AD-A175 207 DEVELOPMENT OF A DEVICE FOR CONTROLLING THE LEADING EDGE VORTICE ON A DELTA WING(U) FLOW RESEARCH CO KENT WA M GAD-EL-HAK JAN 86 FLOW-RR-357 AFOSR-TR-86-2128 1/1

UNCLASSIFIED F49620-85-C-0131 F/G 20/4 NL

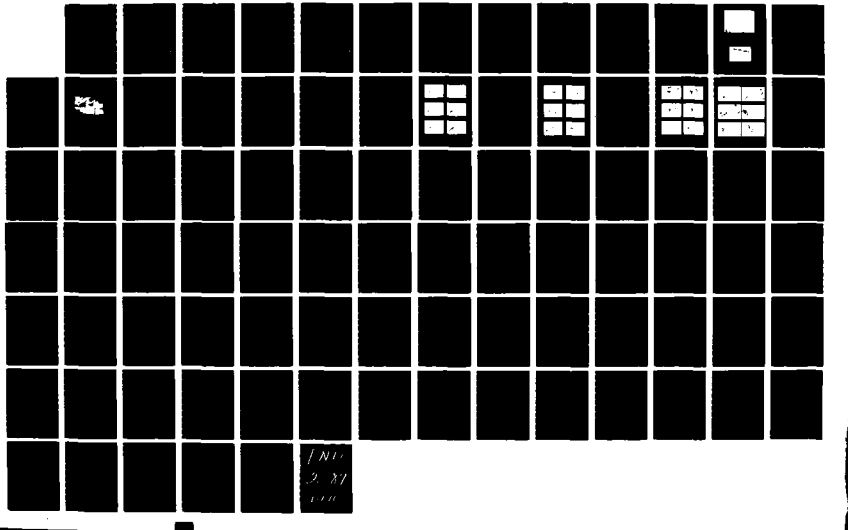

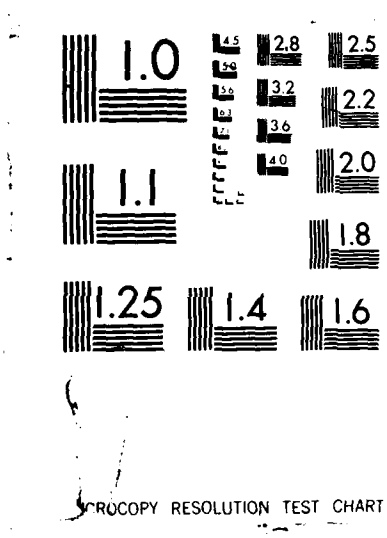
1.0
1.1
1.25
1.4
1.6
1.8
2.0
2.2
2.5
2.8
3.2
3.6
4.0
4.5
CROCOPY RESOLUTION TEST CHART

(2)

Flow Research Report No. 357

AD-A175 207

AFOSR-TR- 86-2128

DEVELOPMENT OF A DEVICE FOR CONTROLLING THE LEADING EDGE VORTICES ON A DELTA WING

(PHASE I SBIR - FINAL TECHNICAL REPORT)

Approved for public release;
distribution unlimited.

A[illegible] (AFSC)
[illegible] is
[illegible].
Information Division

by

Mohamed Gad-el-Hak

Research sponsored by the Air Force Office of
Scientific Research under Contract No. F49620-85-C-0131

DTIC
ELECTE
DEC 1 2 1986
B

January 1986

DTIC FILE COPY

Flow Research Company
21414-68th Avenue South
Kent, WA 98032
(206) 872-8500

390409. SH

86 12 11 114

Unclassified
SECURITY CLASSIFICATION OF THIS PAGE

AD-A175 207

REPORT DOCUMENTATION PAGE

1a. REPORT SECURITY CLASSIFICATION: Unclassified	1b. RESTRICTIVE MARKINGS
2a. SECURITY CLASSIFICATION AUTHORITY	3. DISTRIBUTION/AVAILABILITY OF REPORT: Approved for Public Release; Distribution Unlimited
2b. DECLASSIFICATION/DOWNGRADING SCHEDULE	
4. PERFORMING ORGANIZATION REPORT NUMBER(S): Flow Research Report No. 357	5. MONITORING ORGANIZATION REPORT NUMBER(S): AFOSR-TR- 86-2128
6a. NAME OF PERFORMING ORGANIZATION: Flow Research Company; 6b. OFFICE SYMBOL (If applicable)	7a. NAME OF MONITORING ORGANIZATION: Aerospace Sciences Directorate, Air Force Office of Scientific Research
6c. ADDRESS (City, State and ZIP Code): 21414 68th Ave. S., Kent, WA 98032	7b. ADDRESS (City, State and ZIP Code): Bolling Air Force Base, Washington, D.C. 20332
8a. NAME OF FUNDING/SPONSORING ORGANIZATION: Air Force Office of Scientific Research; 8b. OFFICE SYMBOL (If applicable): NA	9. PROCUREMENT INSTRUMENT IDENTIFICATION NUMBER: SBIR Phase I - Contract F49620-85-C-0131
8c. ADDRESS (City, State and ZIP Code): Bolling Air Force Base, Washington, D.C. 20332	10. SOURCE OF FUNDING NOS.

PROGRAM ELEMENT NO.	PROJECT NO.	TASK NO.	WORK UNIT NO.
61102F	3005	A1	

11. TITLE (Include Security Classification): Development of a Device for Controlling the Leading Edge Vortices on a Delta Wing

12. PERSONAL AUTHOR(S): Gad-el-Hak, Mohamed

13a. TYPE OF REPORT	13b. TIME COVERED	14. DATE OF REPORT (Yr., Mo., Day)	15. PAGE COUNT
Final Technical Report	FROM 85/7/1 TO 85/12/31	86/1/31	82

16. SUPPLEMENTARY NOTATION

17. COSATI CODES		
FIELD	GROUP	SUB GR

18. SUBJECT TERMS (Continue on reverse if necessary and identify by block number): Delta Wings; Vortex Control; Vortex Control Device; Lift Control; Lift Enhancement; Leading Edge Vortices; Super-maneuverability.

19. ABSTRACT (Continue on reverse if necessary and identify by block number)

Experimental observations obtained during a recent research program at Flow Research have shown that a leading edge vortex on a delta wing at constant angle of attack consists of a series of discrete smaller vortices. These vortices pair, much the same as in a free shear layer. A device is proposed to modulate the shedding and the pairing of the discrete vortices by mechanically or acoustically perturbing the leading edge of a delta wing. By applying the perturbation to both leading edges, the total lift of a wing will be altered; alternatively, by using the perturbation preferentially on only one side of the wing, the rolling moment around the axis of symmetry of the aircraft is controlled. The proposed device will enable the pilot of a fighter aircraft to achieve a previously unattained degree of maneuverability.

(Over)

20. DISTRIBUTION/AVAILABILITY OF ABSTRACT	21. ABSTRACT SECURITY CLASSIFICATION
UNCLASSIFIED/UNLIMITED ☒ SAME AS RPT ☐ DTIC USERS ☐	Unclassified

22a. NAME OF RESPONSIBLE INDIVIDUAL	22b. TELEPHONE NUMBER (Include Area Code)	22c. OFFICE SYMBOL
Dr. James D. Wilson; AFOSR	(202) 767-4935	NA

DD FORM 1473, 83 APR — EDITION OF 1 JAN 73 IS OBSOLETE

Unclassified
SECURITY CLASSIFICATION OF THIS PAGE

19. Abstract (continued)

During the first phase of this research program, experiments were conducted in both a water towing tank and a high speed wind tunnel. Flow visualization, fast-response velocity probe surveys, as well as force measurements were conducted to assess the performance of the proposed vortex control device and, more importantly, at this early stage of the reserach, to understand the complex flow field under consideration. This report summarizes our findings based on the research conducted during the period 1 July 1985 through 31 December 1985.

Flow Research Report No. 357

DEVELOPMENT OF A DEVICE FOR CONTROLLING THE LEADING EDGE VORTICES ON A DELTA WING (PHASE I SBIR - FINAL TECHNICAL REPORT)

by

Mohamed Gad-el-Hak

Research sponsored by the Air Force Office of Scientific Research under Contract No. F49620-85-C-0131

DTIC
ELECTE
DEC 12 1986
S
D
B

January 1986

Flow Research Company
21414-68th Avenue South
Kent, WA 98032
(206) 872-8500

TABLE OF CONTENTS

DTIC COPY INSPECTED

Accession For
NTIS GRA&I
DTIC TAB
Unannounced
Justification
By
Distribution
Availability Codes
Dist
A-1

1. INTRODUCTION

With the recent advances in short range infrared guided missiles, a significant change in close air combat characteristics emphasizing instantaneous maneuverability becomes inevitable. This has led to a growing interest in the so called "supermaneuverability" of fighter aircraft, where previously unattained regions of the maneuver envelope are attempted. For example, post-stall flight maneuver and side slipping (Herbst, 1981; 1983). There exists a need for improving existing, and devising novel, vortex control devices that might help achieving the desired high degree of maneuverability.

In a recent research program conducted at Flow Research, it was discovered that the leading edge vortex on a delta wing at a constant angle of attack consists of a series of discrete smaller vortices. These vortices are shed at a predictable frequency. Their trajectories follow the general outline of the classical large bound vortex on each side of the wing. As the discrete vortices follow this course, two vortices would begin to roll around each other and merge to form a single larger vortex. This process was observed to repeat itself several times.

Preliminary attempts to modulate the shedding and the pairing of the discrete vortices were successful. The flow at the leading edge of the delta wing was perturbed by impulsively injecting, at a given frequency, a secondary fluid from a slot along that edge. The flow field was significantly affected when the injection frequency was chosen to be a subharmonic of the shedding frequency of the discrete vortices.

The ultimate goal of the present work is to develop a device that can be used to change the shedding and the pairing of the discrete vortices on a delta wing aircraft. The device will be optimized to significantly change the lift of the airplane at constant speed and constant angle of attack. By applying the method to both leading edges, the total lift of the wing will be altered; alternatively, by using the perturbation preferentially on only one side of the wing, the rolling moment around the axis of symmetry of the aircraft is controlled. Such a device, when successfully developed, will enable the pilot of a delta-wing fighter aircraft to achieve a previously unattained degree of maneuverability.

During Phase I of this research program, experiments were conducted in a water towing tank and a wind tunnel to characterize the flow field around a delta wing with and without the vortex control device. Flow visualizations, velocity surveys using fast-response probes and aerodynamic force measurements were conducted. In this report, a brief background is given in Section 2. The experimental approach is described in Section 3. The flow visualization, velocity and force measurements results are detailed in Sections 4 through 8. Finally, a summary and recommendation for future research are found in the last section.

2. BACKGROUND

The flow over delta wings at constant angle of attack is dominated by two large bound vortices that result from the flow separation at the leading edge (Elle, 1958; Wentz & Kohlman, 1968; Werlé, 1973; Hoerner & Borst, 1975; and Faery et al., 1981). With a sharp leading edge at an angle of attack α, the flow is separated along the entire leading edge forming a strong shear layer. The shear layer is wrapped up in a spiral fashion resulting in a large bound vortex on each side of the wing as sketched in Figure 1a. The two vortices appear on the suction surface of the wing in the form of an expanding helix when viewed from the apex of the lifting surface. The low pressure associated with the vortices produces additional lift on the wing, often called nonlinear or vortex lift, which is particularly important at large angles of attack.

A recent research program, supported by the Air Force Office of Scientific Research, was conducted at Flow Research to determine and examine the structure of the shear layer at the leading edge of a delta wing and other three-dimensional lifting surfaces in steady and unsteady flights (Gad-el-Hak et al., 1983a; 1983b; 1985b; 1985c; 1985d; 1986a; 1986b; 1986c). Flow visualization experiments clearly showed that the shear layer flow near the leading edge of a delta wing at constant angle of attack rolls up into discrete vortices as sketched in Figure 1b. The trajectory of these vortices followed the general outline of the large bound vortex. As they followed this course, two vortices would begin to roll around each other and merge, or pair, to form a single layer vortex, much the same as observed in a free shear layer (Figure 2) originating at a splitter plate between two streams of differing velocity (Winant & Browand, 1974; Brown & Roshko, 1974; and Roshko, 1976).

Examples of the discrete vortices on a delta wing in steady flight are shown in Figures 3 and 4. In Figure 3, a 60° sweep, sharp-leading-edge delta wing was towed in an 18-meter water channel at a root-chord Reynolds number of 1.3×10^4, and at an angle of attack of 10°. Fluorescent dye was injected from a slot near the left hand side leading edge and illuminated with a bank of black lights. The dye marks the discrete vortices with their axes emanating from the apex of the delta wing. Figure 4 is a side view of a 45° sweep delta wing which had a NACA 0012 profile at each spanwise section. The wing had a root-chord Reynolds number of 2.5×10^4. The fluorescent dye is illuminated with a vertical sheet of laser light (Gad-el-Hak et al., 1981) parallel to the

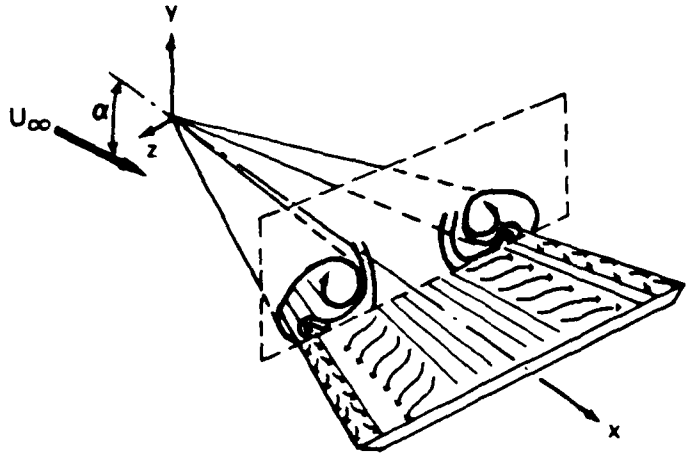

a

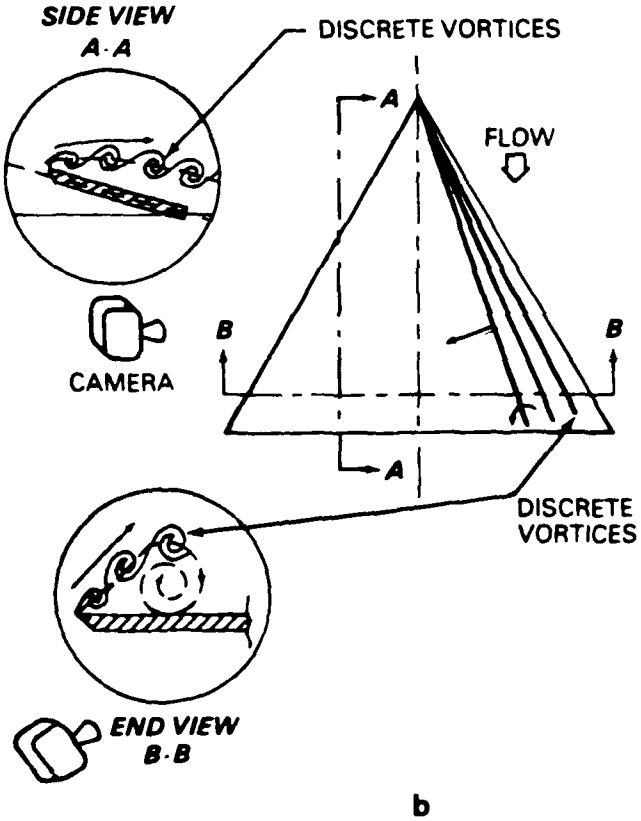

b

Figure 1. Flow Distribution of a Sharp Leading Edge Delta Wing

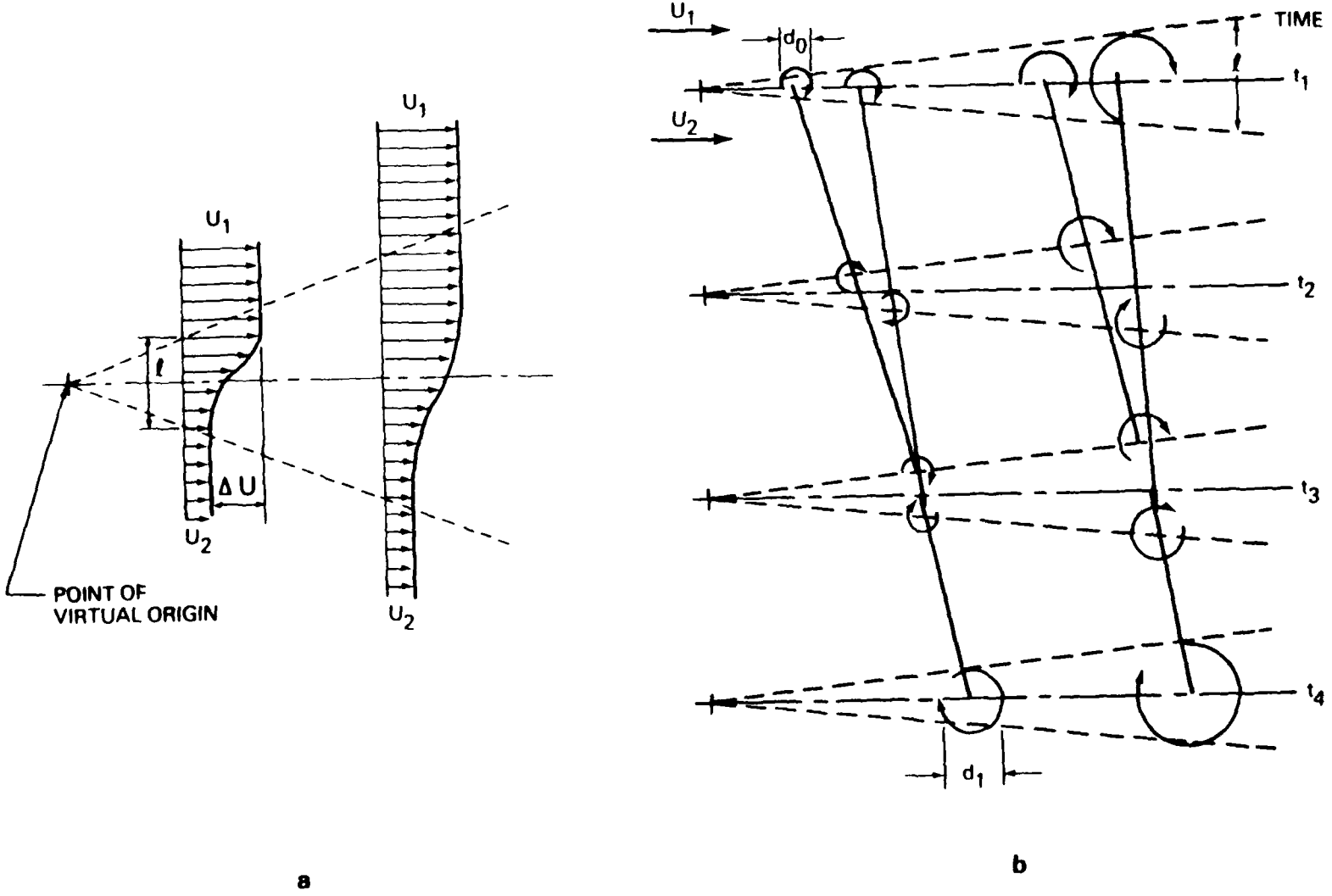

Figure 2. The Growth of a Shear Layer Through Pairing Process

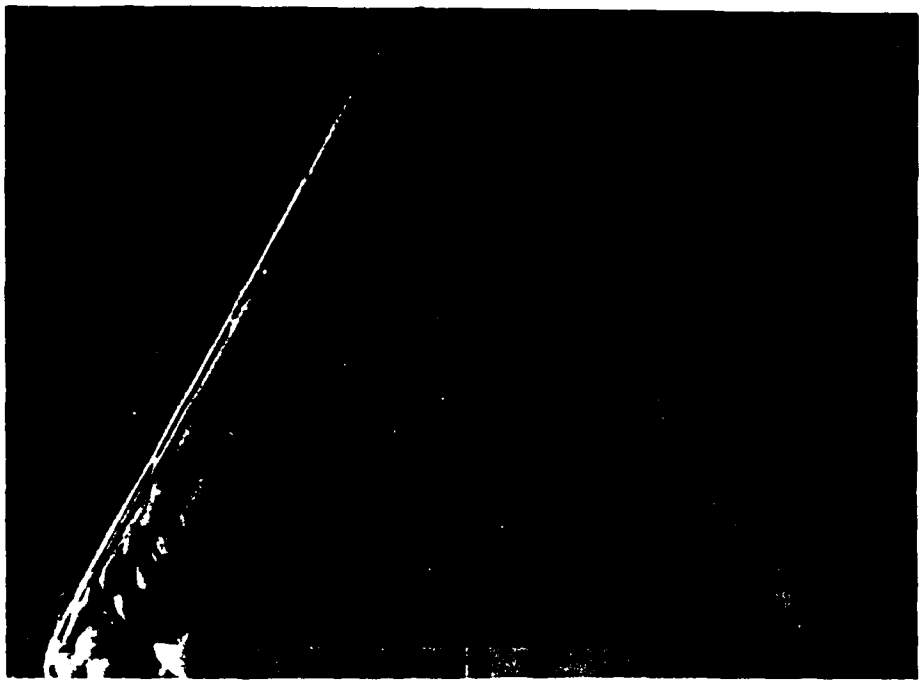

Figure 3. Top View with the Delta Wing at Fixed Angle of Attack $\alpha = 10°$

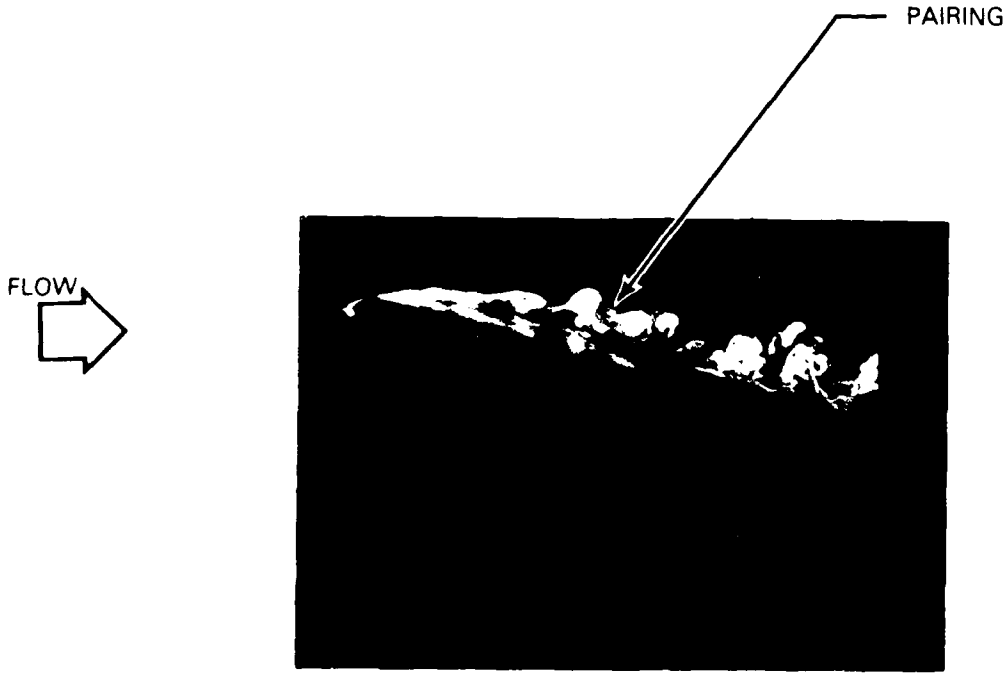

Figure 4. Side View with Wing Fixed at $\alpha = 10°$

flow direction at z = 10 cm (40% of the root-chord length). In this photograph, the pairing process between two discrete vortices is clearly indicated.

For angles of attack below 5°, the pairing process seemed to be inhibited by the proximity of the vortices to the wing surface. The discrete vortices were observed on delta wings with sharp and with blunt leading edges, with delta wings having different sweep angles, and with a Reynolds number varying over at least one order of magnitude. The shedding frequency of the discrete vortices depends on the mean velocity of the wing and the parameters effecting the thickness of the shear layer. This frequency can be modulated by a pitching motion of the wing (Gad-el-Hak et al., 1983b).

It should be noted that the shedding of discrete vortices in a free shear layer has been observed to occur resonantly at all Reynolds numbers investigated in different laboratories around the world (Ho & Huerre, 1984), including Reynolds numbers well in excess of the critical one. We believe that the analogous phenomenon of shedding from a delta wing is also occurring at all Reynolds numbers and, hence, our observations have universal validity. The shedding of discrete vortices from a free shear layer or from the leading edge of a delta wing is to be contrasted to the shedding from a bluff body. In the latter case, the shedding occurs resonantly at subcritical Reynolds numbers but occurs more randomly at higher Reynolds numbers.

During the above mentioned research program, attempts were made to modulate the shedding and the pairing of the discrete vortices from a delta wing at <u>constant</u> angles of attack. This was inspired by the recent attempts to control the growth rate of a free shear layer by perturbing the flow at the end of the splitter plate (Ho & Huerre, 1984). The flow at the leading edge of the delta wing was perturbed by impulsively injecting a secondary fluid from a slot along that edge. The frequency of perturbation was varied over a wide range, and it was found that maximum changes in the flow field occurred when this frequency was a subharmonic of the natural shedding frequency of the unperturbed wing.

3. EXPERIMENTAL APPROACH

3.1 Towing Tank

The present experiments were conducted in both a water towing tank and a high-speed wind tunnel. The flow visualization tests were best suited for the water facility. The towing tank, Figure 5, is 18 meter long, 1.2 meter wide, and 0.9 m deep (see Gad-el-Hak et al., 1981). The delta wing was rigidly mounted on a carriage that rides on two tracks mounted on top of the towing system. During towing, the carriage was supported by an oil film, which ensured a vibrationless tow. The equivalent freestream turbulence was checked using a hot-film probe, and was found to be about 0.1% of the mean towing speed. The carriage was towed by two cables driven through a reduction gear by a 1.5-hp Boston Ratiotrol motor. The towing speed was regulated within an accuracy of 0.1 percent. The system was able to achieve towing speeds between 1 and 300 cm/sec ($R_c = 2.5 \times 10^3 - 7.5 \times 10^5$) for the present study.

3.2 Wind Tunnel

While the flow visualization experiments were conducted in the water towing tank, a wind tunnel was used to measure the lift, drag and pitching moment and to survey the velocity field around the delta wing. The venturi wind tunnel, located at the University of Washington's Department of Aeronautics and Astronautics is an open circuit type and is 6.5 meter long. The test section is of a hexagonal cross section, 1 meter wide, 0.8 meter high and 1 meter long. The wind tunnel is powered by a 10 hp D.C. motor driving, by direct coupling, a 1.6 meter, four bladed propeller. The model is mounted in the test section using a three-point support system consisting of two fixed bayonets forward and a pitch arm aft. The maximum speed of the tunnel is 32 m/sec ($R_c \equiv U_\infty c/\nu = 8.5 \times 10^5$) with a clear test section. The background turbulence in the tunnel is quite high and exceeds 1 percent even with the addition of several turbulence management devices (honeycombs, screens, etc.).

3.3 Delta Wing Models

Four different delta wing models were used in the present investigation. For the flow visualization experiments conducted in the water tank, a delta wing with a leading edge sweep of 45° and a NACA 0012 profile at each spanwise section, a delta wing with similar sweep angle but having a sharp leading edge and a flat surface, and a 60° sweep wing with a sharp leading edge were used.

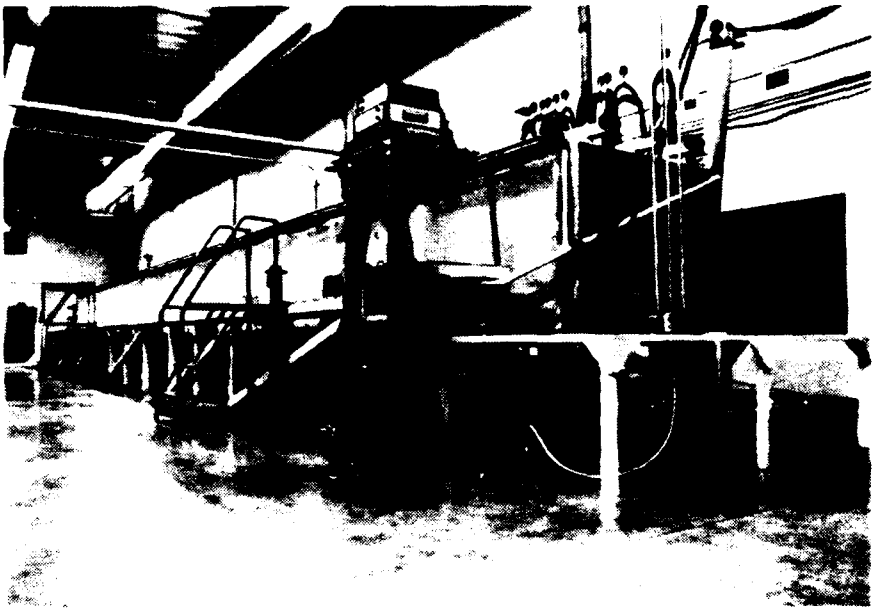

Figure 5. The Flow Industries 18-m Towing Tank

The root chord of all three wings was 25 cm. A larger model having a root chord of 40 cm, a 60° sweep angle and a sharp leading edge was used in the wind tunnel tests. The blunt leading edge model was made of aluminum, while the sharp leading edge models were made of Plexiglas.

3.4 Leading Edge Excitation

To perturb the shar layer originating at the leading edge of a delta wing, a variety of methods are available including the following:

(a) a passive cavity system which is tuned to a frequency range corresponding to the natural frequency of the vortex shedding. The tuning is provided by a piston or a similar device which changes the volume of the cavity so that its natural resonance frequency is comparable to the shedding rate.

(b) acoustical means which for example may utilize an array of speakers perpendicular to the cross section of the wing. The speakers are used to provide a velocity perturbation along a slot in the leading edge of the delta wing.

(c) a piezoelectric array embedded in the wing near the leading edge. The vibration of the piezoelectric surface perpendicular to the flow would provide the disturbance. In a field application this has the advantage that there is less chance of fouling because no slots are used.

(d) a heating element could be utilized to provide an unsteady perturbation to the flow before separation. Because this device may not respond to as high frequency as the above methods, it may be most useful in hydrofoil applications where the frequency requirements are lower.

(e) blowing and/or sucking through spanwise slots similar to those in (b) above. This would provide a larger amplitude disturbance than the acoustical technique.

(f) mechanical devices, such as a vibrating ribbon, in the shape of leading edge slots or other configurations.

In this preliminary phase of the research, only method (e) above was tested. Periodic blowing or suction was applied through both leading edges of a delta wing model. A slot 0.2-mm wide was formed at each leading edge and plumbed to a system of grooves inside the model. In the towing tank experiments, a constant head tank was used together with a solenoid value to inject water at a given frequency and amplitude out of the leading edge slots. The solenoid valve was driven by a square-wave signal generator having the desired frequency. A 100-psi compressed air line was used to periodically inject air through the leading edge slots in the model placed in the wind tunnel. The secondary air flow rate was varied using a pressure regulator and the perturbation frequency was controlled using a home-made rotary valve driven by an external motor.* The same valve was used together with a vacuum chamber to achieve periodic suction in the wind tunnel experiments.

The peak injection or suction speeds from the leading edge slots varied over the wide range of 0 to 2 U_∞. While the upper limit of this speed may seem excessive, the resulting perturbation were still weak because of the extremely small area of the leading edge slot compared to the area of the delta wing ($1/2\ \rho\ U_j^2\ A_j << 1/2\ \rho\ U_\infty^2\ A_{wing}$).

3.5 Flow Visualization Methods

The water towing tank was used to conduct flow visualization experiments to assess the nature of the discrete vortices shed from a delta wing with and without perturbation at its leading edge. Food color and fluorescent dyes were used in the present investigation. The food color dyes were illuminated with conventional flood lights and were used to obtain overall views of the flow field using a camera mounted on top of the towing tank. The fluorescent dyes were excited with sheets of laser light projected in the desired plane. To produce a sheet of light, a 5-W argon-ion laser (Spectra Physics, Model 164) was used with a mirror mounted on an optical scanner having a 720-Hz natural frequency (General Scanning, Model G124). A sine-wave signal generator, set at a frequency equal to the inverse of the camera shutter speed, drove the optical scanner to produce light sheets approximately 1-mm thick.

---

*The required frequencies in the wind tunnel experiment were higher than those used in the water tests.

Side views of the flow field were obtained using a vertical sheet of laser light in the x-y plane at z = 10 cm (40% of the semispan of the 45° sweep wing) and a camera towed with the wing but located outside the tank, as shown in Figure 1. End views were obtained using a vertical sheet of laser light in the y-z plane at x = 20 cm (80% of the root chord) and an underwater camera towed behind the wing using the same carriage.

Dye sheets or dye lines were seeped into the boundary layer through a system of slots and holes on the suction side of the delta wings. The slots were 0.2-mm wide, milled at a 45° angle to minimize the flow disturbance. The holes were 0.4 mm in diameter, spaced at 1 cm center to center.

Dye was also placed in the flow field by laying several thin, horizontal sheets prior to towing the wing. The dye layers remained thin, about 1-mm thick, due to the inhibition of vertical motion caused by introducing a weak saline stratification in the tank. The dye layers remained quiescent until disturbed by the flow field on and around the wing. Thus, the boundary-layer flow as well as the potential flow could be observed since the dye layers existed in both flow regions. Ciné films of the runs presented in this report are available upon request.

For the dye-layer runs, the density gradient in the tank was about 10^{-4} g/cm^4, which yields a Brunt-Väisälä frequency of N = 0.05 Hz. The time scale associated with this weak stratification is large compared to a typical convection time scale; hence, the stratification should have little effect on the dynamics of the flow. This was verified experimentally by conducting two runs using the dye injection method, in the presence and in the absence of stratification in the tank. The visualization patterns in the two runs were indistinguishable.

3.6 Velocity Probes

Hot-film and hot-wire probes were used to survey the velocity field around the delta wing mounted in the venturi wind tunnel. Miniature, single-element probes (TSI Model 1260) having a diameter of 0.025 mm and a sensing length of 0.25 mm were used. A three-dimensional traverse was used to survey the longitudinal velocity fluctuations in the vicinity of the delta wing. Conventional turbulence statistics such as the mean, root-mean-square, spectrum, correlation and probability distribution were computed from the velocity signals.

The fast-response probe signals were first recorded on an instrumentation tape recorder (Hewlett-Packard Model 3964A). The FM analog tape recorder has 4 channels, uses 6 mm tape and accepts very low frequencies including DC. The data are stored in the analog tape and digitized later using the analog-to-digital converter on the NOVA 800 minicomputer. Data analysis are then performed on the NOVA and on the mainframe computer PRIME P750.

3.7 Force Balance

The venturi wind tunnel described in Section 3.2 has a three-component balance system to measure lift, drag and pitching moment. The delta wing is mounted on a three-point support type system, consisting of two fixed bayonets forward and a pitch arm aft. The force readings appear on a motor driven beam balance having a resolution of 10 gram. However, due to the continuous motion of the force balance caused by insufficient damping in the feedback circuit, the smallest force change that was accurately readable was about one order of magnitude higher than the nominal resolution. As will be discussed in Section 8, the balance resolution was not sufficient to detect the expected changes in the aerodynamic forces due to the vortex control device. The short period available for the present project (6 months) did not allow enough time for considering alternative facilities including building a new force balance. However, during the second phase of this research a new force balance with sufficient resolution will be designed and built.

4. FLOW VISUALIZATION RESULTS

Three delta wing models were tested in the 18-m towing tank. Different views of the flow field around the perturbed and unperturbed lifting surfaces were obtained using food color and fluorescent dyes. Figure 3 shows a plane view of the 60°, sharp leading edge delta wing at an angle of attack of $\alpha = 10°$ and a root-chord Reynolds number of 1.25×10^4. The flow is from top to bottom and the flow field on the left side of the wing is visualized using a dye slot at the leading edge. Note that the dye sheet has alternating dark and light regions near the leading edge and extending along it. Although these regions become more obscure as they are wrapped up into the large vortex structure, they do indicate that a substructure is present in the flow field.

Figure 4 is a side view of the 45° sweep delta wing which had a NACA 0012 profile at each spanwise section. The angle of attack is $\alpha = 10°$ and the Reynolds number is $R_c = 2.5 \times 10^4$. The fluorescent dye is illuminated with a vertical sheet of laser light parallel to the flow direction at z = 10 cm. In this picture, the pairing process between two discrete vortices is clearly indicated.

A cross-sectional view of the discrete leading edge vortices is depicted in the sequence of photographs in Figure 6. In here, the 60°, sharp leading edge delta wing at an angle of attack of $\alpha = 10°$ and a Reynolds number of $R_c = 1.25 \times 10^4$ is visualized using fluorescent dye seeped from the leading edge slot and excited with a vertical sheet of laser light perpendicular to the axis of the primary leading-edge vortex. Six frames from the ciné film are shown in Figure 6 at times t = 0, 0.14, 0.20, 0.34, 0.49 and 0.56 sec.* It is clear that the dye rolls up into regions of strong concentration immediately after separation, much the same as in the case of a free shear layer. The discrete vortices are separated by a very thin braid of dye and two vortices are observed to roll around each other and merge to form a single larger vortex. This process repeats itself at least three times before reaching the trailing edge of the wing at the Reynolds number range used in the present investigation.

The ciné films were used to determine the natural shedding frequency, f_o, by counting the number of vortices passing a fixed position near the leading edge per unit time. The shedding frequency was independent of the wing's

---

*The origin of time is arbitrary.

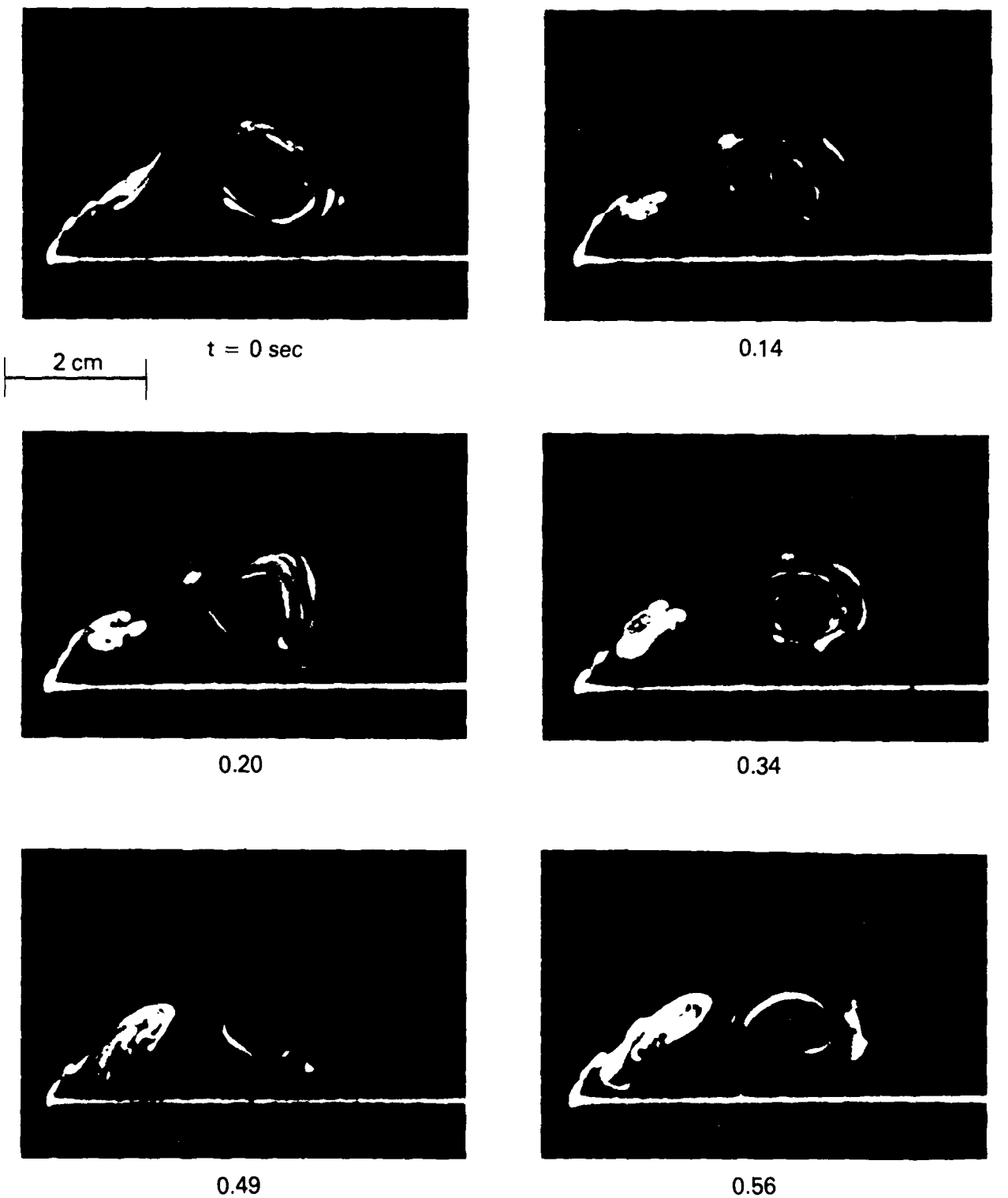

Figure 6. End View of the Discrete Leading Edge Vortices. $R_c = 1.25 \times 10^4$; $\alpha = 10^0$. Natural Shedding Frequency $f_0 = 2.2$ Hz.

sweep angle and leading edge shape. At constant U_∞, the observed number of vortices shed per unit time tended to decrease as α increased. At constant α, the measured frequency is proportional to the square root of the towing speed. A least squares fit of the data at $\alpha = 15°$ yields the empirical relation:

$$f_o = 1.3\sqrt{U_\infty} \quad ; \alpha = 15°, \; R_c = 1.25\times10^4 - 3.33\times10^5,$$

or

$$f_o c/U_\infty = 1625/\sqrt{R_c} \quad .$$

If the vortices are shed at a constant Strouhal number, this would imply that the length scale also increases as the square root of the velocity. Since the frequency is very sensitive to slight changes in the shear layer, this result may have been influenced by increasing the dye flow rate at higher velocities in order to improve the visual image.

The principal result of the visualization results depicted in Figures 3, 4 and 6 is that the classical large vortices on delta wings originate as a series of smaller vortices shed from the leading edge of the airfoil. They rotate around each other and pair to form larger vortices while simultaneously moving downstream. As was depicted by Roshko (1976) for a free shear layer, the pairing process is an important contributor to the growth of the vortical region. Turbulent diffusion* can correctly but imprecisely describe that growth.

The best attack angle to observe the shedding and pairing of the discrete vortices was in the range of 10 to 15°. At angles below 5°, the pairing process seemed to be inhibited by the proximity of the solid boundary. At large angles of attack, the flow was more turbulent and masked the observed phenomenon.

By perturbing the leading edge of a delta wing, the shedding and the pairing of the discrete vortices are modulated much the same as the changes in the growth rate achieved in perturbed free shear layers. The flow at the leading edge of the delta wing was perturbed in the tow tank experiments by impulsively injecting a secondary fluid from the leading edge slots. The results for a subharmonic perturbations are shown in the sequence of photographs in Figure 7. The run conditions were the same as those depicted in Figure 6, but a square-wave perturbation was applied with a peak injection speed equal to the towing speed ($U_j = U_\infty = 5$ cm/sec) and a frequency equal half

*Or molecular diffusion in the case of a laminar flow.

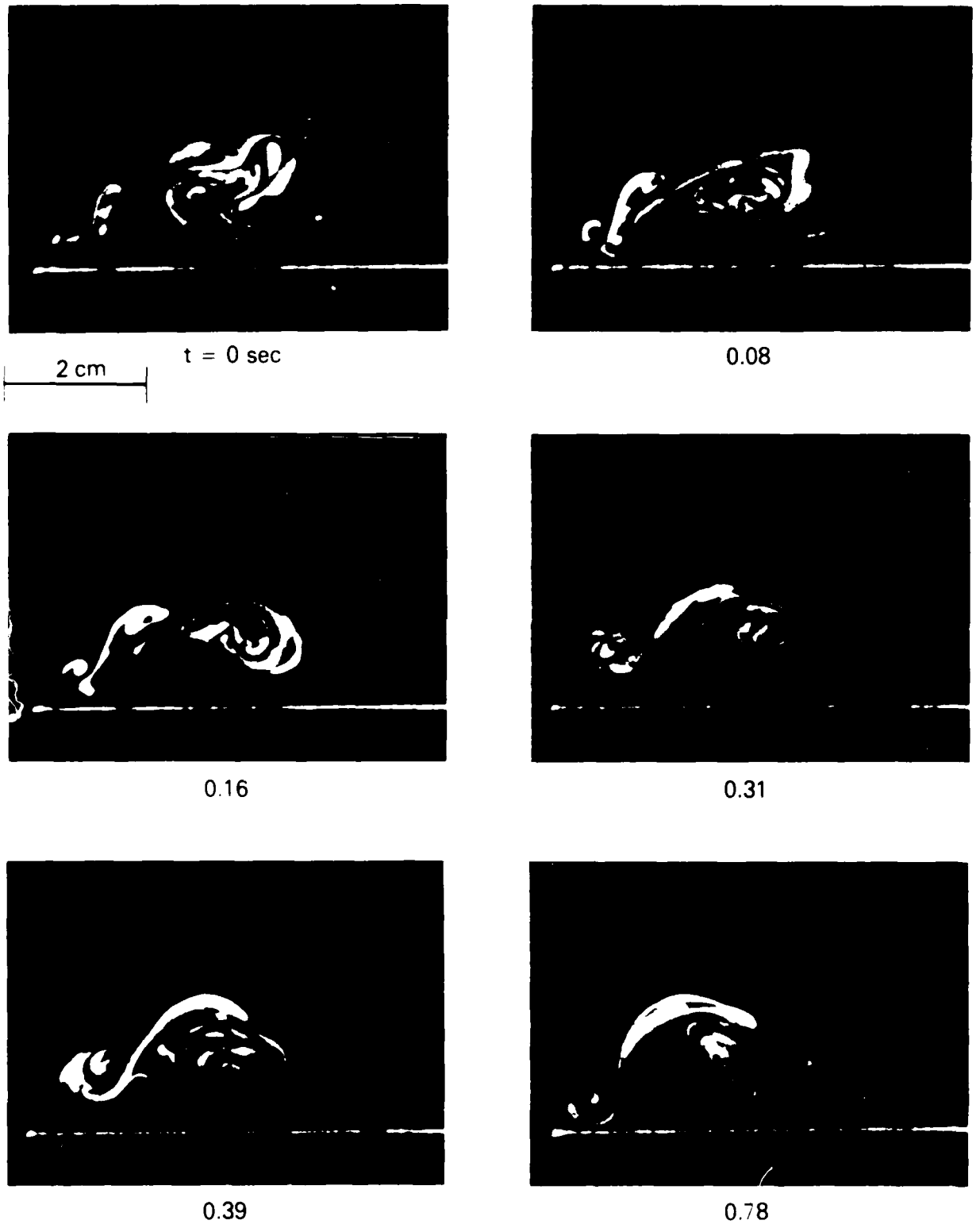

Figure 7. End View. Subharmonic Perturbation Applied at the Leading Edge. Pairing is Enhanced and the Large Vortex is More Organized.

the natural shedding frequency ($f = 0.5\ f_o = 1.1$ Hz). It is clear that the perturbed shear layer is quite different from the natural one. The first pairing occurs closer to the leading edge and the primary leading edge vortex is more intense and larger by about 30% than the one observed in the unperturbed case.

Higher injection rates seem to be counter-productive. As shown in Figure 8, when the subharmonic perturbations were doubled in amplitude ($U_j = 2\ U_\infty =$ 10 cm/sec), the resulting large vortex was less organized and the pairing process was not enhanced. This was also observed, Figure 9, when the perturbation frequency was quarter of the natural shedding frequency ($f = 0.25\ f_o = 0.55$ Hz) while the perturbation amplitude remained high ($U_j = 2\ U_\infty = 10$ cm/sec).

In summary, the visualization experiments indicate that the classical large vortices on a delta wing originate as a series of smaller vortices shed from the leading edge. The pairing process between these vortices is dynamically significant and can be modulated by perturbing the leading edge of the wing. Weak, subharmonic perturbations seem to enhance the pairing and result in a more organized large vortex.

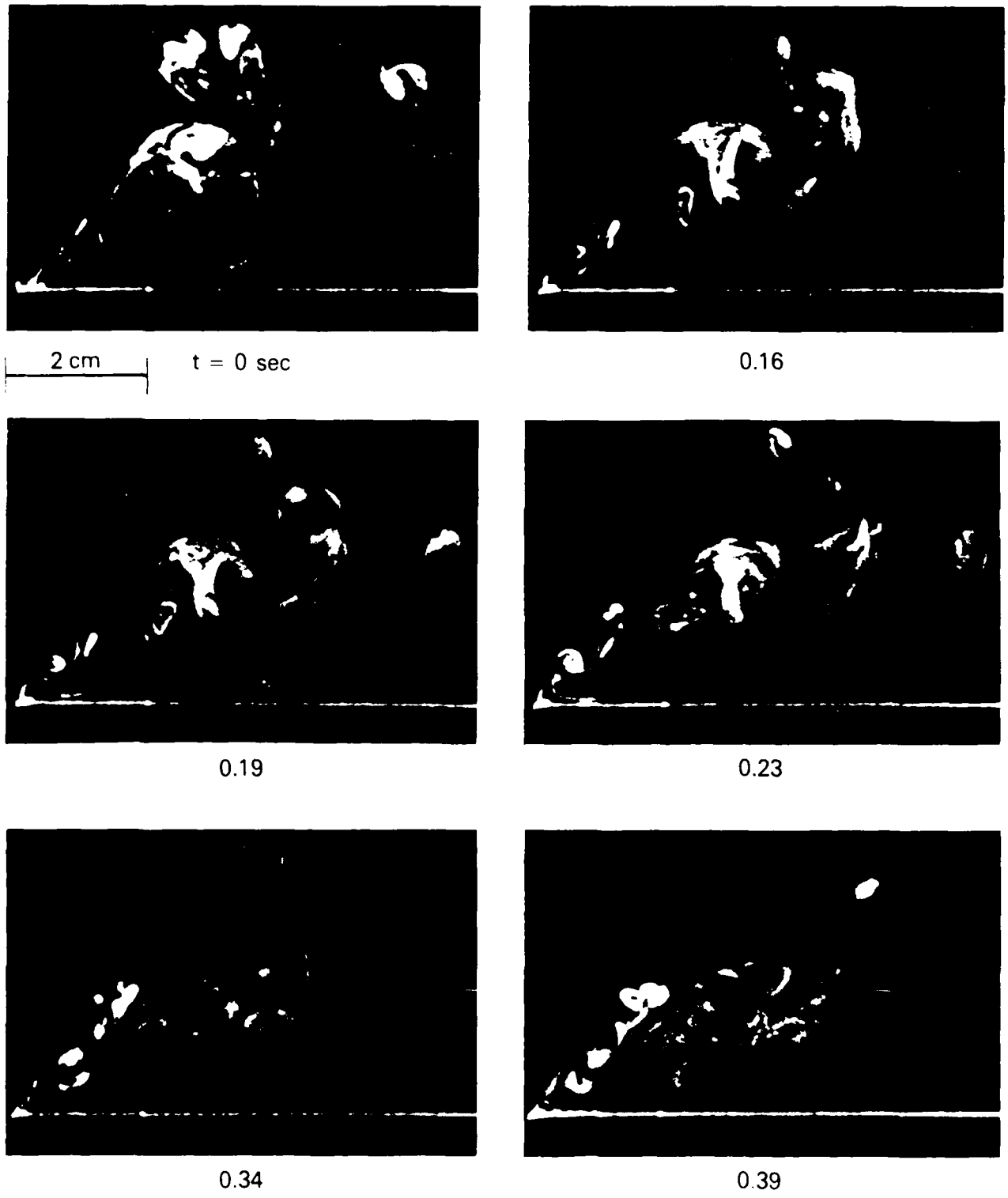

Figure 8. Higher Injection Rate at the Leading Edge Seems to be Counter Productive. The Resulting Large Vortex is Less Organized.

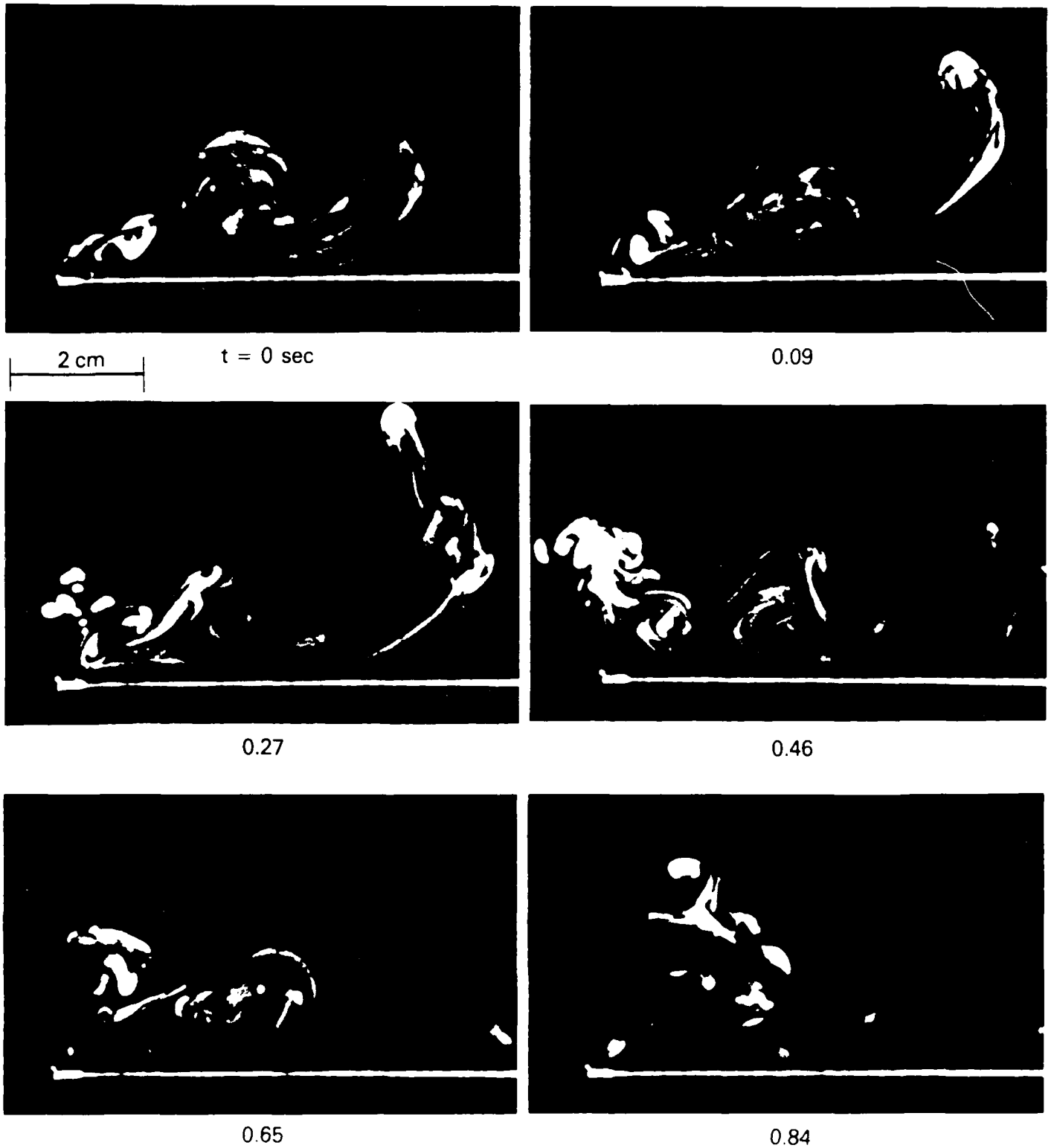

Figure 9. The Perturbation Frequency is 25% of the Natural Shedding Frequency. The Perturbation is Again Too Strong, Resulting in a Less Organized Vortex.

5. VELOCITY MEASUREMENTS

The large delta wing model was tested at the venturi wind tunnel to obtain velocity and force measurements. The 60° sweep angle, sharp leading edge wing is made of Plexiglas and has a root chord of 40 cm. The root chord Reynolds number in the experiment was varied in the range of $1x10^5$ to $4x10^5$. Miniature, single element hot-wire and hot-film probes were used to survey the instantaneous longitudinal velocity at different positions within the leading edge vortices and at different run conditions.

The coordinate system is shown in Figure 1, where the origin is at the apex of the delta wing, x is along the root chord, y is normal to the model surface and z is in the spanwise direction. Measurements were conducted at the attack angles of 10° and 28°, at two stations, 0.3 c and 0.6 c, and at different y's and z's. The complex, three-dimensional shear layer was investigated without perturbation, with periodic injection at the leading edge and with periodic suction.

A sample of the instantaneous longitudinal velocity signal, normalized with the tunnel speed, is shown in Figures 10 through 13. The unperturbed shear layer is surveyed for a Reynolds number $R_c = 1.3x10^5$ and angle of attack $\alpha = 28°$. The measurements were conducted along a line perpendicular to the x-y plane at x = 0.6 c and y = 0.01 c, where C is the root chord. Four different z's position are shown in the figures: z/c = 0.349; 0.346 (leading edge); 0.344 and 0.326. All four positions are very close to the leading edge, yet dramatic differences exist between each profile, consistent with the presence of an intense shear layer.

In Figure 10, the negative spikes in the instantaneous longitudinal velocity are consistent with the passing of the discrete vortices at the fixed probe location. As these vortices turn, lower speed fluid is transported on the high speed side of the shear layer. Note that the mean speed at z/c = 0.349 is higher than the tunnel speed ($\bar{U}(x,y,z) > U_\infty$). A well defined mean shedding frequency is apparent and will be computed from the spectrum peak of the raw velocity data.

The negative spikes are still apparent in Figure 11 but are now embedded in the background turbulence. The mean speed is now lower. Positive spikes are observed as the probe is traversed inward from the leading edge (Figures 12 and 13), and the mean speed continues to drop indicating a strong spanwise shear.

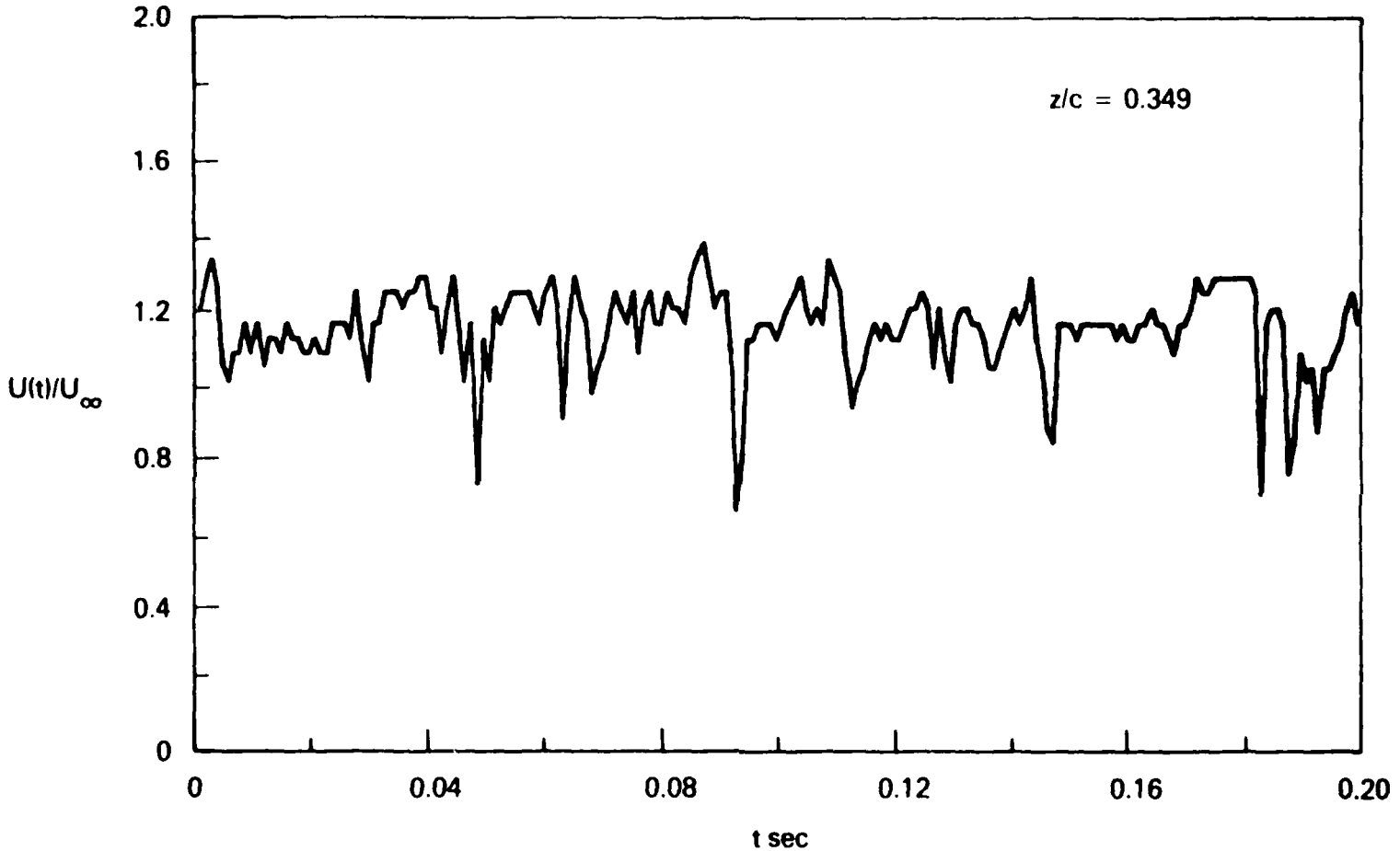

Figure 10. Instantaneous Longitudinal Velocity. x/c = 0.6; y/c = 0.01; $R_c = 1.3 \times 10^5$; $\alpha = 28°$; $U_j/U_\infty = 0$.

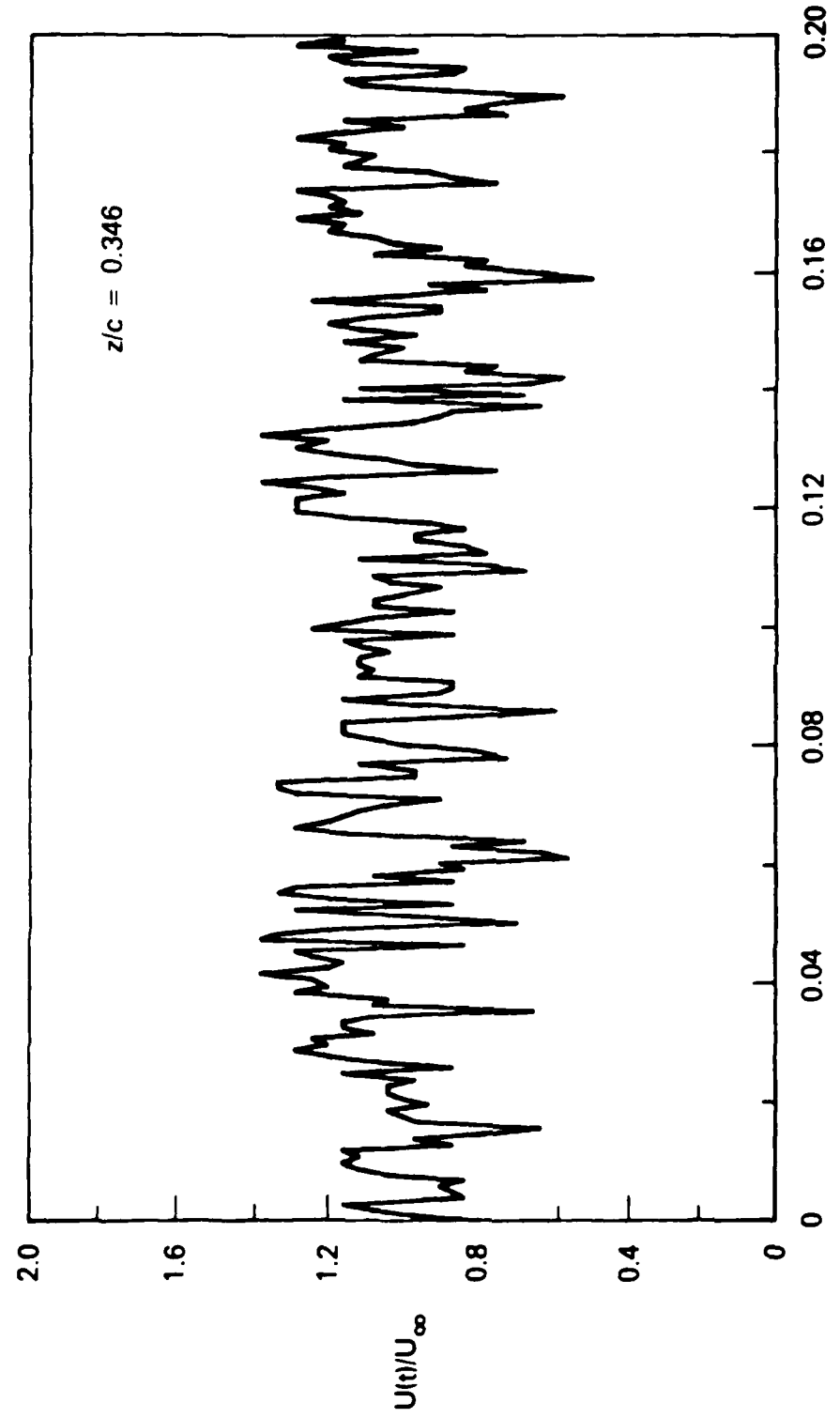

Figure 11. Instantaneous Longitudinal Velocity. x/c = 0.6; y/c = 0.01; $R_c = 1.3 \times 10^5$; $\alpha = 28°$; $U_j/U_\infty = 0$.

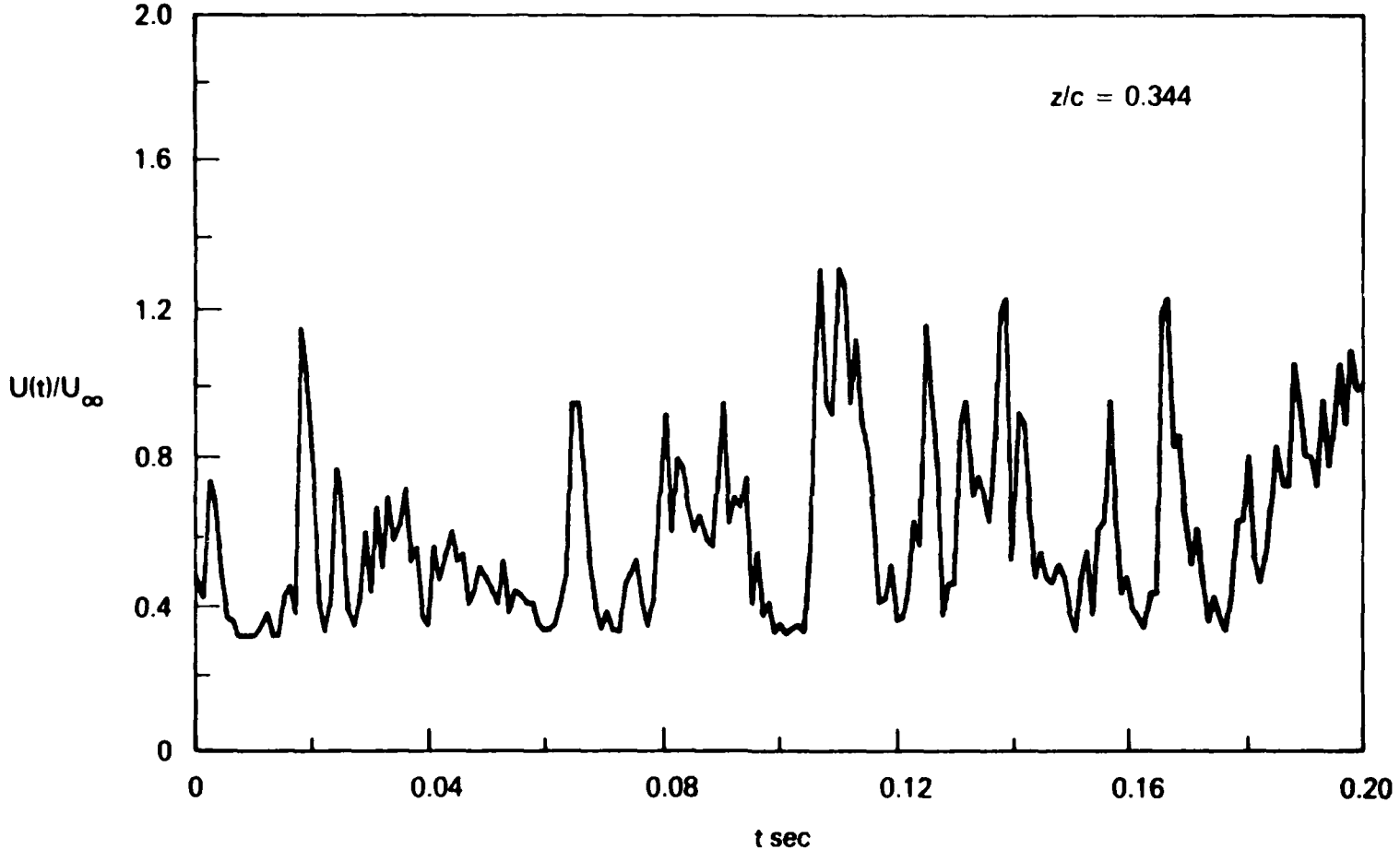

Figure 12. Instantaneous Longitudinal Velocity. x/c = 0.6; y/c = 0.01; $R_c = 1.3 \times 10^5$; $\alpha = 28°$; $U_j/U_\infty = 0$.

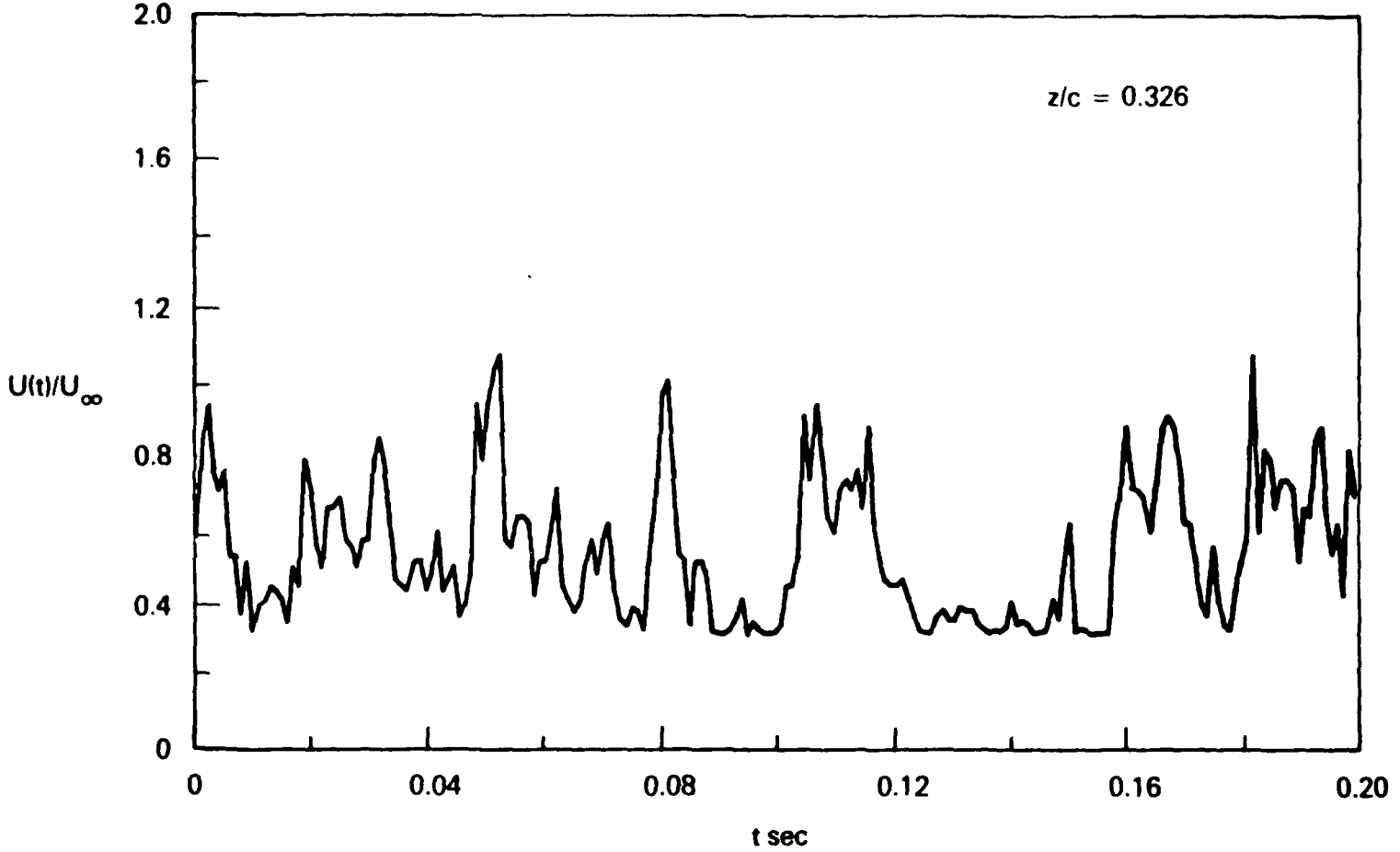

Figure 13. Instantaneous Longitudinal Velocity. x/c = 0.6; y/c = 0.01; $R_c = 1.3 \times 10^5$; $\alpha = 28°$; $U_j/U_\infty = 0$.

The longitudinal mean velocity profiles at different spanwise locations is shown in Figure 14 for the same run conditions depicted in Figures 10 through 13. At the centerline of the delta wing, z/c = 0, the velocity near the suction surface is twice that of the ambient speed. It drops to a low of 0.6 U_∞ at z/c = 0.3 just inward of the leading edge, then rises quite fast and drops again just outside the leading edge. This strong shear region is where the discrete vortices are pairing and are dynamically interacting.

The root-mean-square profiles obtained from the same signal are shown in Figures 15 and 16. In the first figure, $\sqrt{\overline{u2}}$ is normalized with the tunnel speed U_∞, while in Figure 16 the RMS velocity fluctuations are normalized with the local mean velocity $\bar{U}$. The two peaks in the velocity fluctuations correspond to the positions of maximum shear (the zero crossings inward of the leading edge in Figure 14). The RMS is as high as 27% of the local mean velocity at these regions of intense shear.

Leading edge perturbations could dramatically affect the intense shear layer. From the visualization results, it was found that subharmonic perturbations could favorably change the growth of the shear layer and enhance pairing. In Figures 17 and 18, the mean and rms profiles are depicted for three cases: no perturbation, subharmonic injection (U_j = 1.73 U_∞) and subharmonic suction (U_j = -0.87 U_∞), where U_j is the mean injection speed from the leading edge slot. The Reynolds number in all three cases is $R_c = 1.3 \times 10^5$, the angle of attack is 28°, and the spanwise profiles are taken at x/c = 0.3 and y/c = 0.003. The leading edge perturbations shift the interface of the shear layer inward towards the wing centerline. The maximum speed near the leading edge is not affected, but the minimum speed is dramatically reduced by the periodic suction or injection. Both the mean and rms profiles appear to be more complex in the case of subharmonic suction perturbation. Note that the second peak in the rms profiles is not quite developed at this upstream station (x/c = 0.3 in Figure 18) compared to the further downstream location shown in Figure 15 (x/c = 0.6).

The mean and rms profiles at four different heights above the suction surface of the delta wing are shown in Figure 19 and 20. The Reynolds number is $R_c = 1.3 \times 10^5$ and the attack angle is α = 28°. Subharmonic perturbations were applied at the leading edge of the delta wing with U_j = 0.73 U_∞, and the spanwise profiles are taken at x/c = 0.6 and y/c = 0.01, 0.03, 0.05 and 0.08. It is clear from these four profiles that the shear layer is extremely complex.

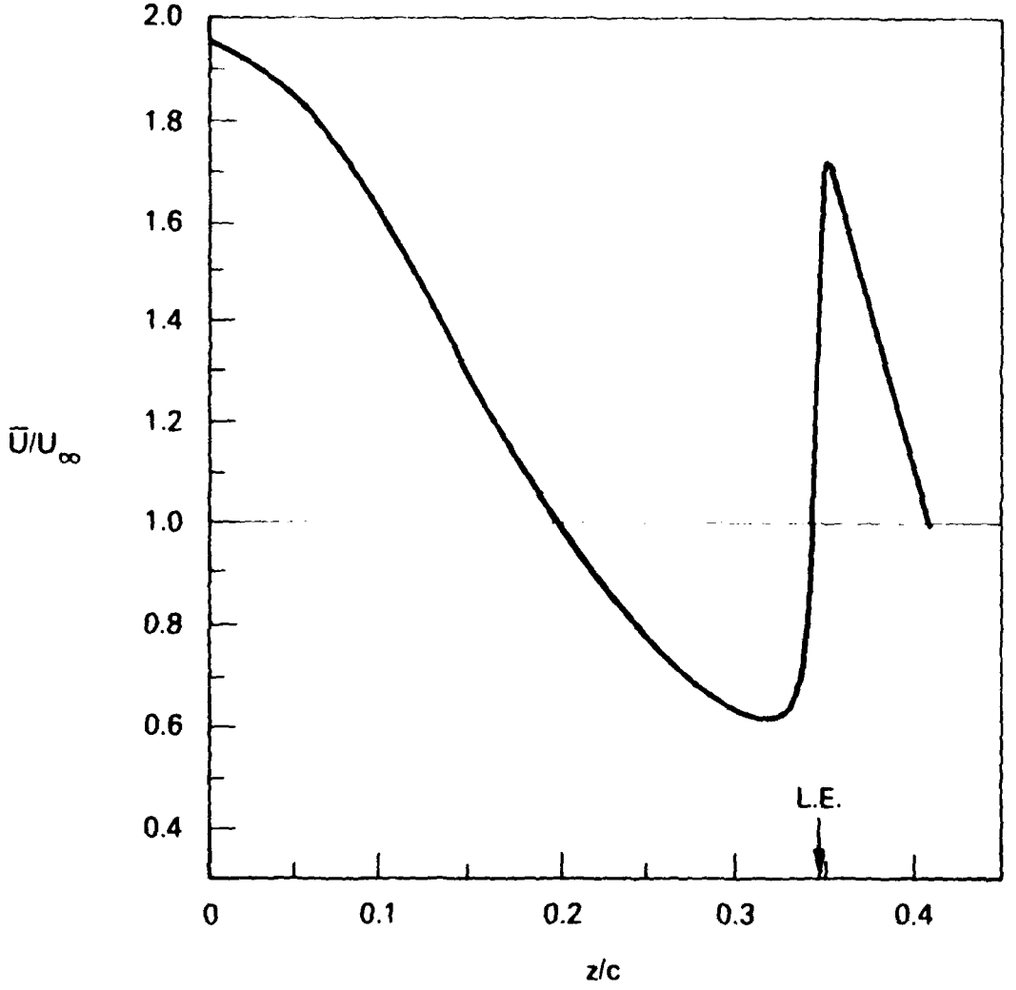

Figure 14. **Longitudinal Mean Velocity Profile. x/c = 0.6; y/c = 0.01; $R_c = 1.3 \times 10^5$; $\alpha = 28°$; $U_j/U_\infty = 0$.**

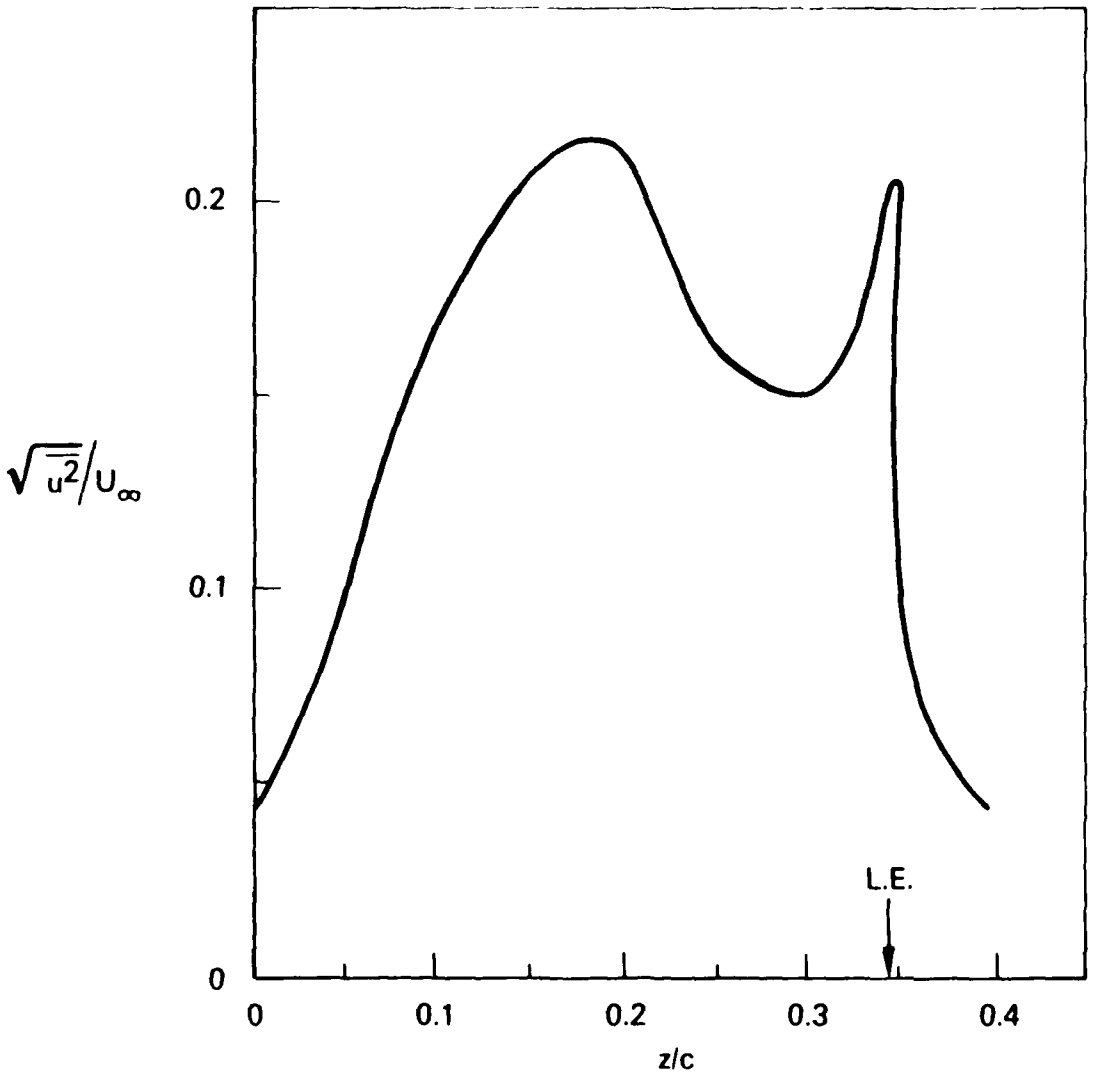

Figure 15. **RMS Velocity Fluctuations. x/c = 0.6; y/c = 0.01; $R_c = 1.3 \times 10^5$; $\alpha = 28°$; $U_j/U_\infty = 0$.**

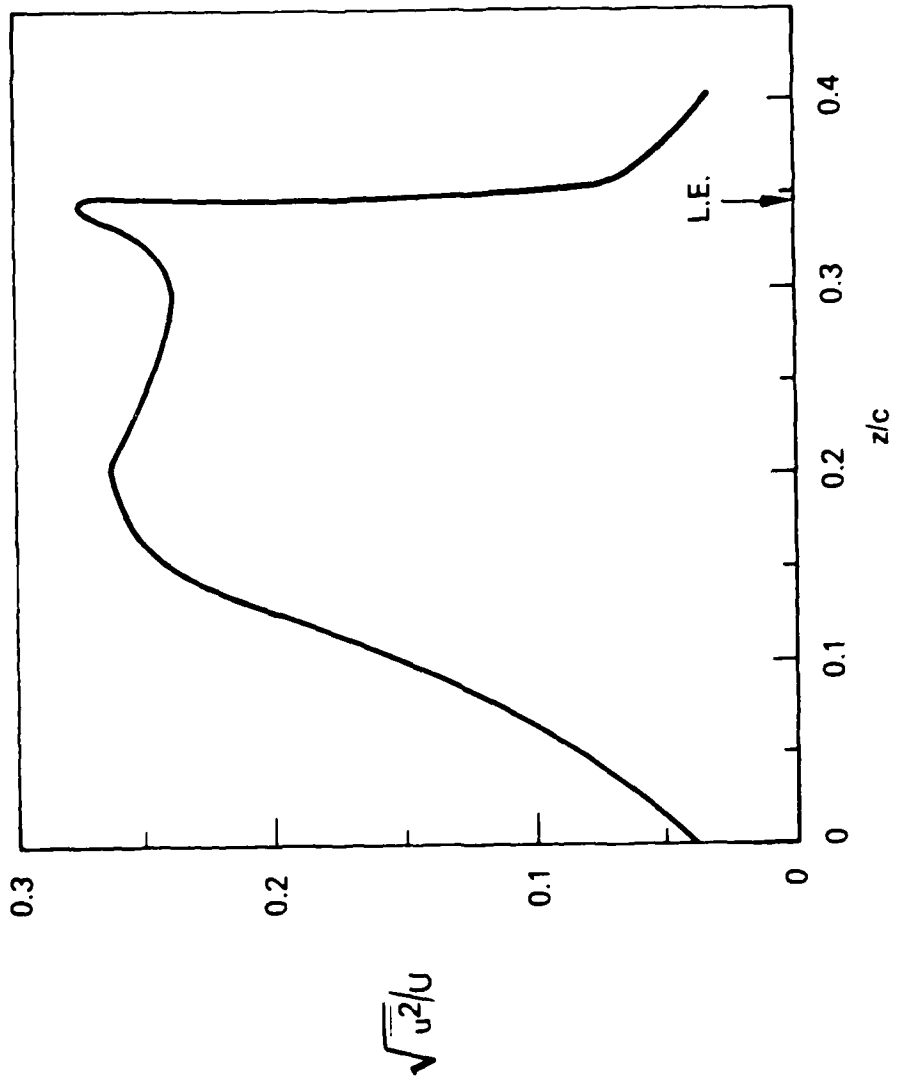

Figure 16. RMS Velocity Fluctuations. x/c = 0.6; y/c = 0.01; $R_c = 1.3 \times 10^5$; $\alpha = 28°$; $U_j/U_\infty = 0$.

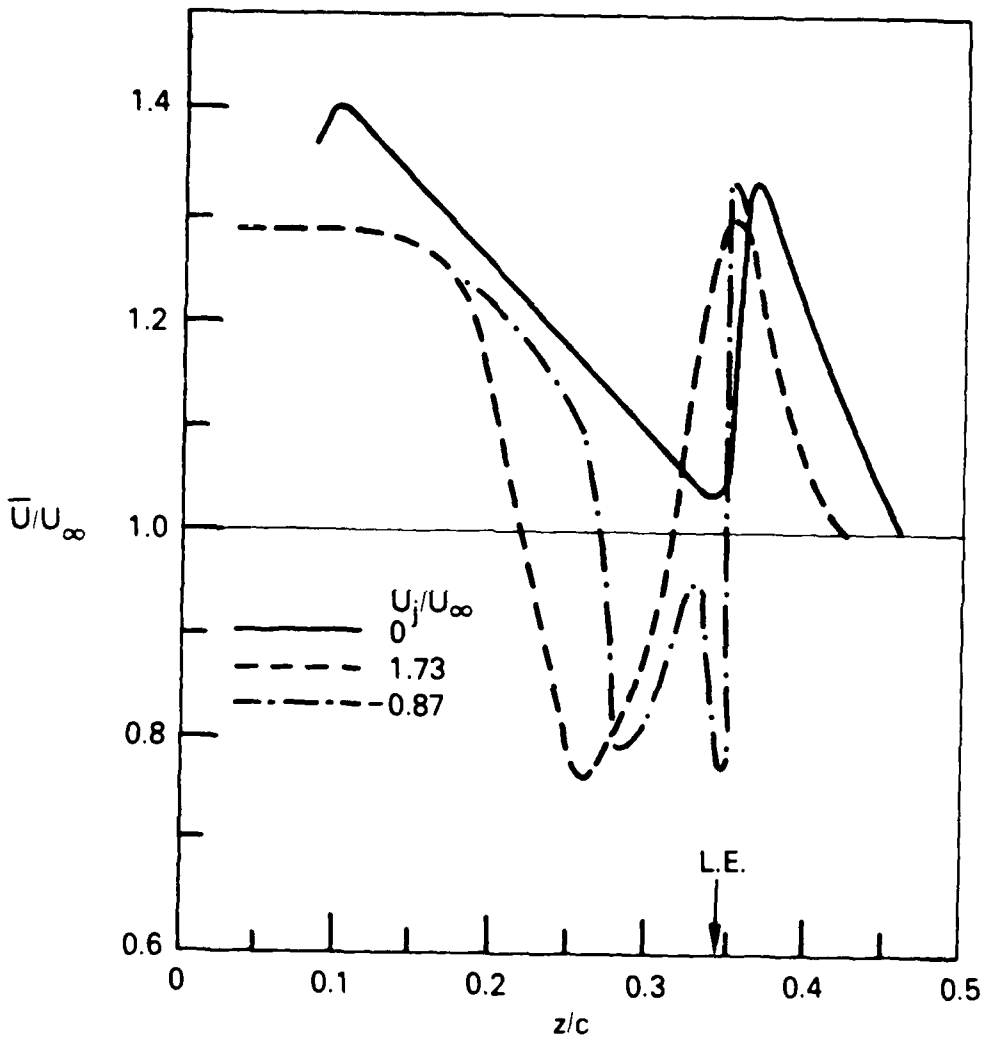

Figure 17. Mean Velocity Profiles. x/c = 0.3; $R_c = 1.3 \times 10^5$; $\alpha = 28°$; y/c = 0.003.

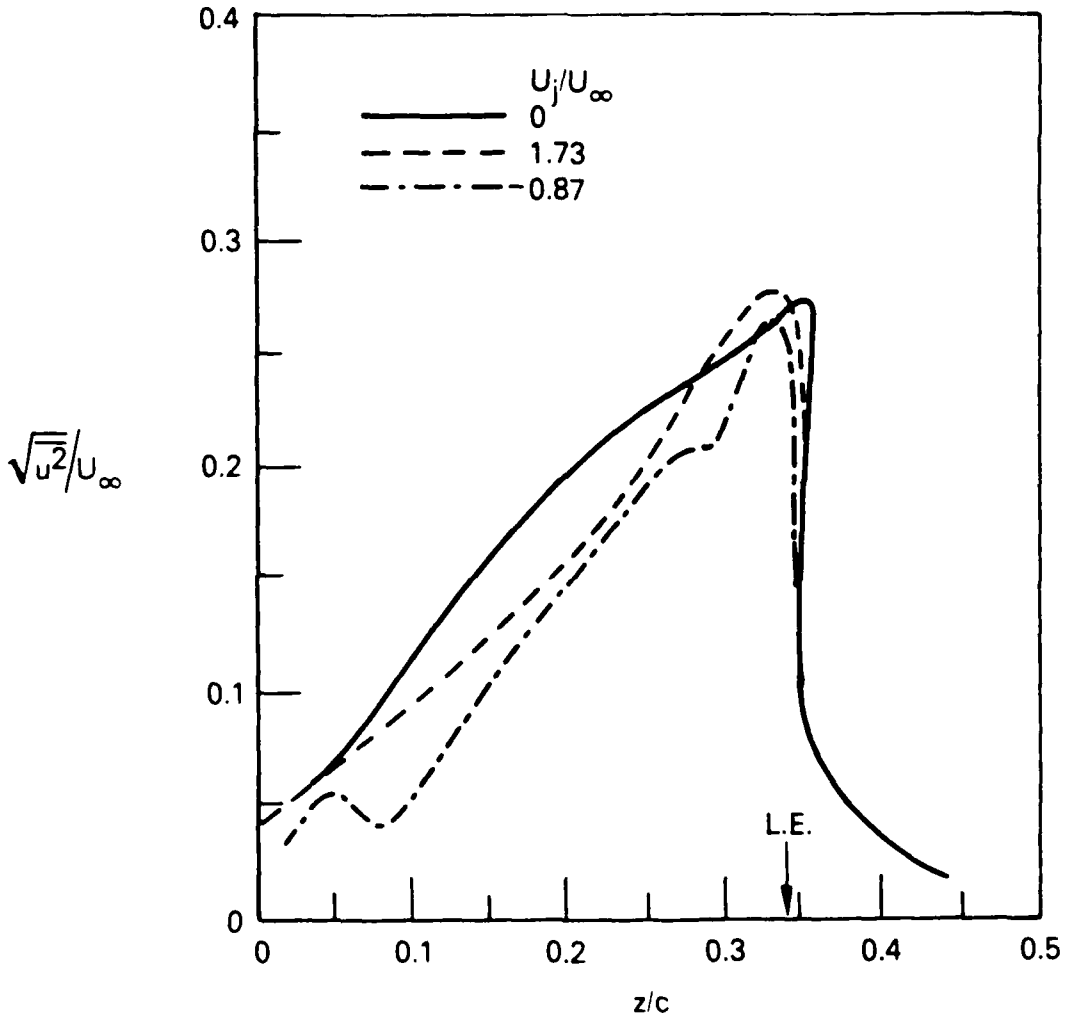

Figure 18. RMS Velocity Fluctuations. x/c = 0.3; $R_c = 1.3 \times 10^5$; $\alpha = 28°$; y/c = 0.003

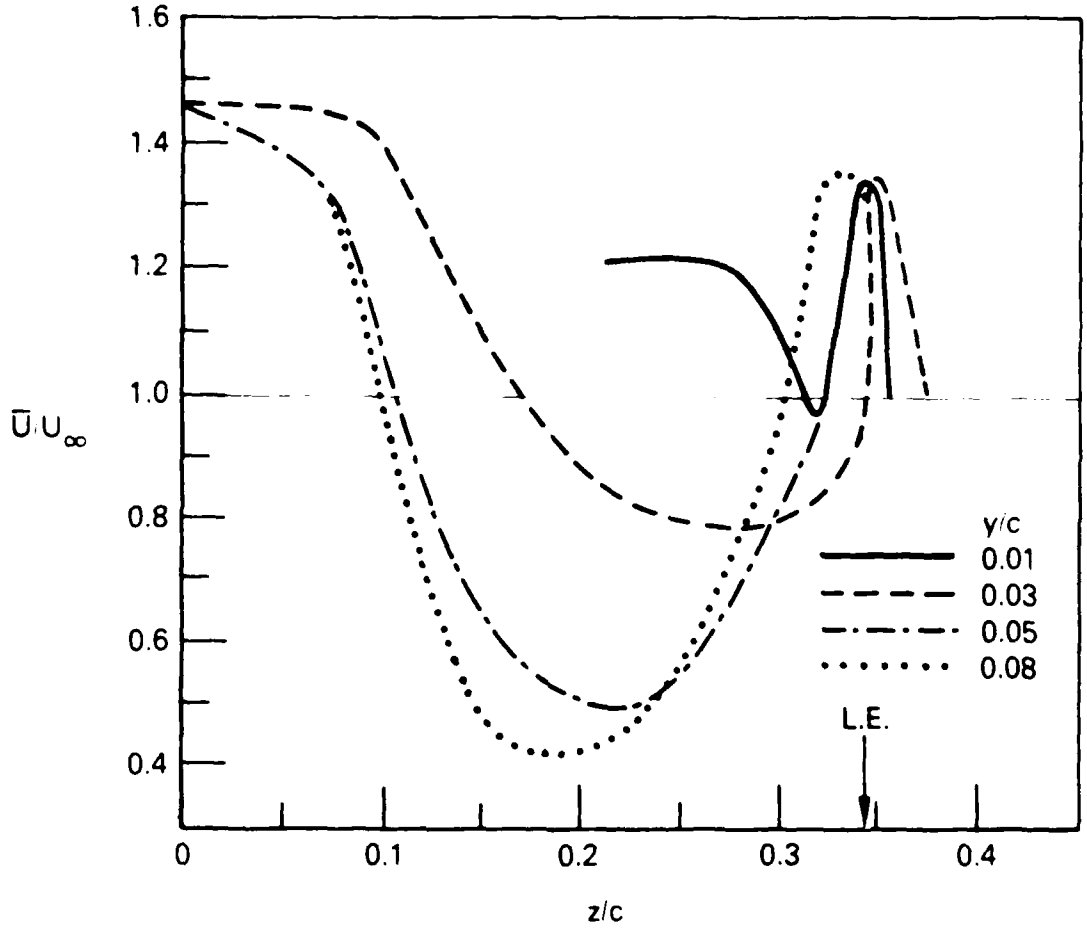

Figure 19. Mean Velocity Profiles. x/c = 0.6; $R_c = 1.3 \times 10^5$; $\alpha = 28°$; $U_j/U_\infty = 1.73$.

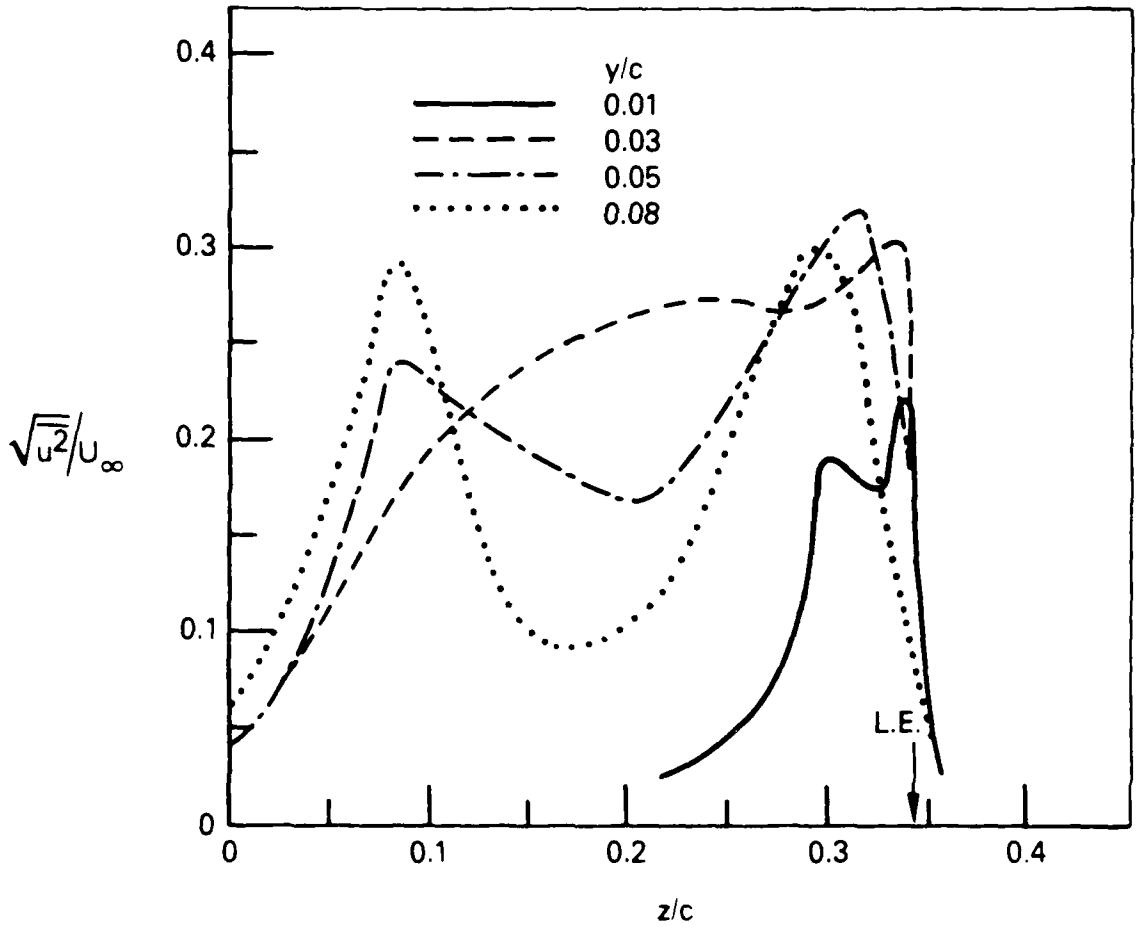

Figure 20. RMS Velocity Fluctuations. x/c = 0.6; $R_c = 1.3 \times 10^5$; $\alpha = 28°$; $U_j/U_\infty = 1.73$.

Simple statistical quantities such as the mean and the root-mean-square are obviously not sufficient to understand the nature of this three-dimensional, unsteady flow field. More complex statistical quantities will be presented in the next two sections.

6. PROBABILITY DISTRIBUTION

A useful statistical quantity that may shed some light on the phenomenon of discrete vortices and the effects of leading edge perturbations on the shear layer is the probability density function of the longitudinal velocity fluctuations (Lumley, 1970), which is a measure of the relative amount of time that U(t) spends at various levels. We start with plots of this function for different spanwise locations near the suction surface of the unperturbed delta wing. Figure 21 depicts the probability density function at x/c = 0.6, y/c = 0.005 for three spanwise positions very near the leading edge: z/c = 0.349, 0.348 and 0.344. The Reynolds number is $R_c = 1.3 \times 10^5$ and the angle of attack is $\alpha = 28°$. In the figure, the ordinate is a normalized histogram slot. Thus, slot 0 is the minimum longitudinal velocity recorded by a hot-wire probe at this location, slot 50 is the mean velocity, and slot 100 is the maximum longitudinal velocity. The abscissa is a normalized probability density function such that the area under the curve is unity. Just outside the leading edge (Figure 21a at z/c = 0.349), the discrete vortices manifest themselves as negative spikes in the instantaneous velocity record and the probability density function is biased towards the low end of the histogram slots (0 to 50). This situation is reversed just inward of the leading edge (z/c = 0.344 in Figure 21c), which indicates higher probability of finding velocities higher than the mean in the instantaneous velocity records.

Similar trends but with a shifted spanwise position of the shear layer are observed at a higher normal position y/c = 0.03, as shown in Figure 22. In here, four spanwise locations are recorded: z/c = 0.346 (leading edge position), 0.345, 0.344 and 0.22. At this higher normal position, low speed fluctuations are more probable even inward of the leading edge (z/c = 0.344 in Figure 22c), and this trend reverses further inward of the leading edge as shown in Figure 22d at z/c = 0.22.

Perturbing the leading edge with subharmonic injection of secondary fluid will shift the shear layer and modulate the pairing process as was indicated in the mean and root-mean-square velocity profiles shown in Section 5. At a fixed position, leading edge perturbations should undoubtly affect the probability density function. This is demonstrated in Figures 23a and 23b for $U_j/U_\infty = 0$ and 1.66, respectively. The Reynolds number was $R_c = 2.6 \times 10^5$ and the angle of attack was $\alpha = 10°$, and the hot wire was located at x/c = 0.3, y/c = 0.01 and z/c = 0.17. The probability density function is wider in the

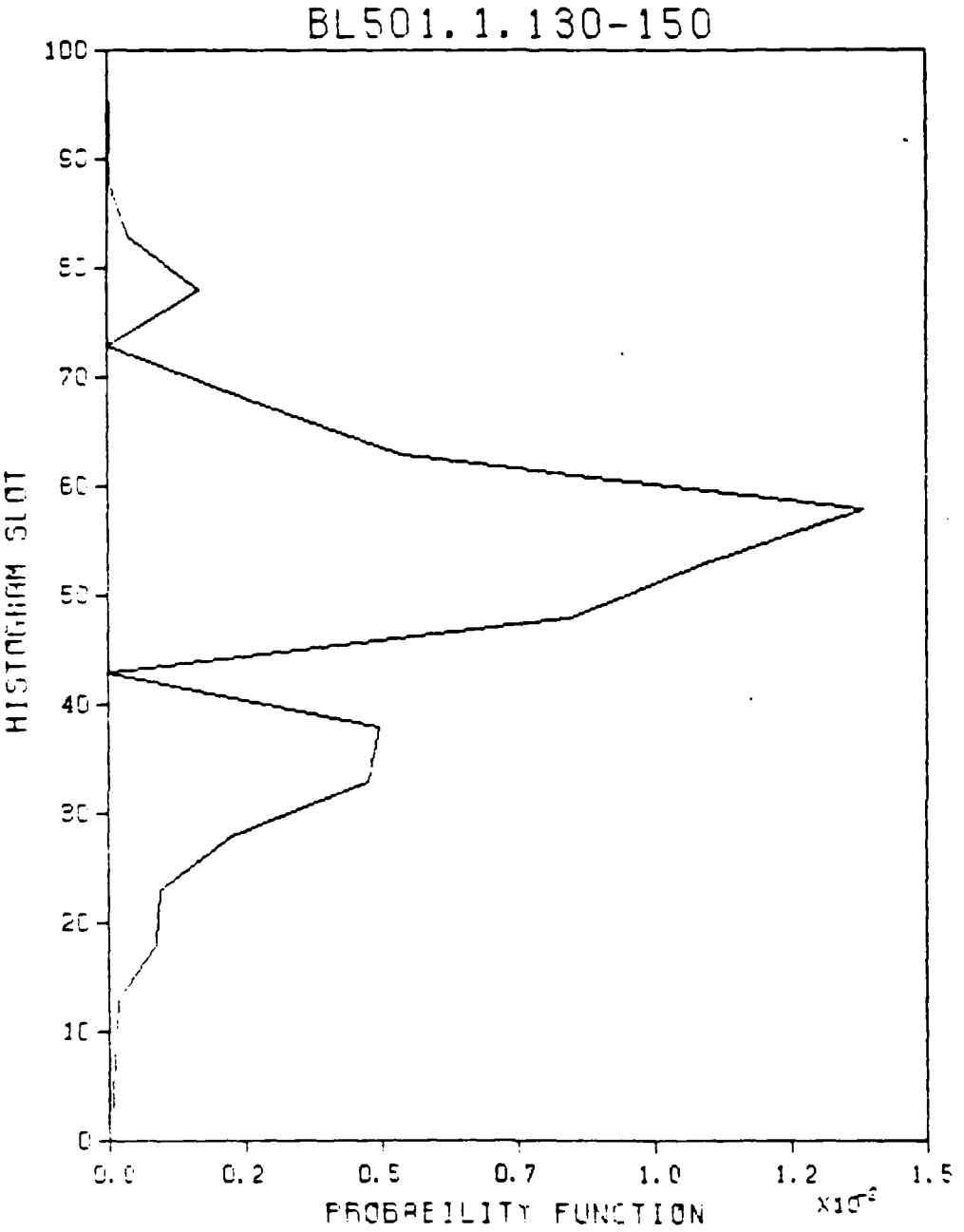

a. z/c = 0.349

Figure 21. Probability Density Function. x/c = 0.6; y/c = 0.005; R_c = 1.3x10^5; α = 28°; U_j/U_∞ = 0

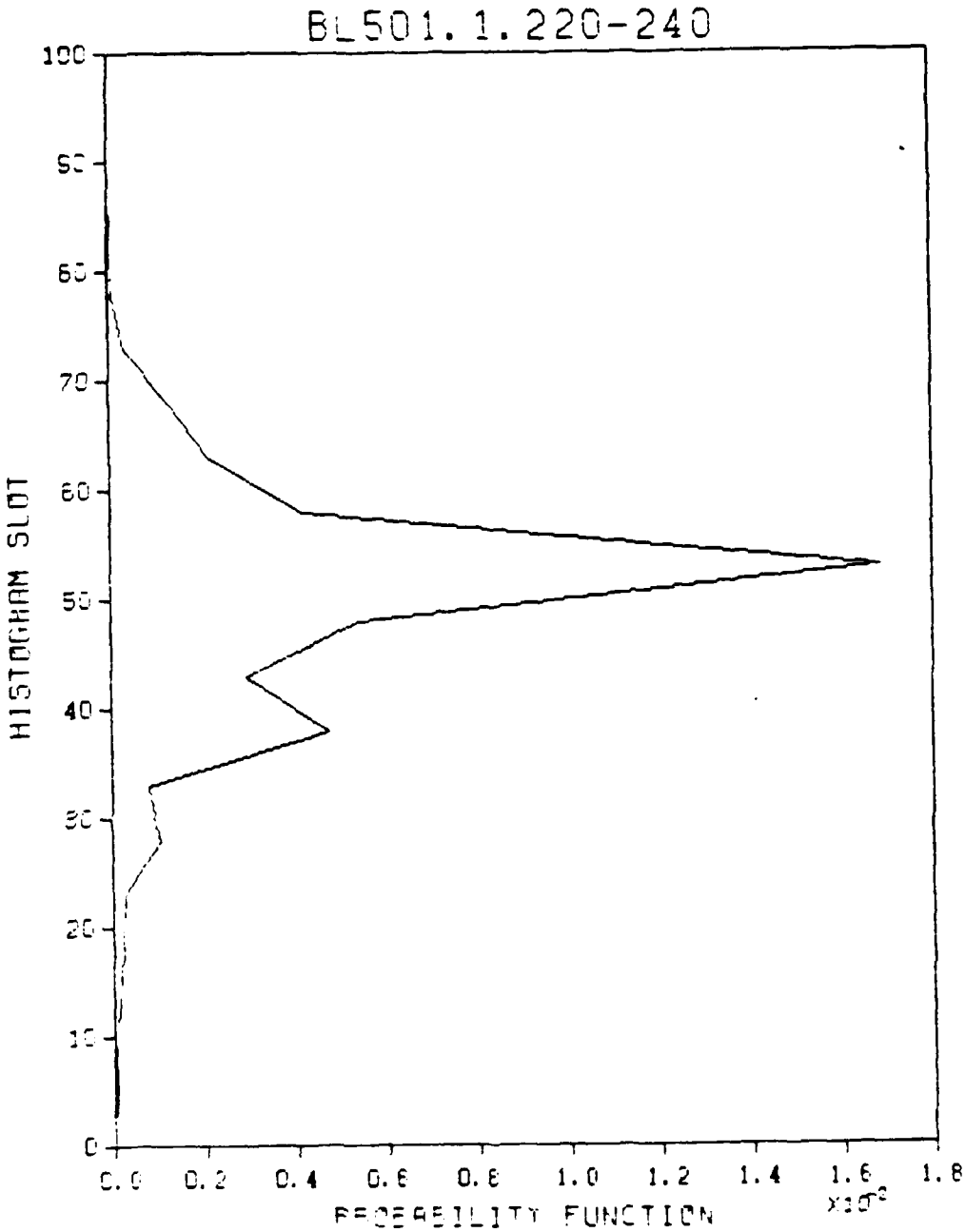

b. z/c = 0.348

Figure 21. (Continued)

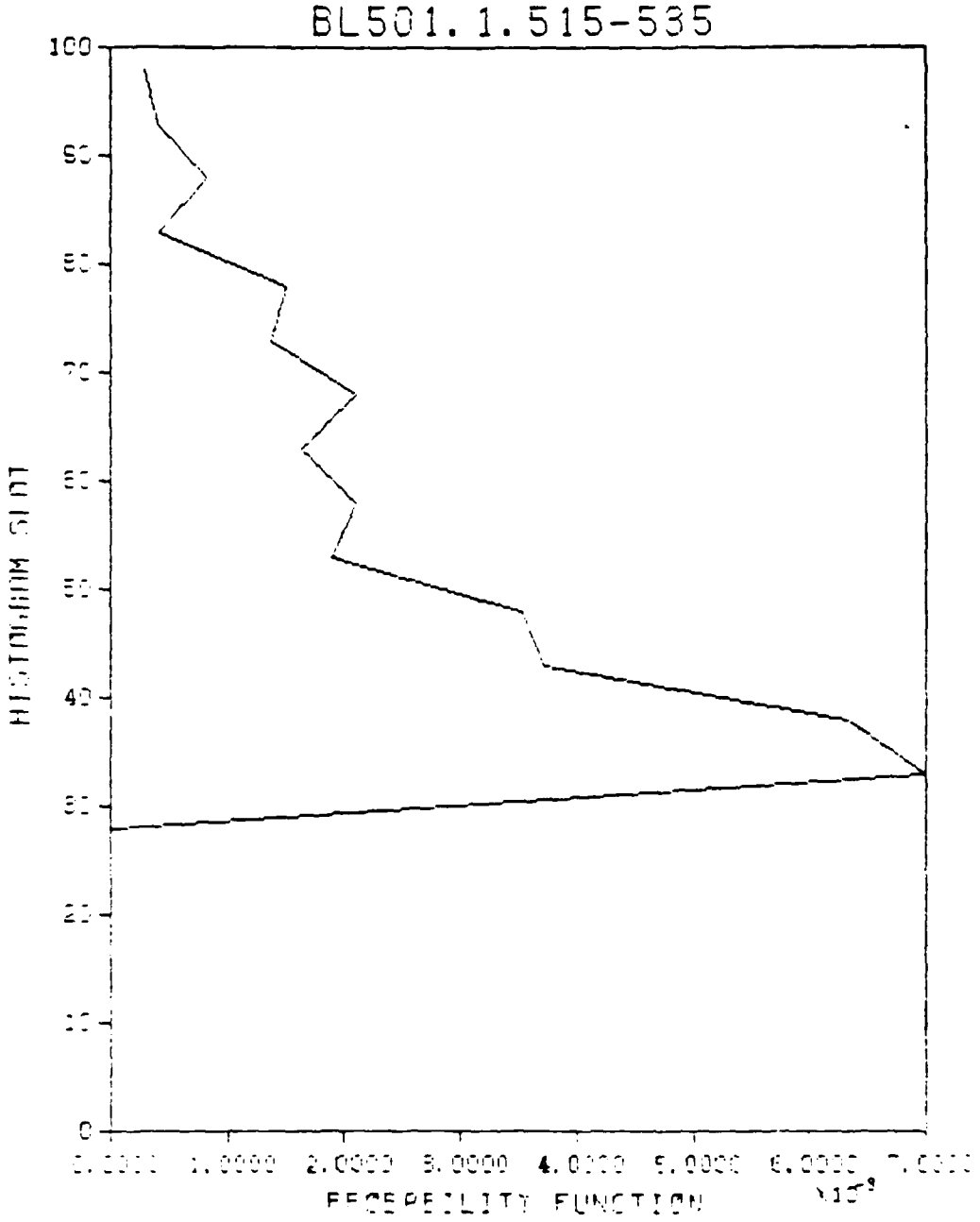

c. z/c = 0.344

Figure 21. (Continued)

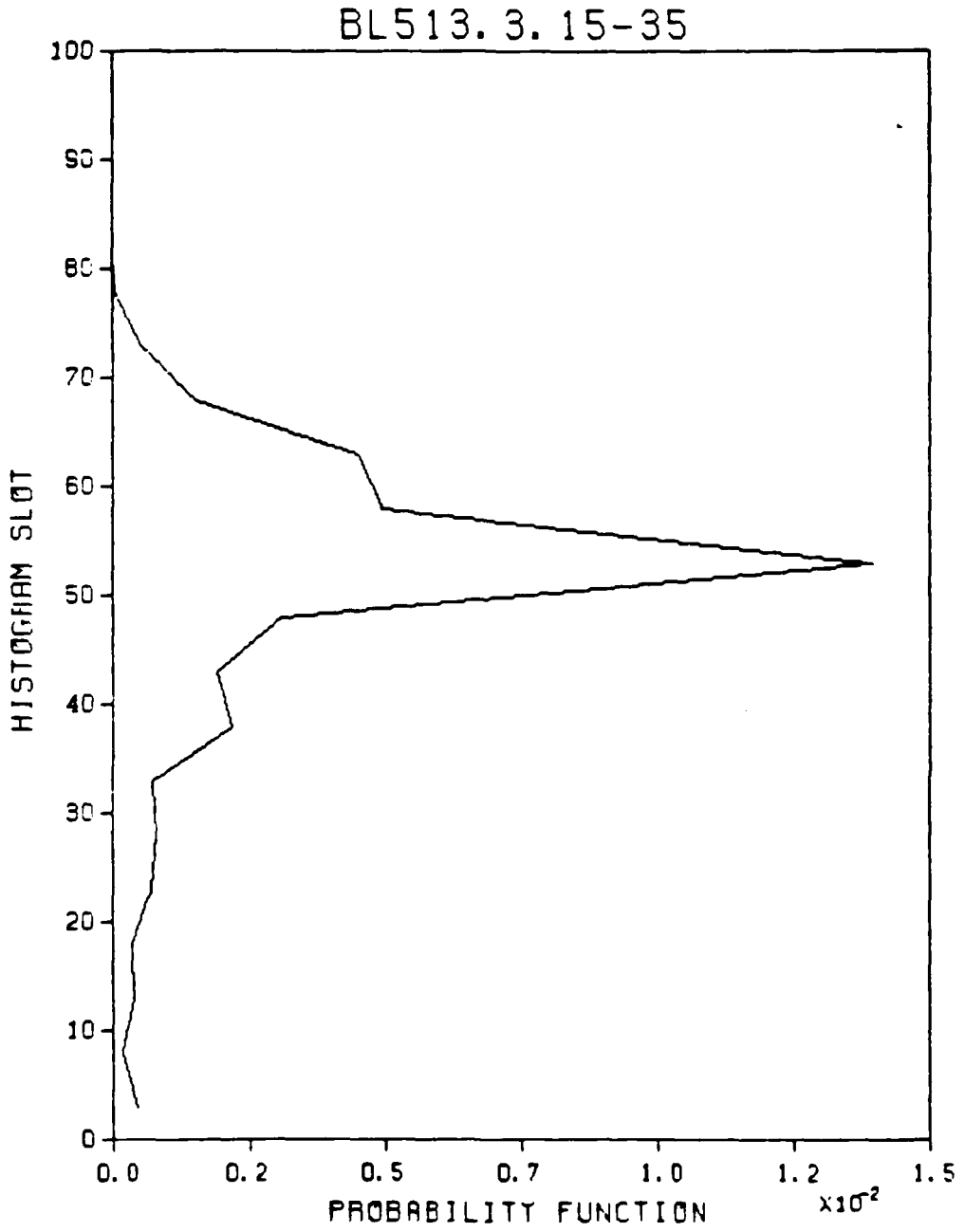

a. z/c = 0.346

Figure 22. Probability Density Function. x/c = 0.6; y/c = 0.03; $R_c = 1.3 \times 10^5$; $\alpha = 28°$; $U_j/U_\infty = 0$

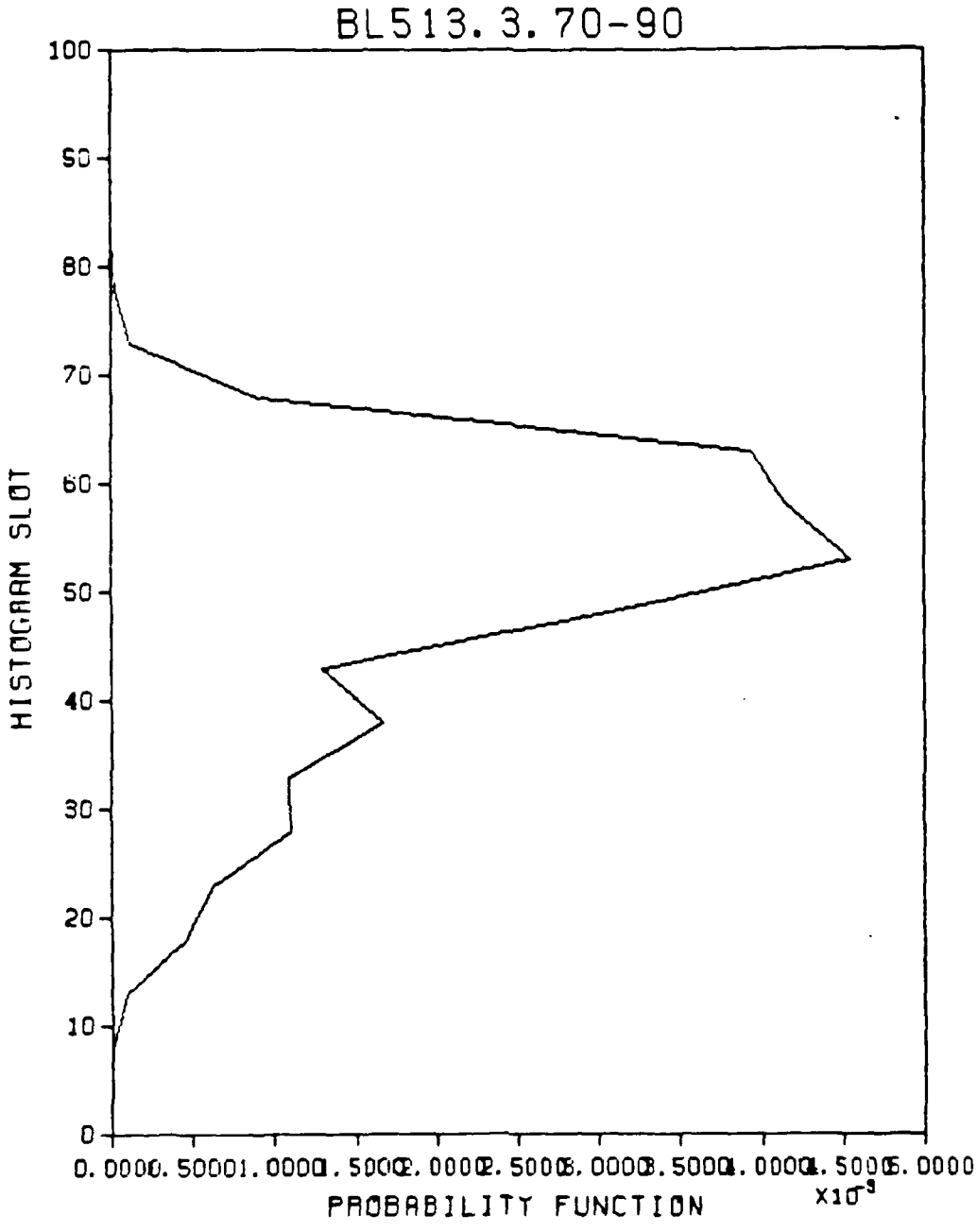

b. z/c = 0.345

Figure 22. (Continued)

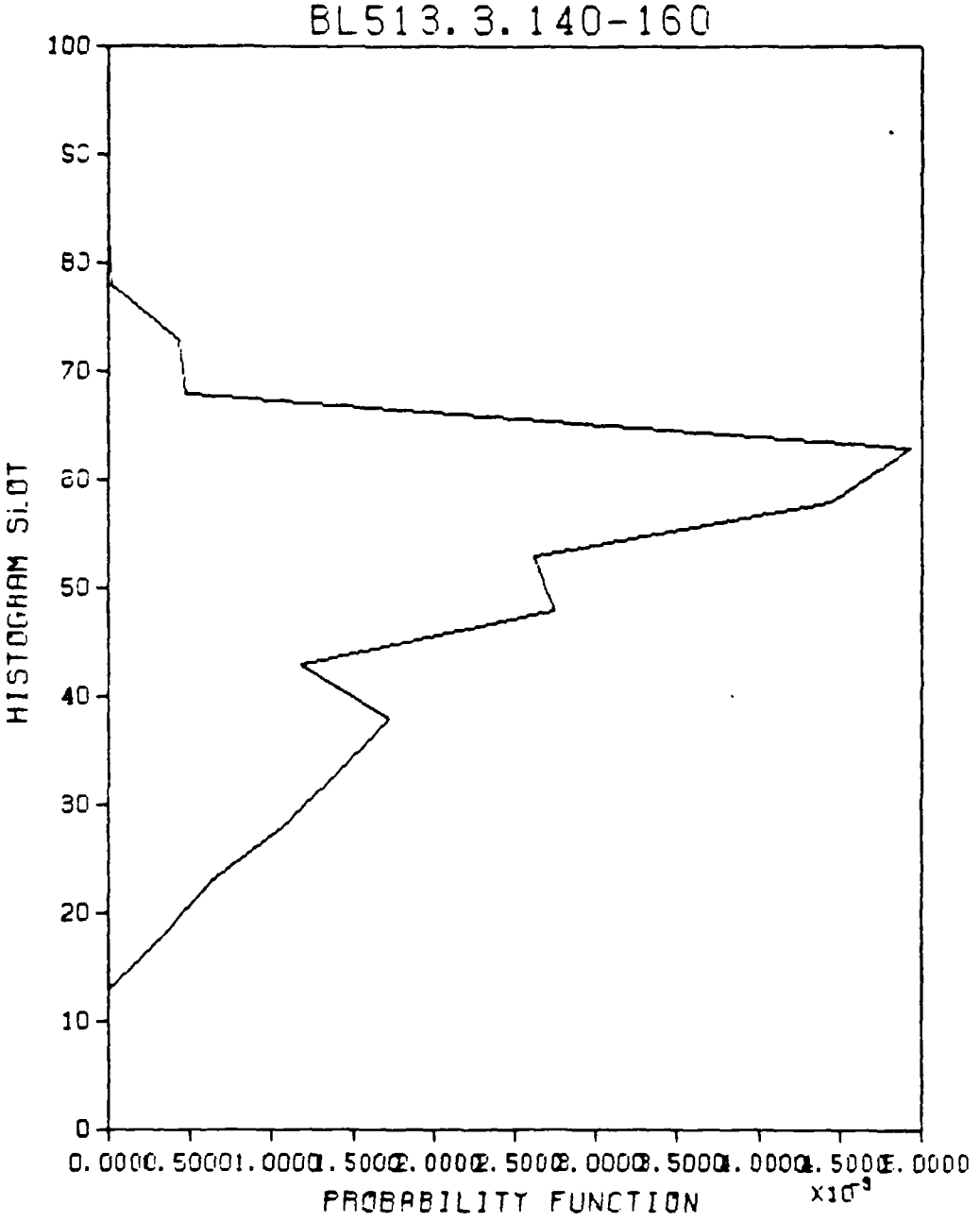

c. z/c = 0.344

Figure 22. (Continued)

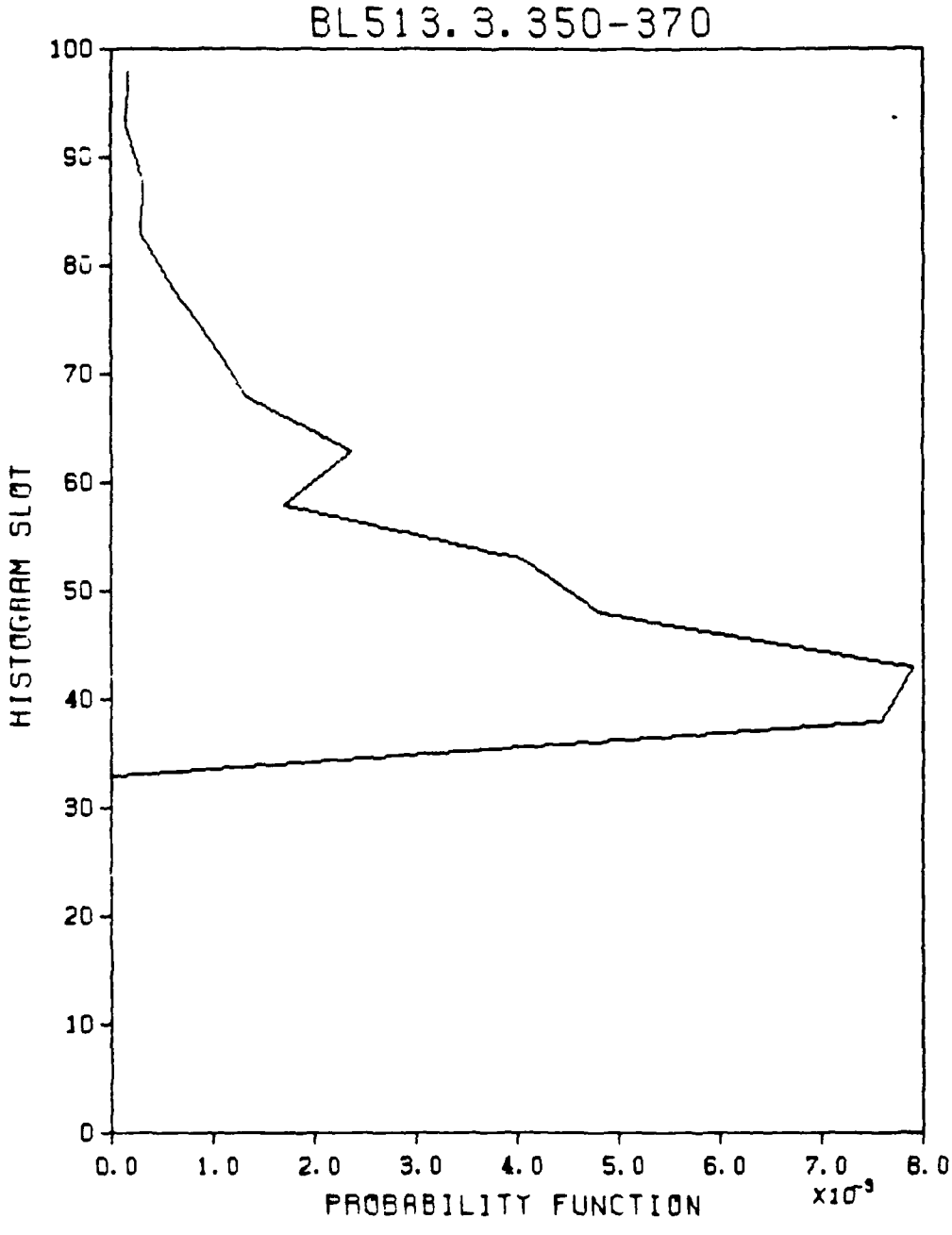

d. z/c = 0.22

Figure 22. (Continued)

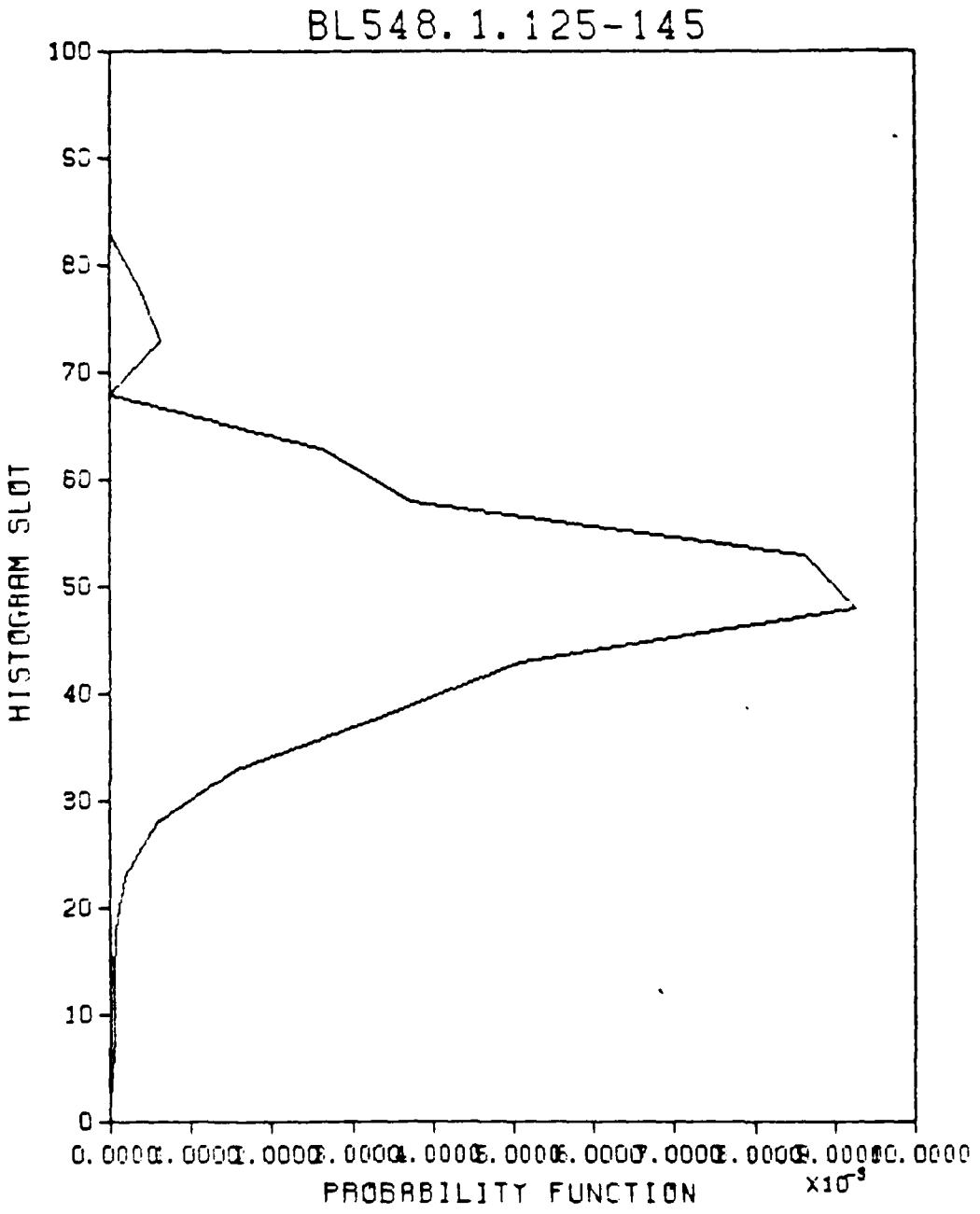

a. $U_j/U_\infty = 0$

Figure 23. Effects of Leading Edge Perturbations on Probability Density Function. x/c = 0.3; y/c = 0.01; $R_c = 2.6 \times 10^5$; $\alpha = 10°$; z/c = 0.17

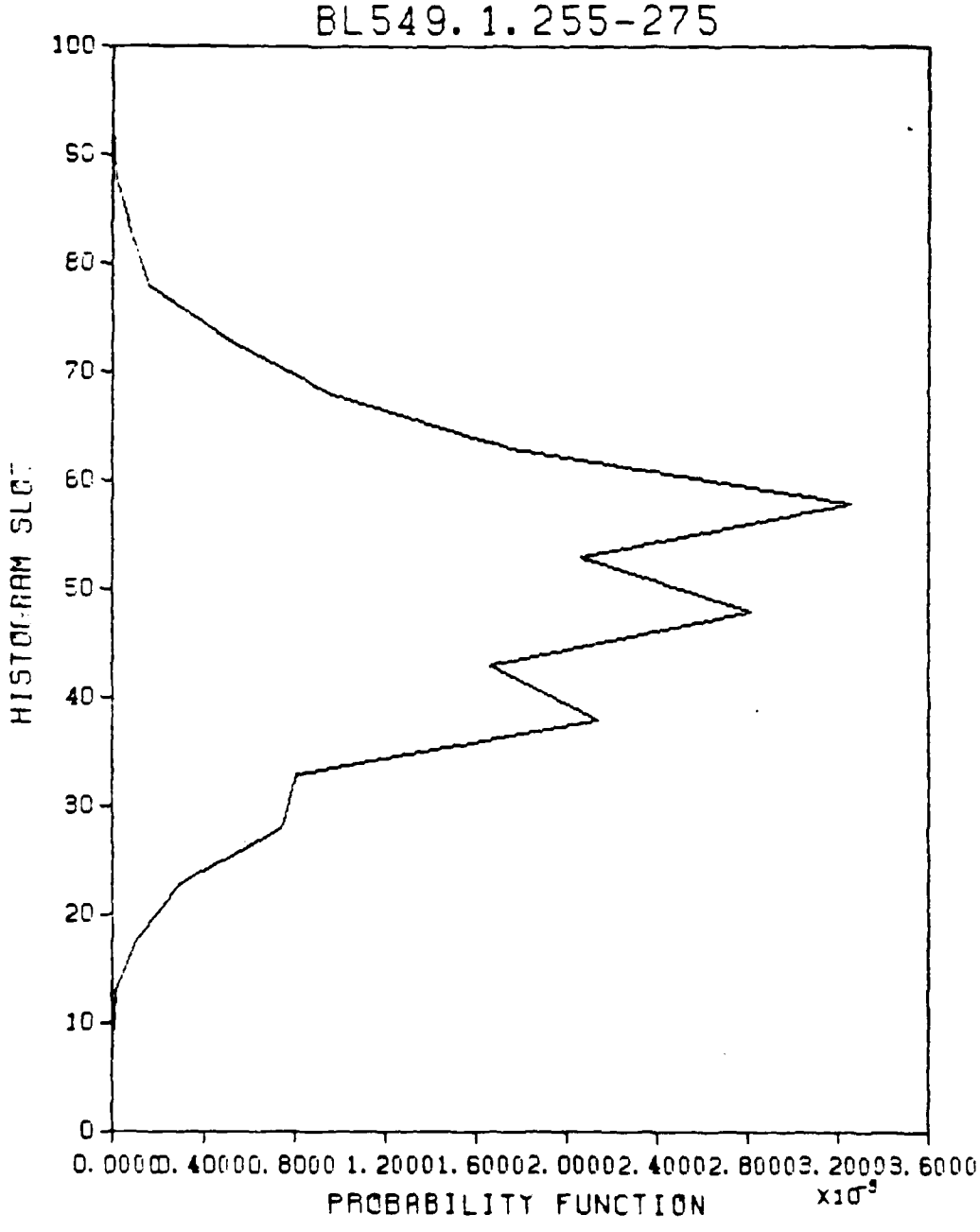

b. $U_j/U_\infty = 1.66$

Figure 23. (Continued)

case of subharmonic leading edge perturbations. The negative spikes are also more intense as indicated by the higher probability in the lower speed regions.

The probability density function in the case of subharmonic suction perturbations is indicated at a different run condition in Figure 24. The maximum suction speed from the leading edge slot was $U_j/U_\infty = -0.87$ and the perturbation frequency was $f = 0.5\ f_o \approx 30$ Hz. Other parameters of this run were $R_c = 1.3 \times 10^5$, $\alpha = 28°$, and the probe position was $x/c = 0.3$, $y/c = 0.27$ and $z/c = 0.17$. At this position the probability density function is quite narrow but is still biased towards the low velocity fluctuations.

More spanwise variations of the probability density function is shown in Figures 25, 26 and 27, at three different heights above the suction surface of the delta wing: $y/c = 0.01$, 0.05 and 0.08, respectively. In all three figures the Reynolds number was $R_c = 1.3 \times 10^5$, the angle of attack was $\alpha = 28°$, and the leading edge was perturbed with a subharmonic perturbation having a maximum injection speed of $U_j = 1.73\ U_\infty$. The hot wire probe was always at a fixed downstream distance of $x = 0.6$ c. Again, useful insight into the behavior of the leading edge vortices and the accompanying shear layer could be derived from observing the changes in the probability density function with height and spanwise location.

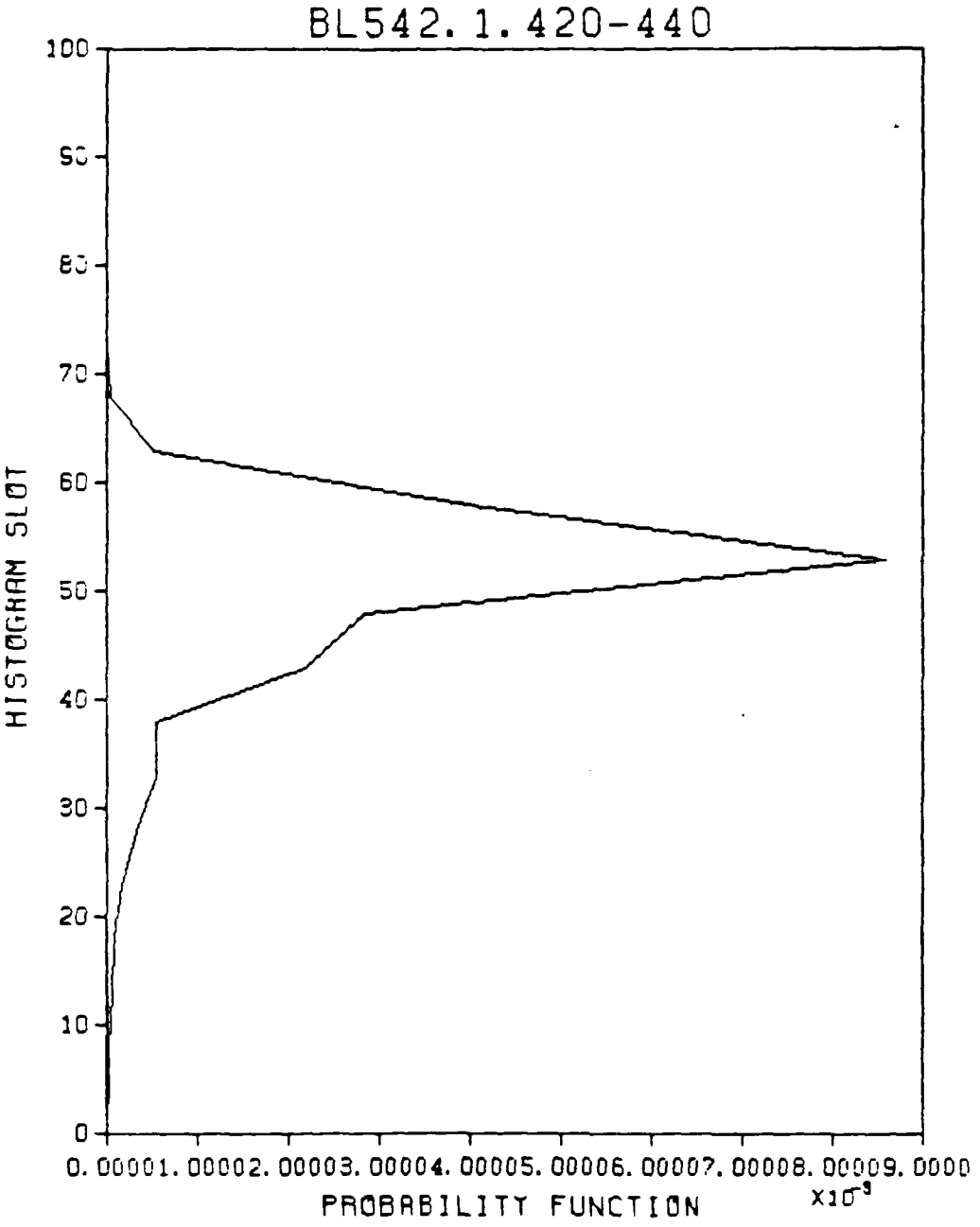

Figure 24. **Probability Density Function with Subharmonic Suction Perturbations.** $x/c = 0.3$; $y/c = 0.27$; $R_c = 1.3 \times 10^5$; $\alpha = 28°$; $z/c = 0.17$; $U_j/U_\infty = -0.87$

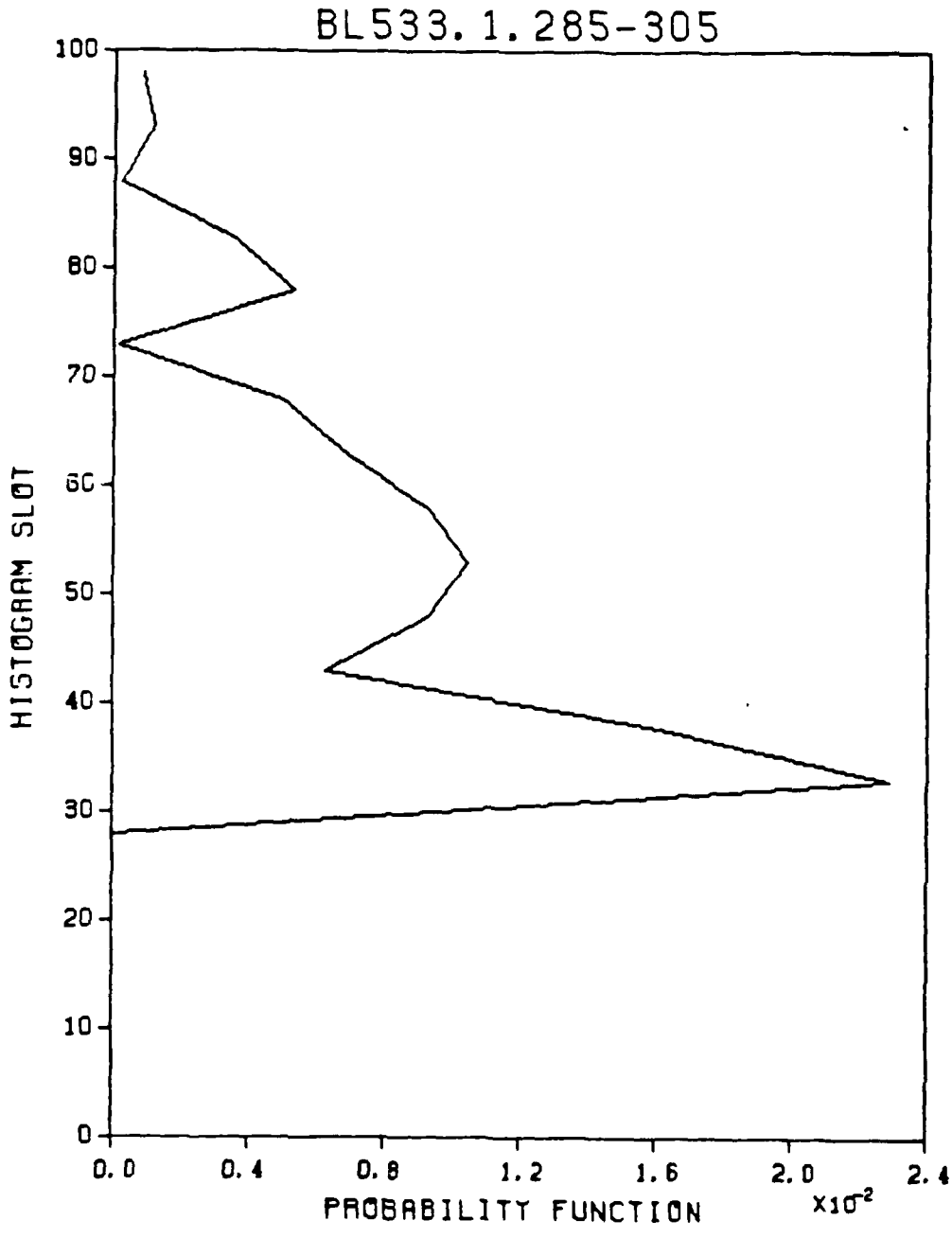

a. z/c = 0.345

Figure 25. Spanwise Changes of Probability Density Function. x/c = 0.6; y/c = 0.01; $R_c = 1.3 \times 10^5$; $\alpha = 28°$; $U_j/U_\infty = 1.73$

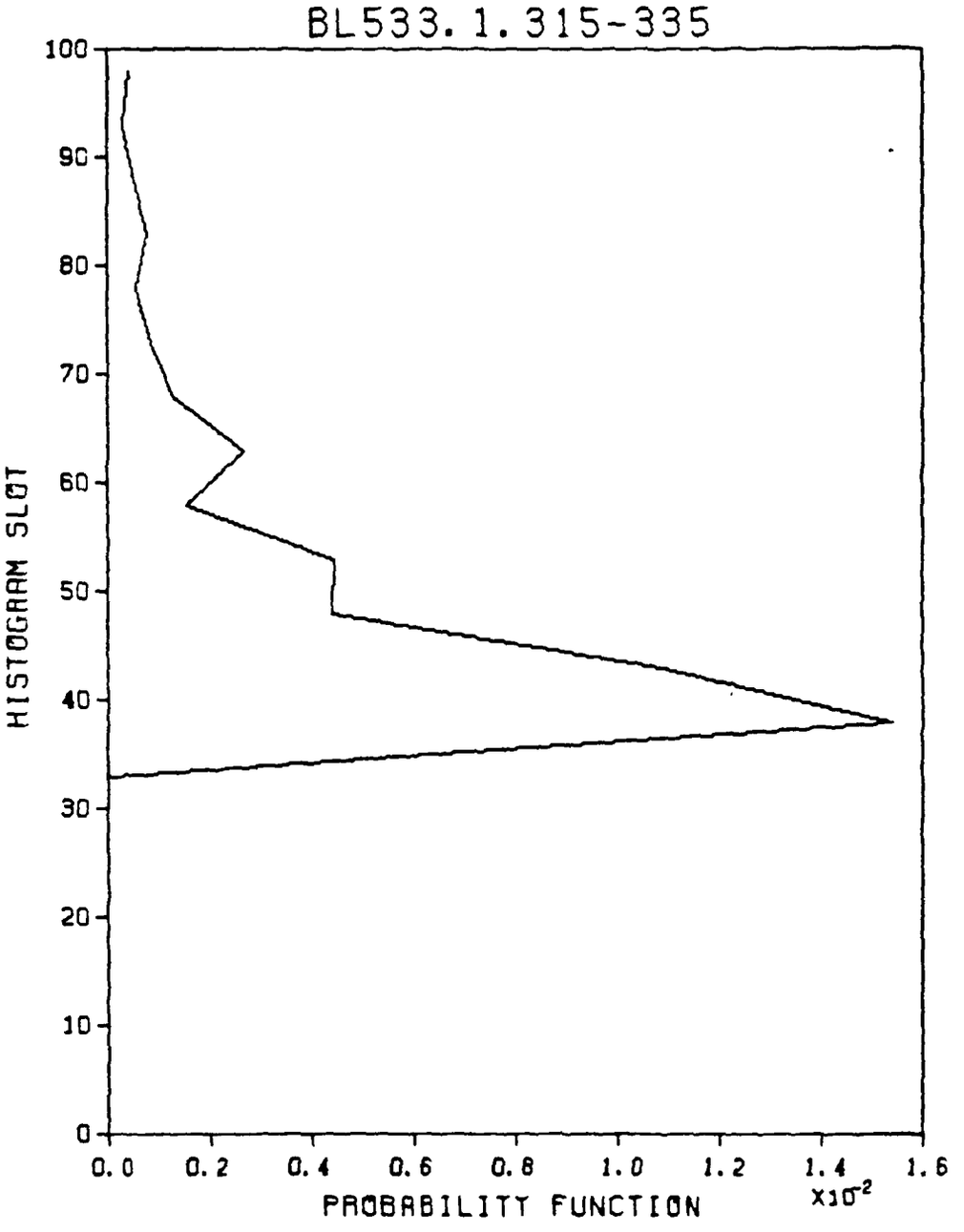

b. $z/c = 0.344$

Figure 25. (Continued)

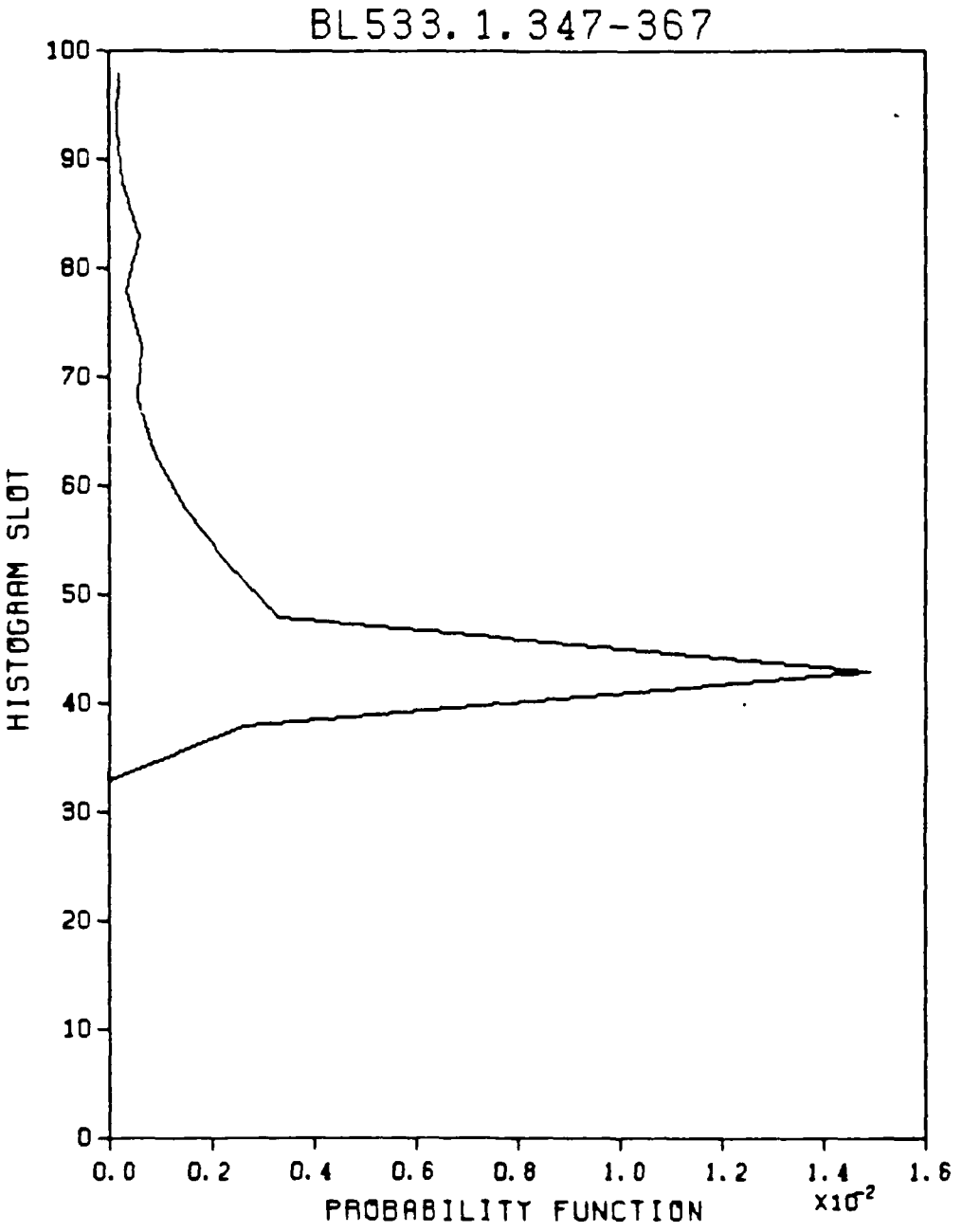

c. z/c = 0.341

Figure 25. (Continued)

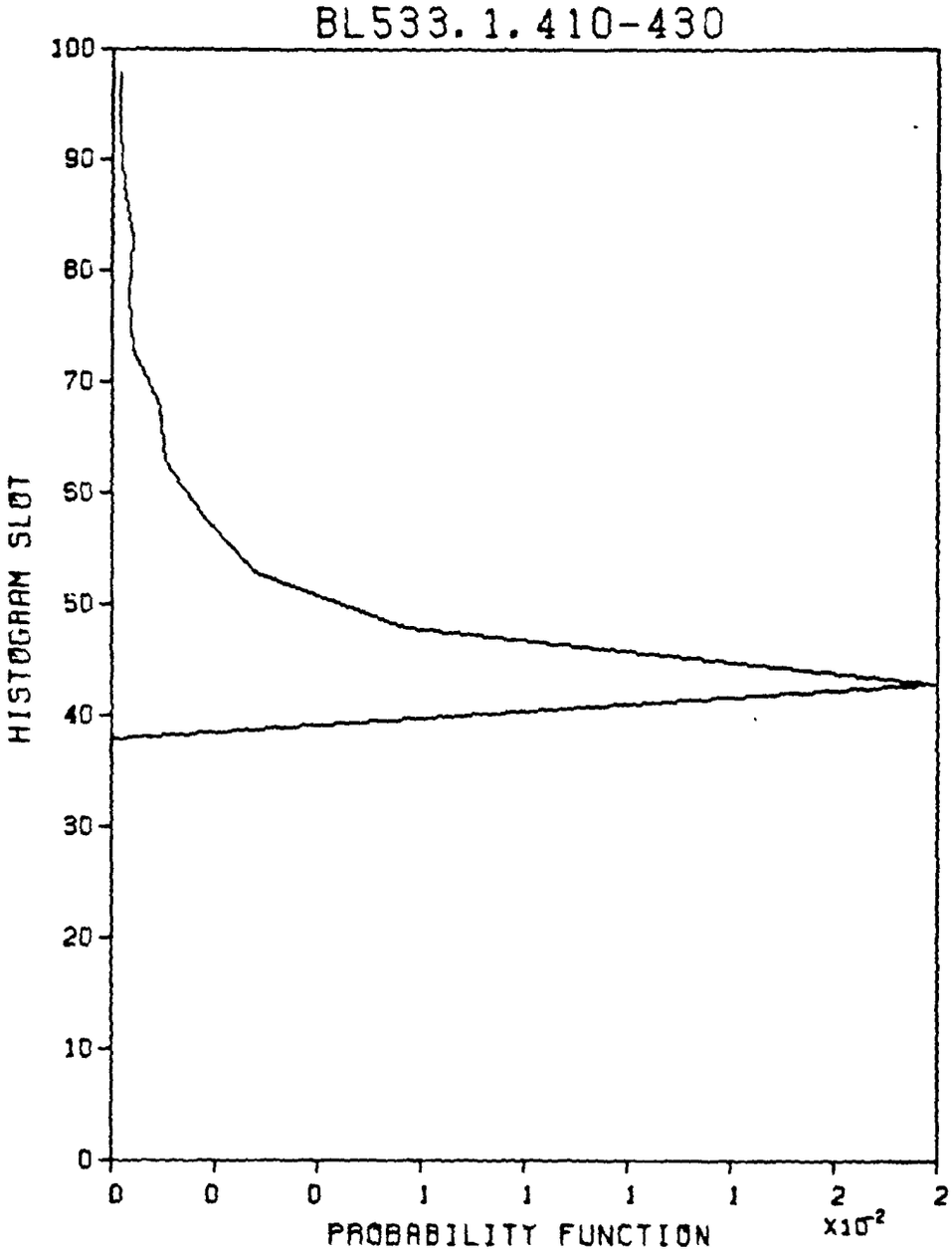

d. z/c = 0.336

Figure 25. (Continued)

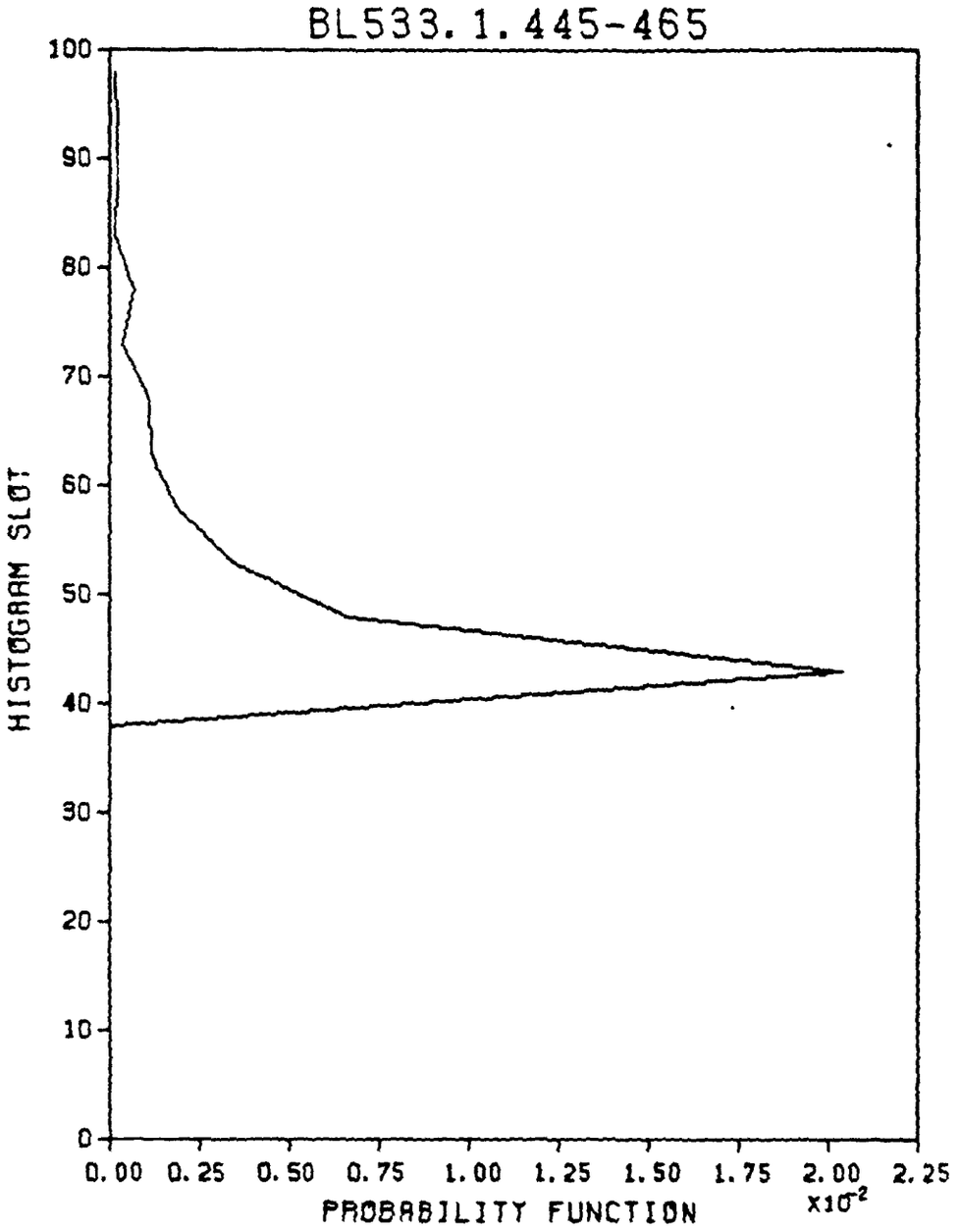

e. z/c = 0.326

Figure 25. (Continued)

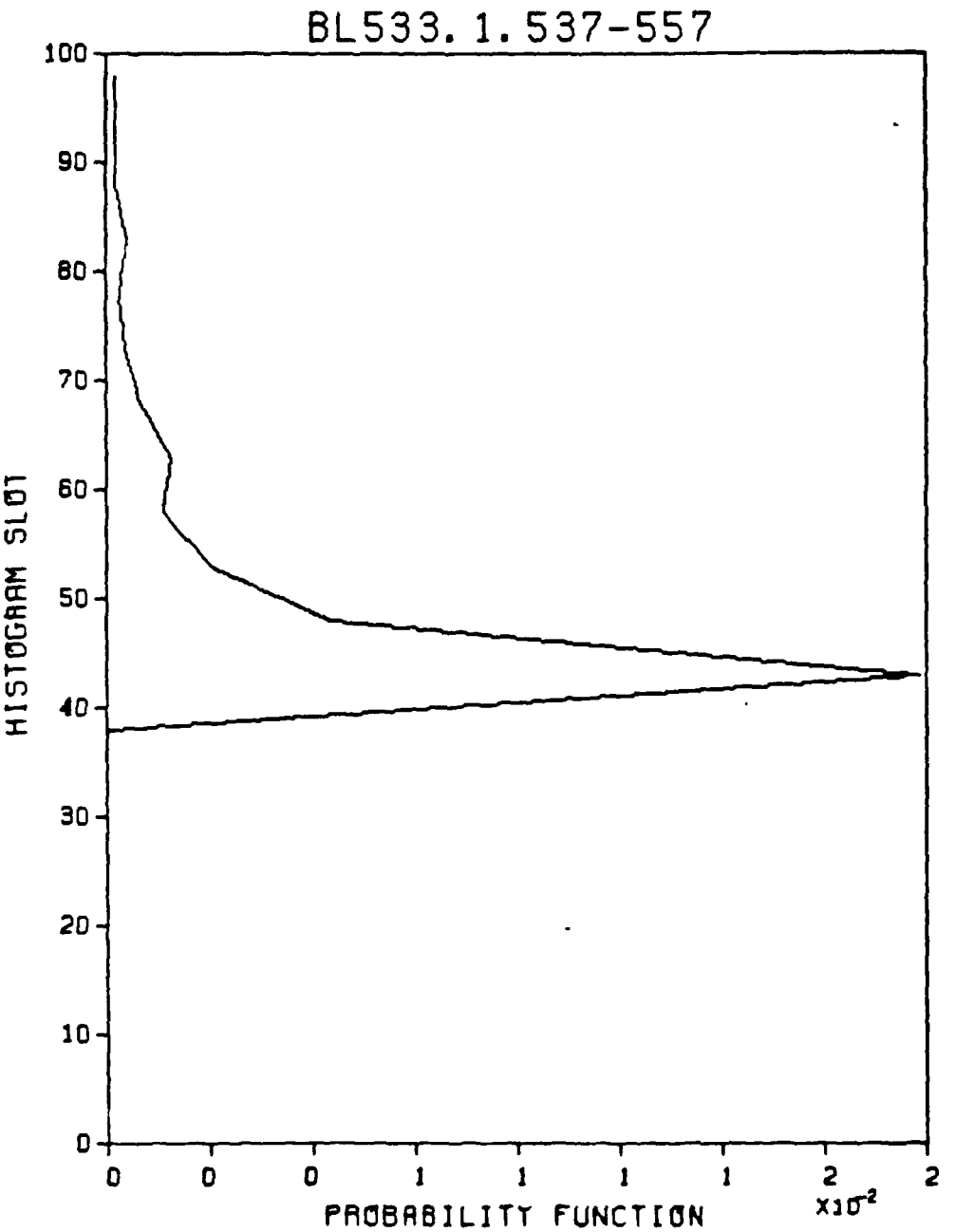

f. *z/c = 0.296*

Figure 25. (Continued)

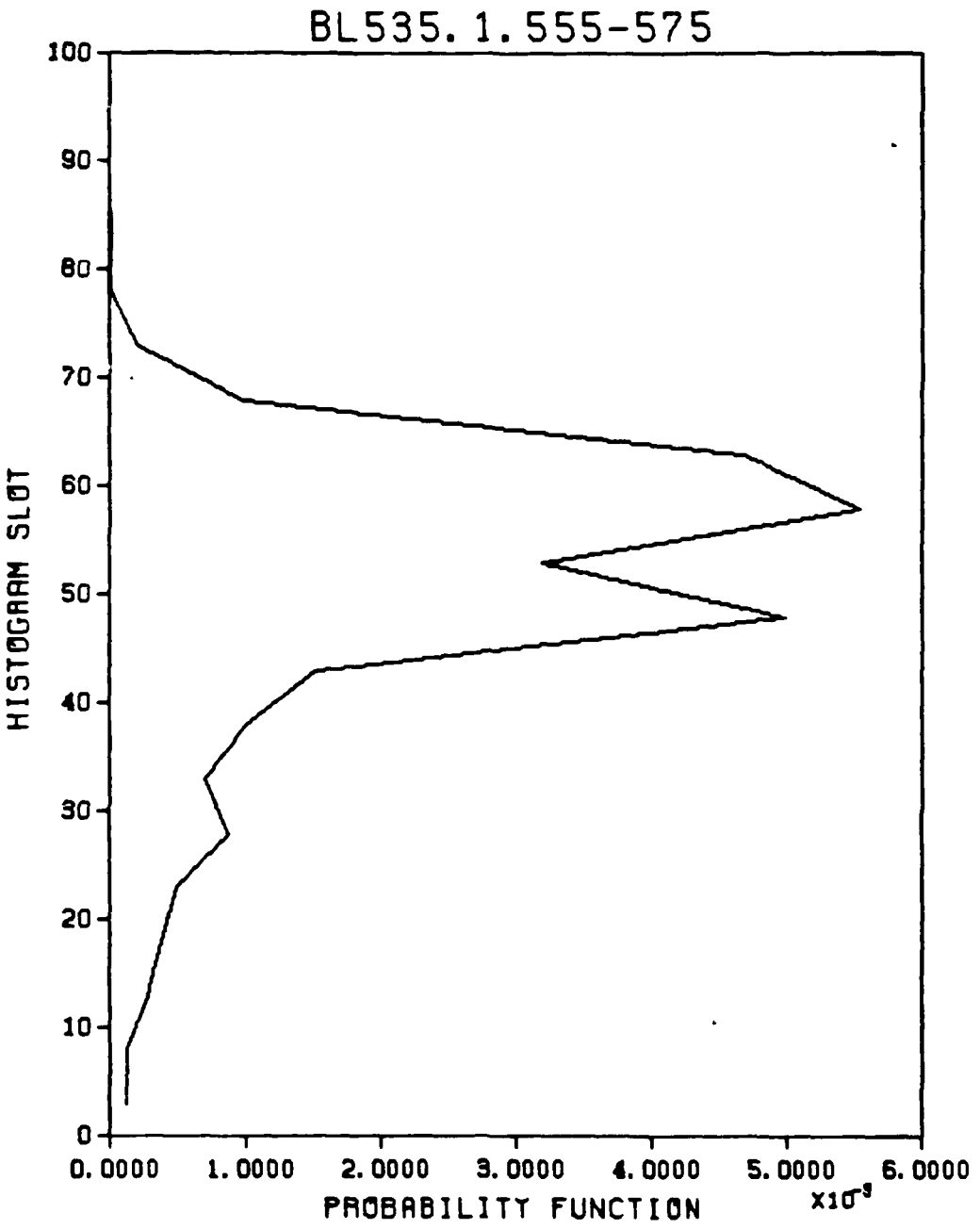

a. z/c = 0.339

Figure 26. Spanwise Changes of Probability Density Function. x/c = 0.6; y/c = 0.05; $R_c = 1.3 \times 10^5$; $\alpha = 28°$; $U_j/U_\infty = 1.73$

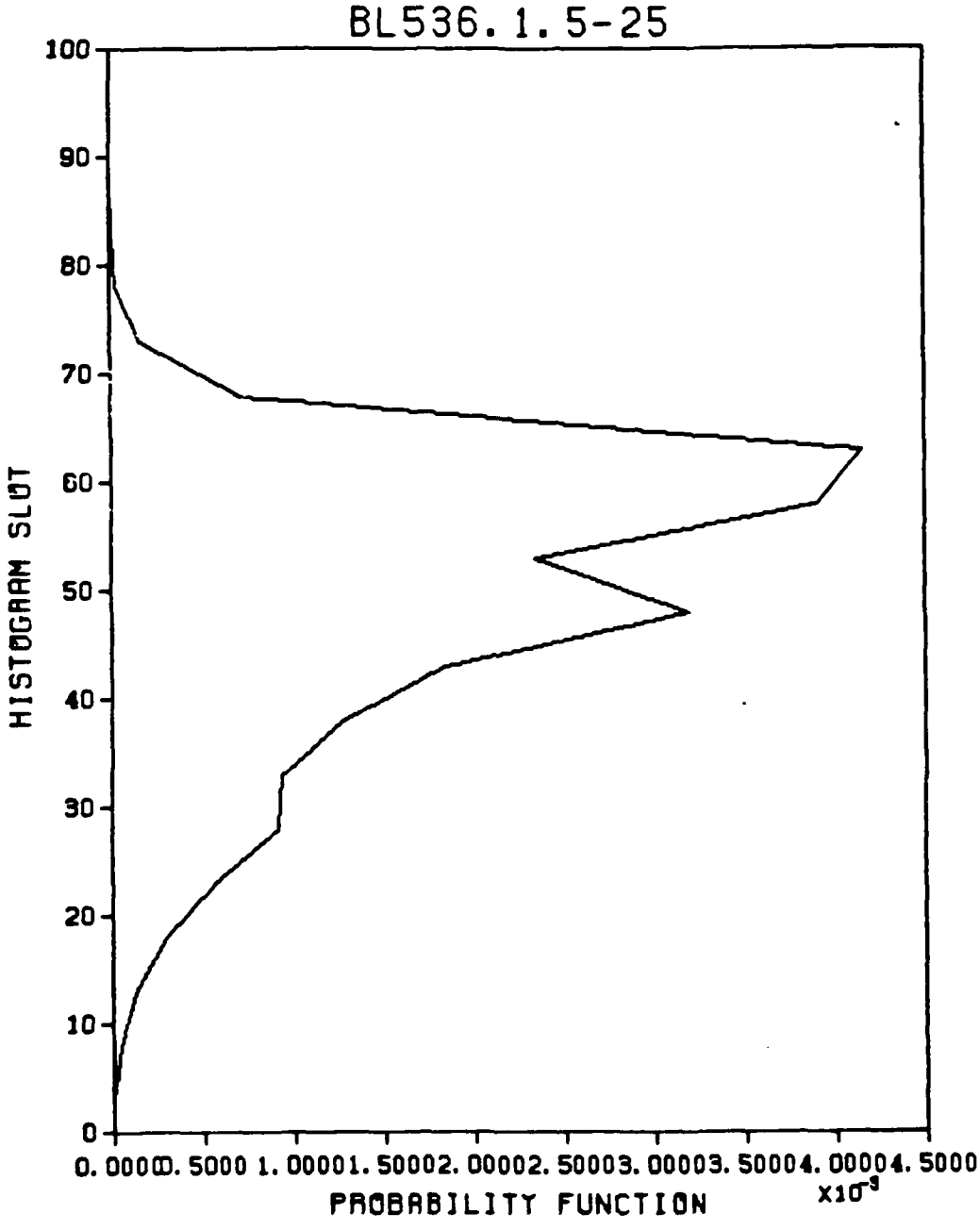

b. z/c = 0.336

Figure 26. (Continued)

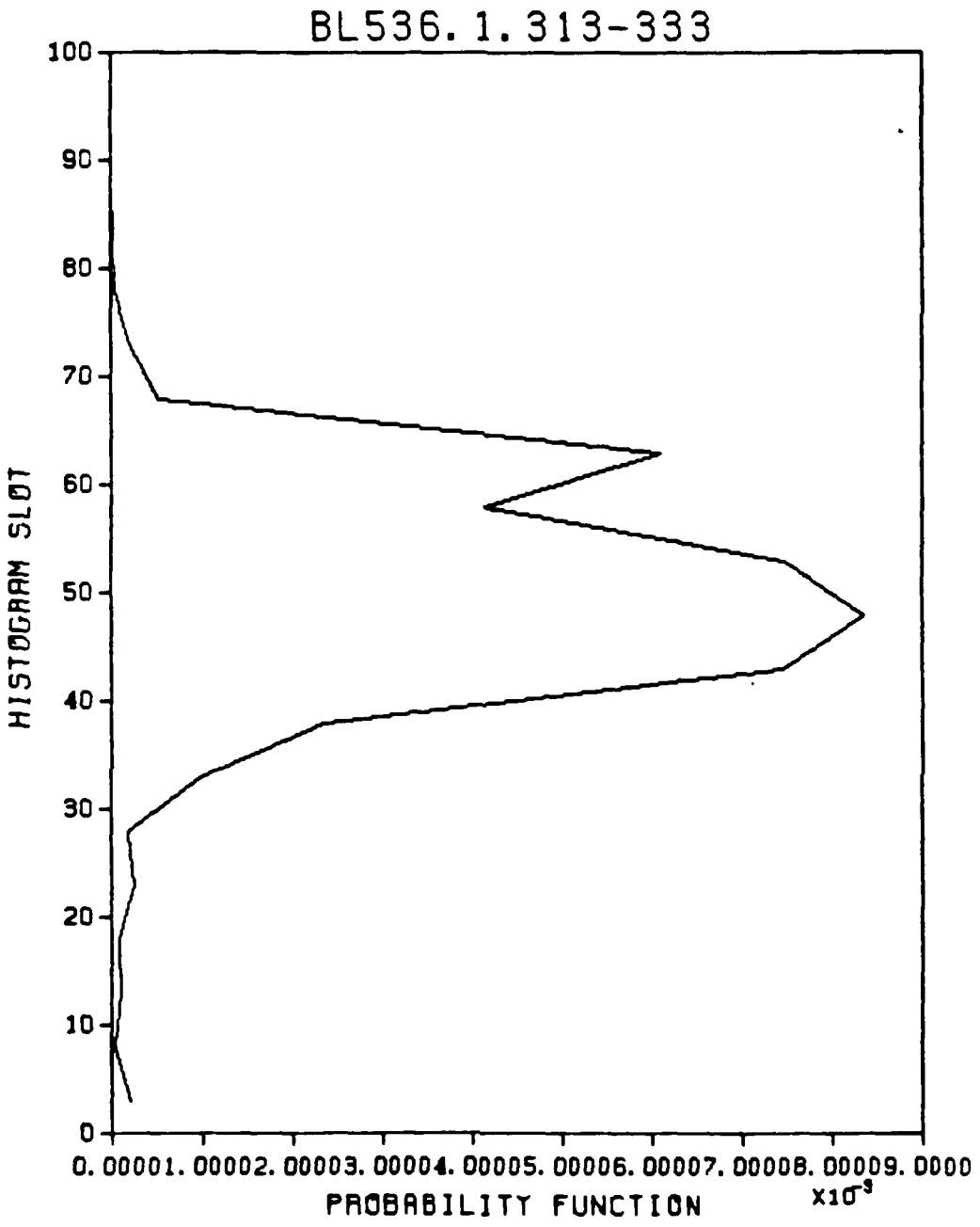

a. z/c = 0.334

Figure 27. Spanwises Changes of Probability Density Function. x/c = 0.6; y/c = 0.08; $R_c = 1.3 \times 10^5$; $\alpha = 28°$; $U_j/U_\infty = 1.73$

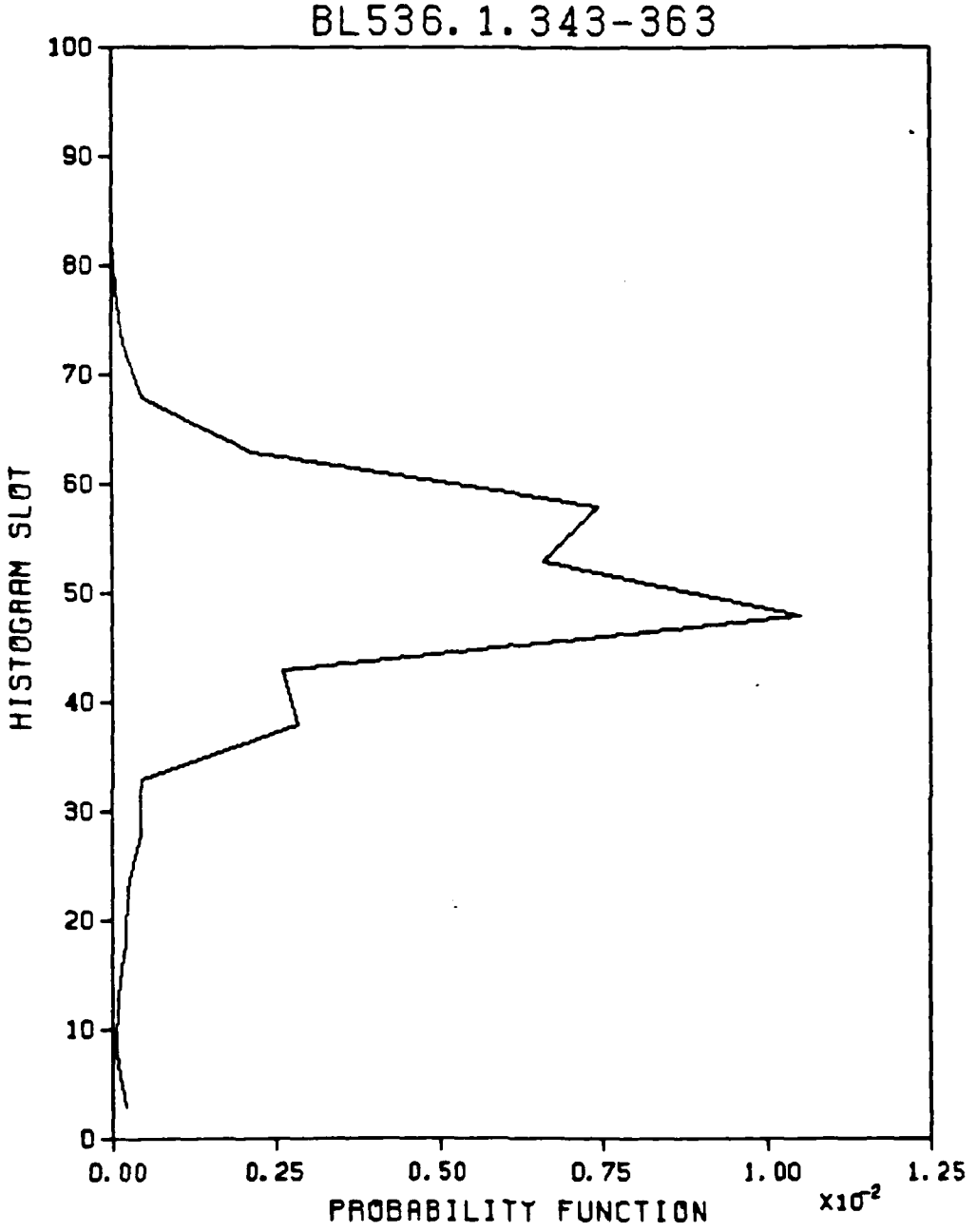

b. z/c = 0.331

Figure 27. (Continued)

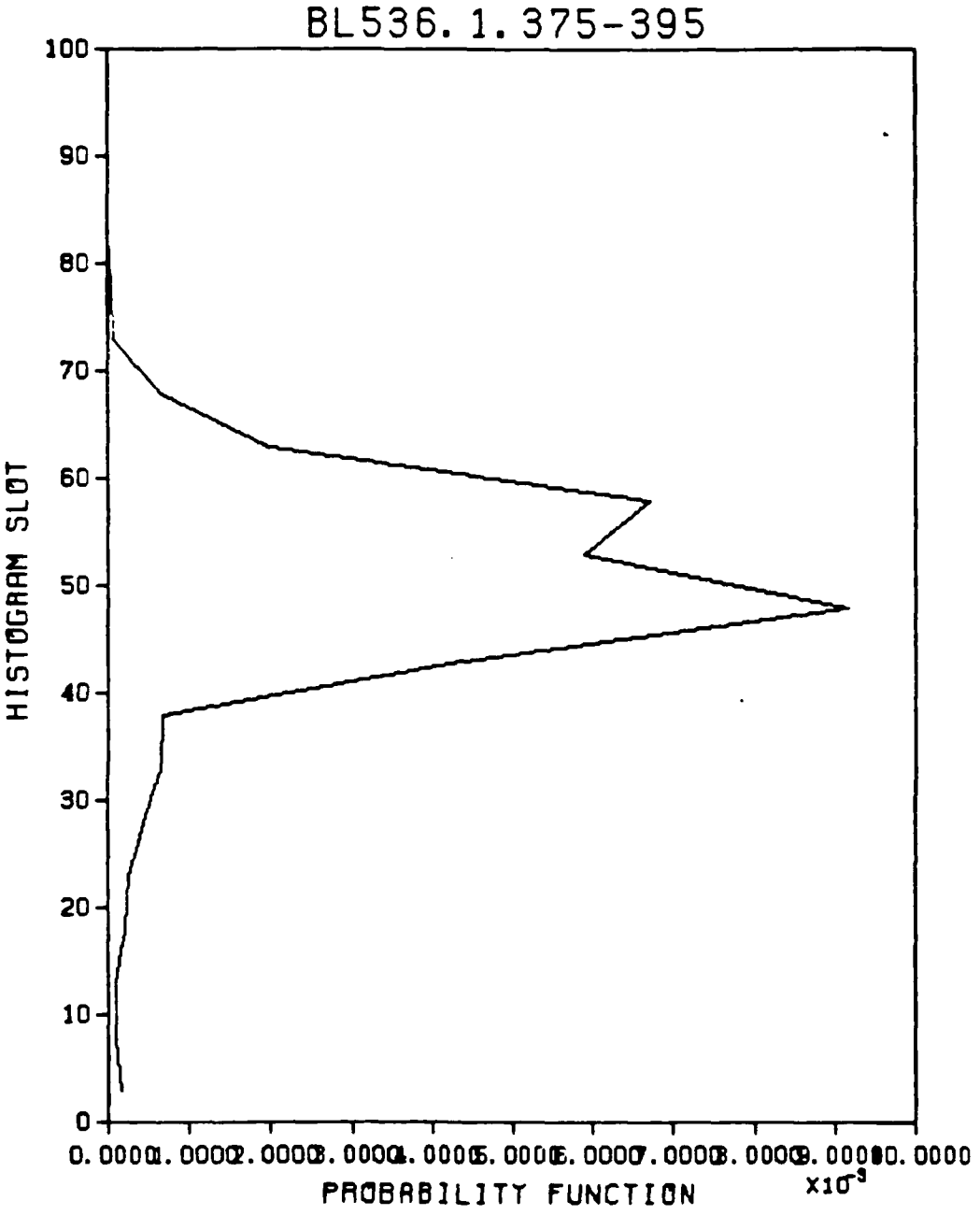

c. z/c = 0.329

Figure 27. (Continued)

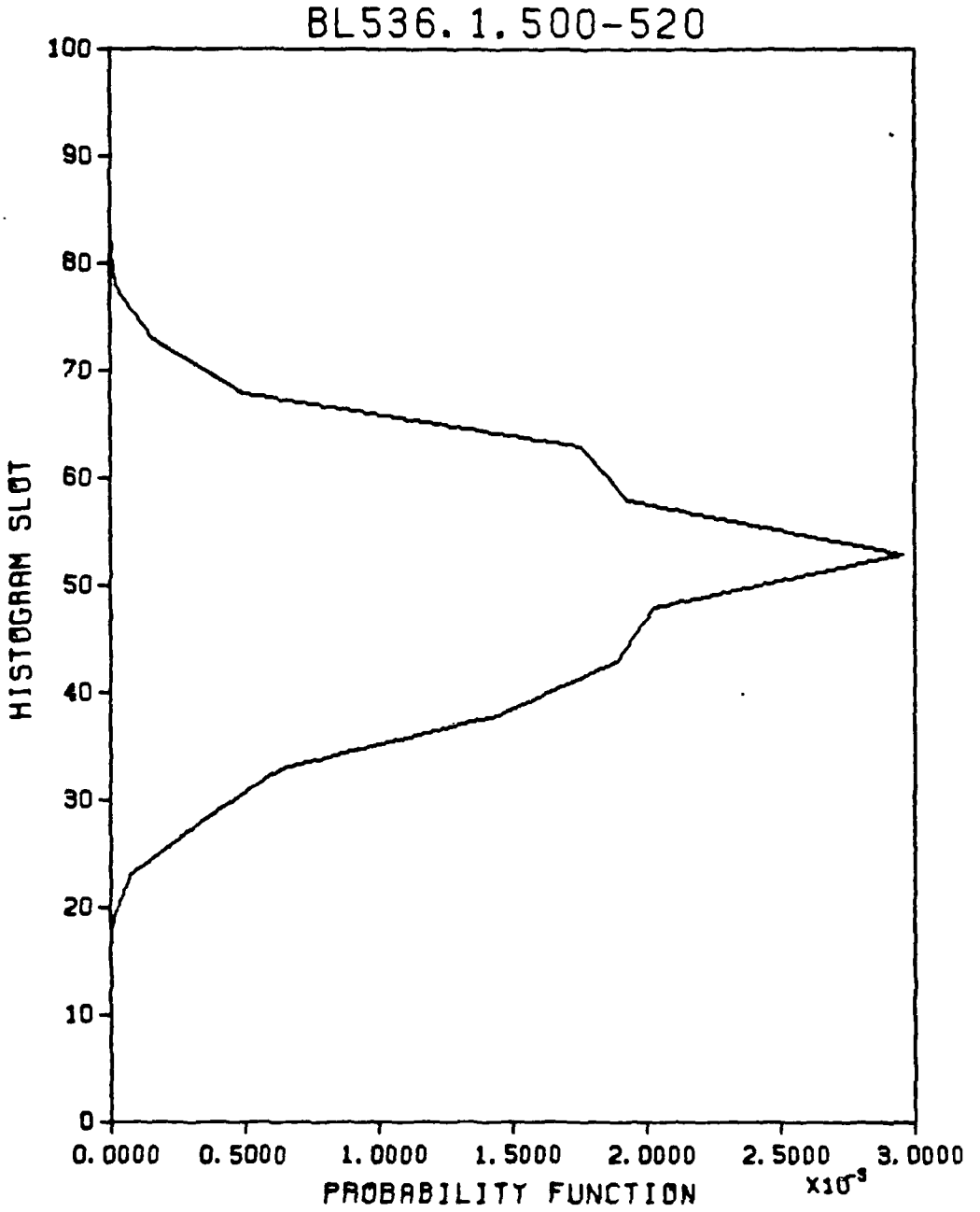

d. z/c = 0.308

Figure 27. (Continued)

7. SPECTRAL ANALYSIS

Two more statistical quantities are useful in analyzing the discrete vortices shed from the leading edge of the delta wing and the effects of the perturbation device on these vortices. These are the autocorrelation and spectrum of the longitudinal velocity fluctuations. The autocorrelation coefficient is the correlation between the values of u at two different times nondimensionalized using the mean square:

$$R(\tau) = \frac{\overline{u(t)\ u(t-\tau)}}{\overline{u^2}} \quad ,$$

where the overbar denotes time average. This coefficient indicates how the values of the longitudinal velocity fluctuations at different times are related. The Fourier transform of the autocorrelation coefficient is the power spectral density:

$$S(f) = \frac{1}{2\pi} \int_{-\infty}^{\infty} e^{-2\pi\tau f}\ R(\tau)\ d\tau \quad ,$$

which is the normalized spectral distribution of the squared intensity of the longitudinal velocity fluctuations (see, for example, Hinze, 1975; Tennekes & Lumley, 1972).

Variations of these two statistical quantities are shown in the next four figures for different run conditions. In Figure 28, the Reynolds number was $R_c = 1.3 \times 10^5$, the angle of attack was $\alpha = 28°$, and the leading edge vortices were not perturbed ($U_j = 0$). The probe was located at x/c = 0.6, y/c = 0.005 and four different spanwise locations: z/c = 0.351, 0.349, 0.348 and 0.344. The peak in the velocity spectrum and the period of oscillation in the autocorrelation correspond to the natural shedding frequency of the leading edge vortices. At this height very close to the wing surface, that peak is not very strong but become more pronounced as the probe moves inward from the leading edge (Figure 28d). The first zero crossing of the correlation coefficient is an indication of the integral time scale. This is about 15 msec at z/c = 0.351 decreasing to about 6 msec at z/c = 0.344.

The spectrum and autocorrelation coefficient at the same run conditions but at a higher elevation above the wing, y/c = 0.03, are depicted in Figure 29 for four different spanwise locations: z/c = 0.346, 0.345, 03.44 and 0.22.

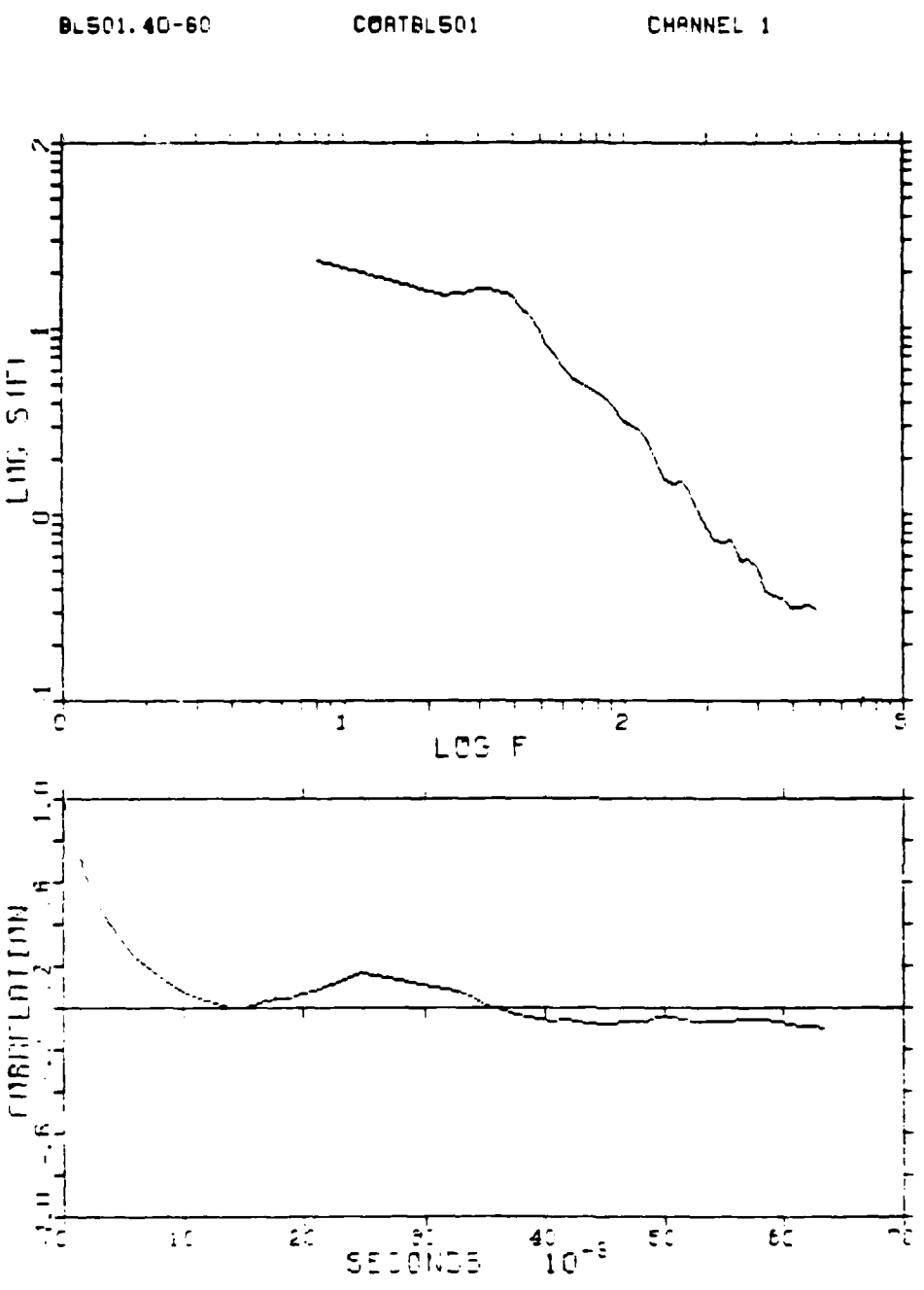

a. z/c = 0.351

Figure 28. Spectrum and Autocorrelation of the Longitudinal Velocity Fluctuations. x/c = 0.6; y/c = 0.005; $R_c = 1.3 \times 10^5$; $\alpha = 28°$; $U_j/U_\infty = 0$

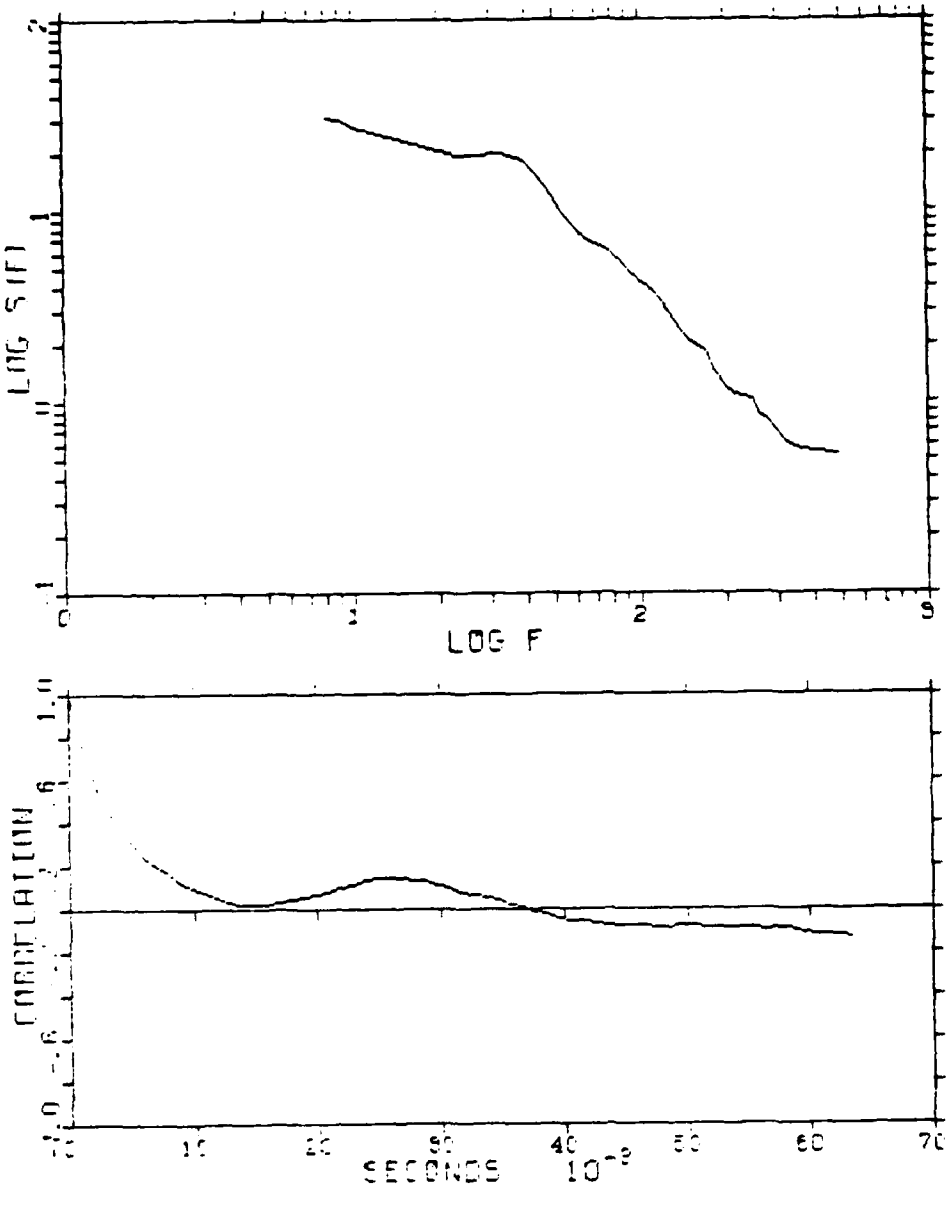

b. z/c = 0.349

Figure 28. (Continued)

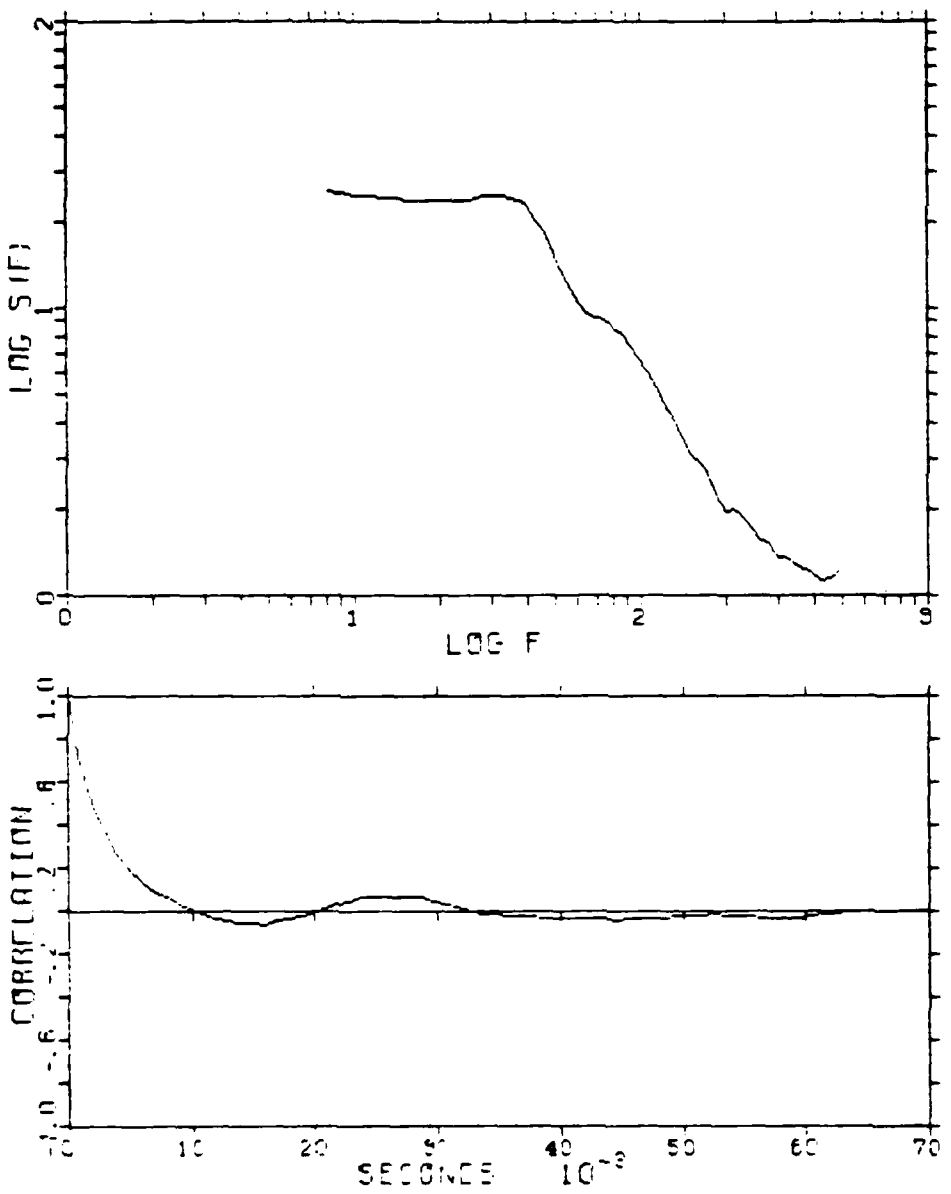

c. z/c = 0.348

Figure 28. (Continued)

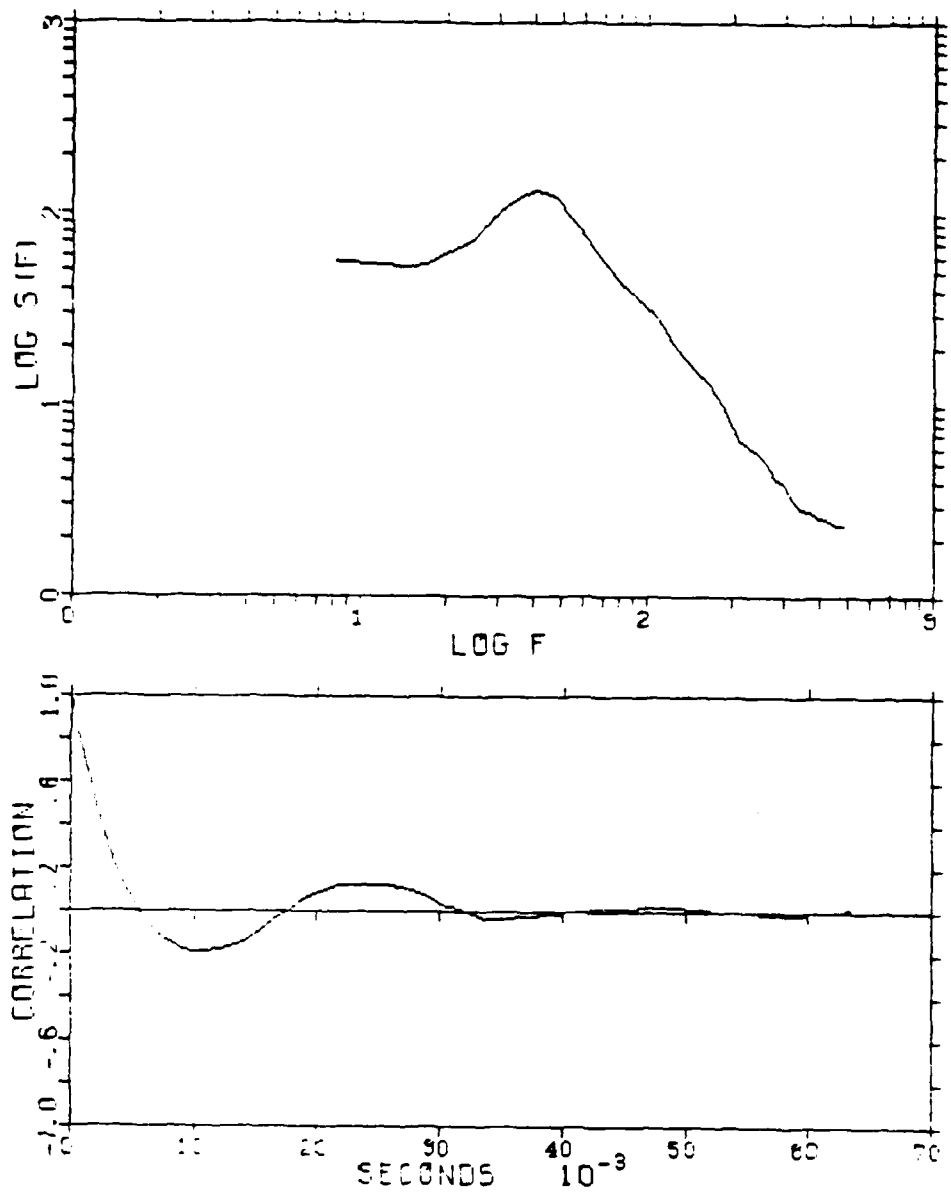

d. z/c = 0.344

Figure 28. (Continued)

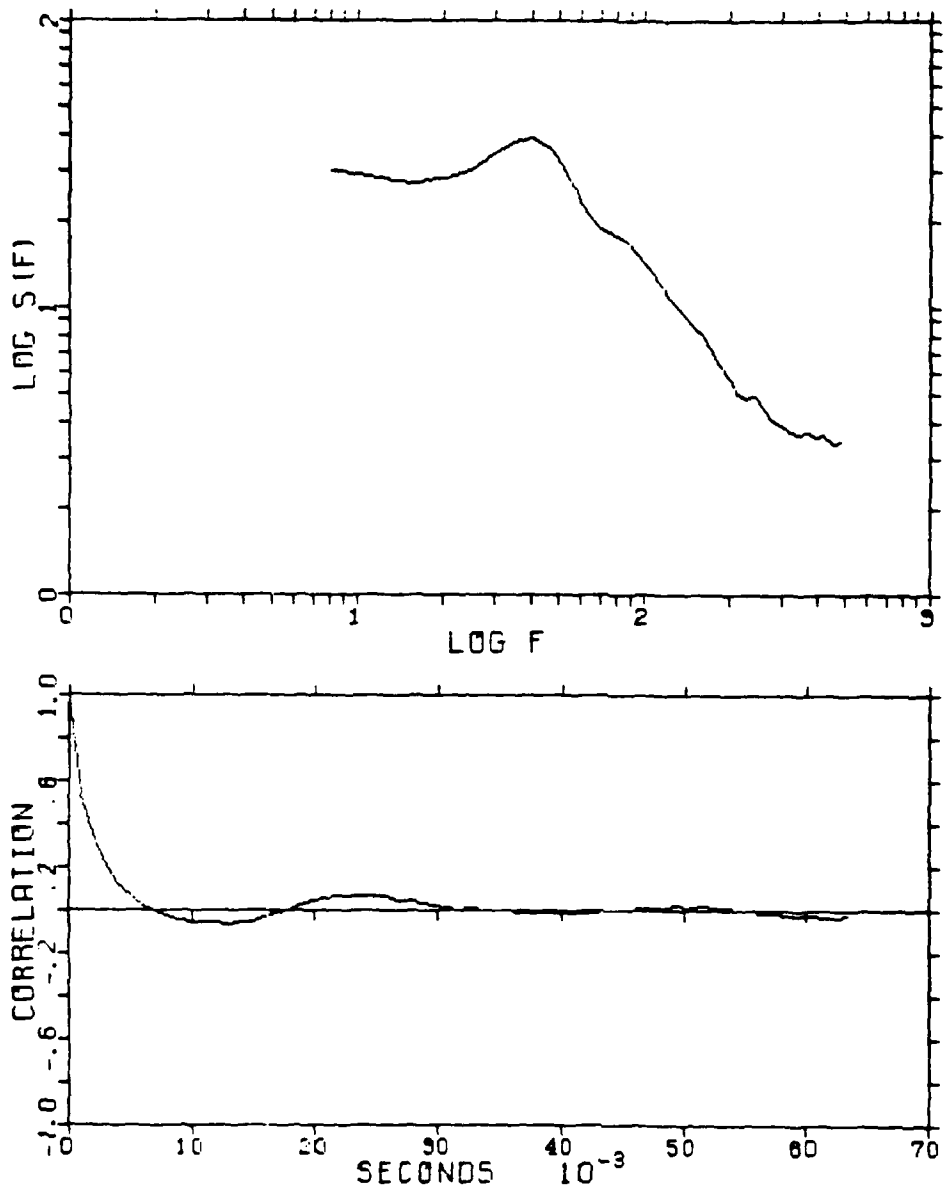

a. z/c = 0.346

Figure 29. Spanwise Changes of Spectrum and Autocorrelation. x/c = 0.6; y/c = 0.03; $R_c = 1.3 \times 10^5$; $\alpha = 28°$; $U_j/U_\infty = 0$

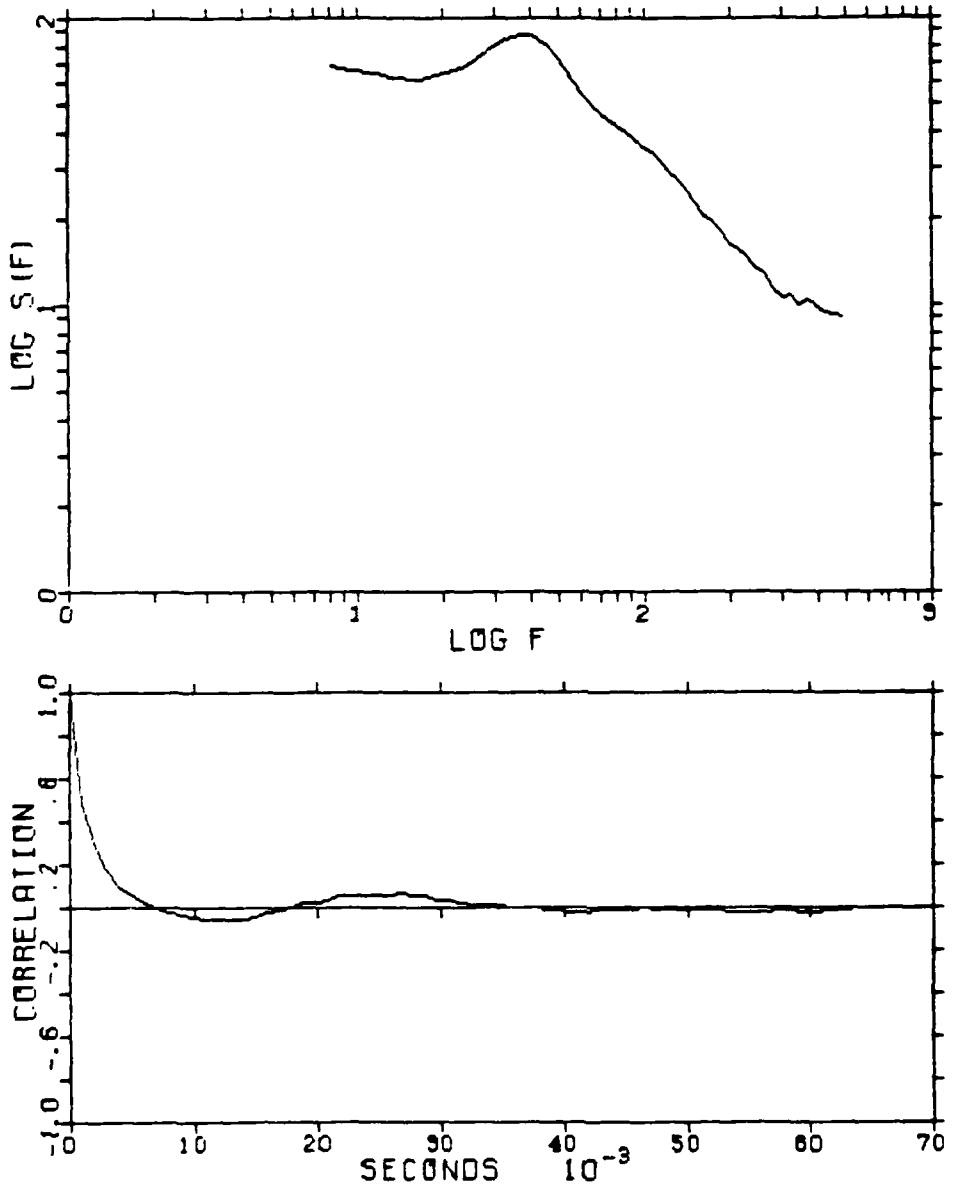

b. z/c = 0.345

Figure 29. (Continued)

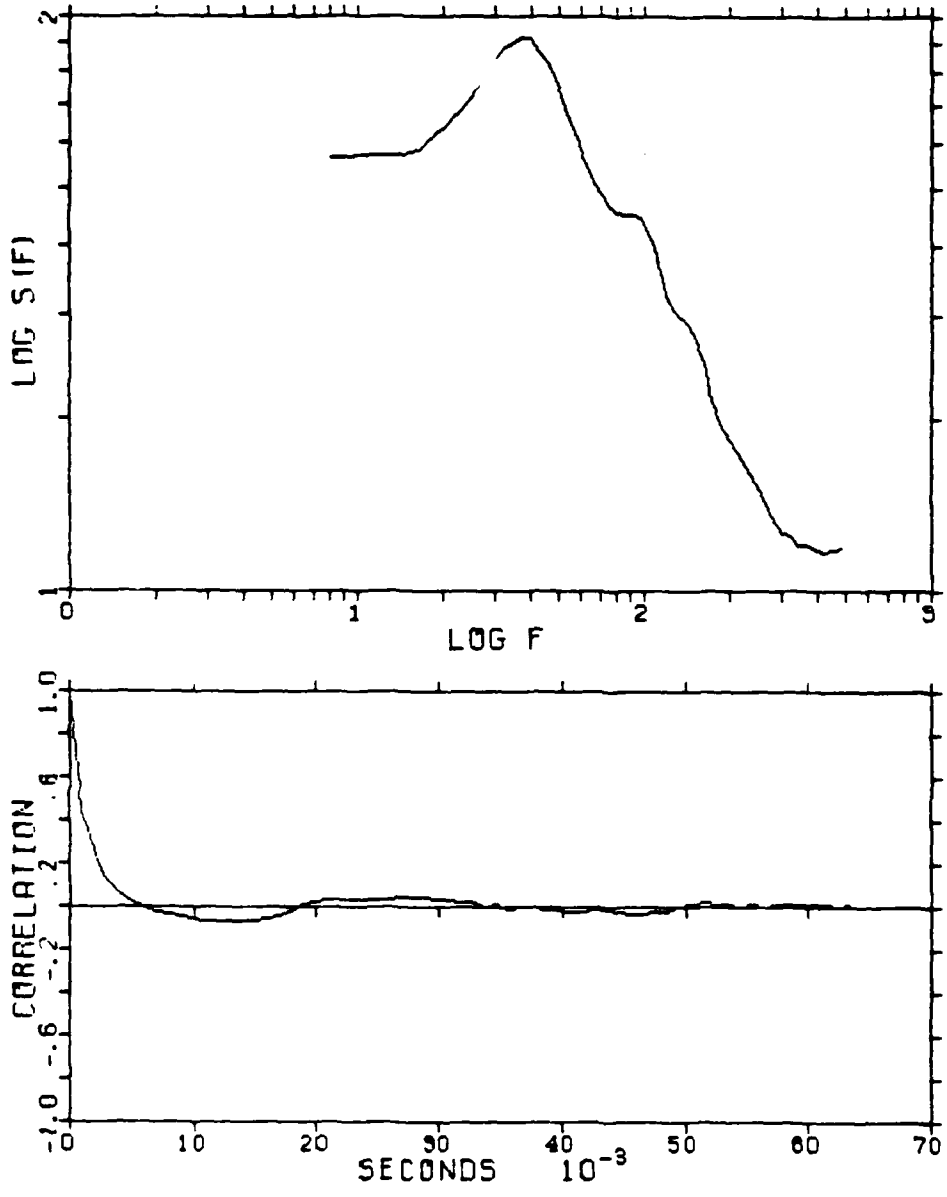

c. z/c = 0.344

Figure 29. (Continued)

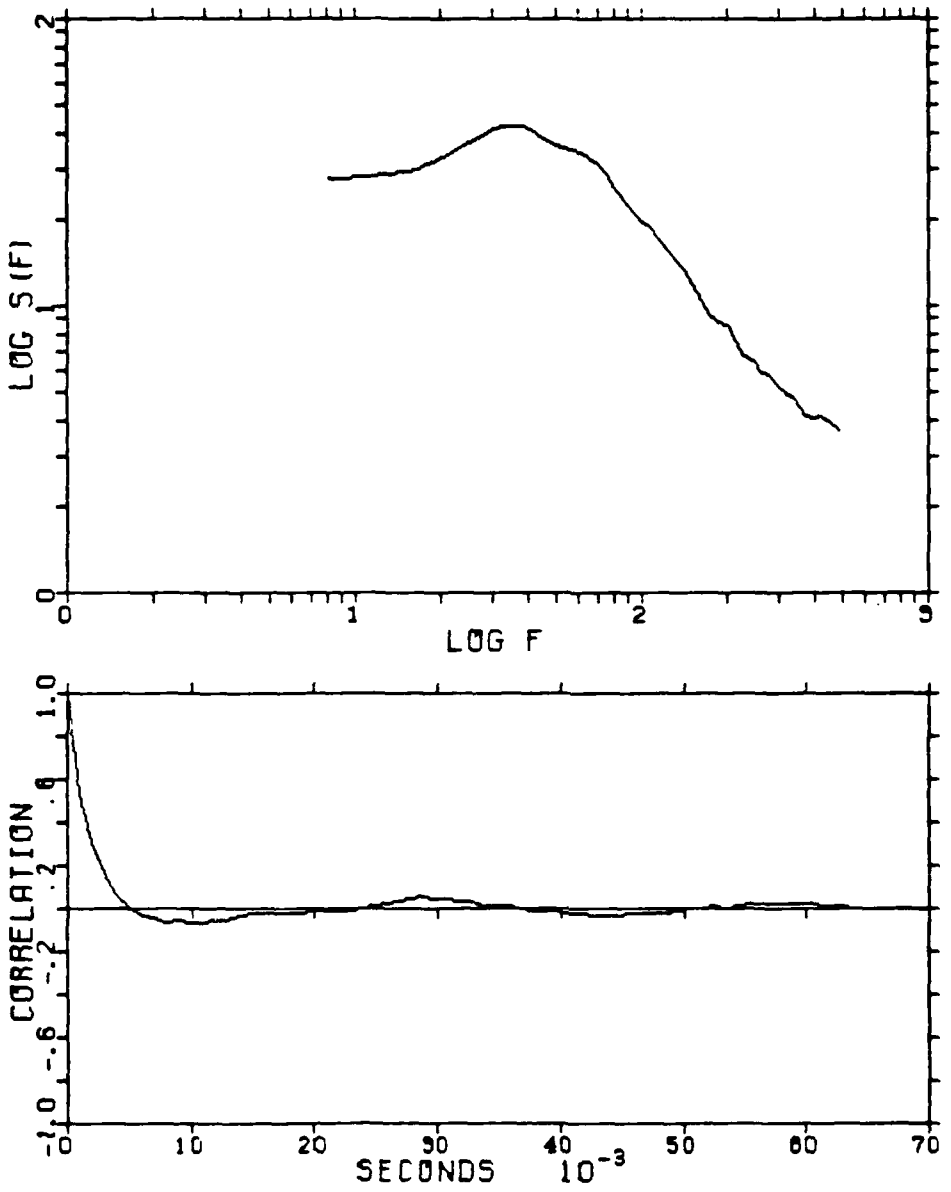

d. z/c = 0.22

Figure 29. (Continued)

At this elevation, the peak in the spectrum corresponding to the natural shedding frequency is more pronounced, particularly at $z/c = 0.344$ (Figure 29c).

The effects of subharmonic perturbation at the leading edge of the delta wing are shown in Figures 30 and 31 at two different heights above the wing: $y/c = 0.03$ and 0.08, respectively. The Reynolds number and angle of attack are the same as that in the run depicted in Figure 29, but a periodic injection perturbation, with maximum jet speed from the leading edge of $U_j = 1.73\ U_\infty$, is applied in the runs shown in Figures 30 and 31. Different spanwise locations are depicted in the two figures. Comparisons between Figures 29b and 30a, and Figures 29c and 30b, which represent the same position relative to the wing in the two respective cases with and without leading edge perturbations, reveal differences in the spectrum and autocorrelation that are consistent with the shift in the position of the shear layer and the corresponding change in the mean velocity and the root-mean-square (Section 5).

At the higher elevation $y/c = 0.08$ shown in Figure 31, the spectrum peak is weak near the leading edge, becoming more pronounced at $z/c = 0.321$ and 0.308 (Figures 31d and 31e), consistent with the general outline of the shear layer as sketched in Figure 1.

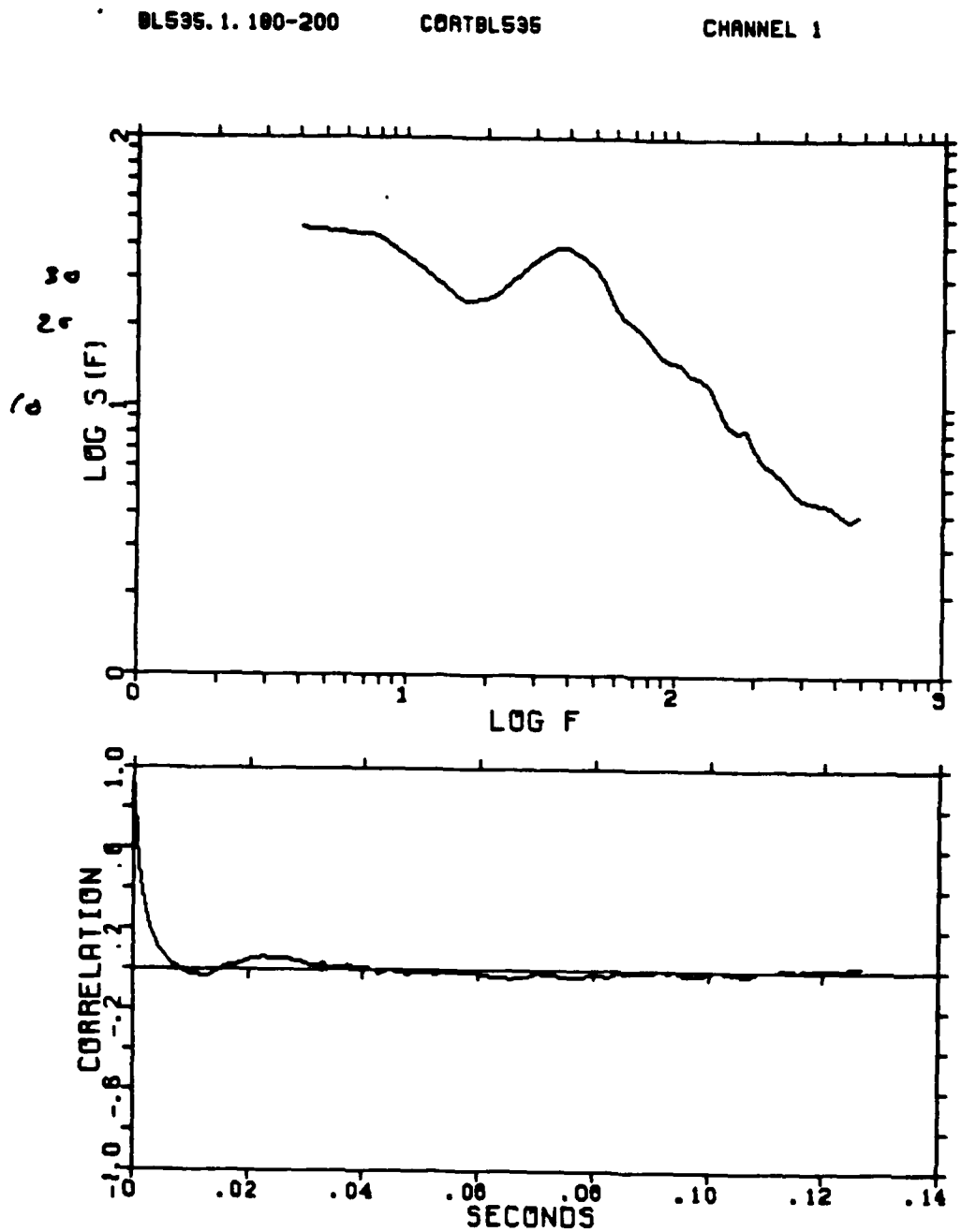

a. z/c = 0.345

Figure 30. Effects of Leading Edge Perturbation on Spectrum and Autocorrelation. x/c = 0.6; y/c = 0.03; $R_c = 1.3 \times 10^5$; $\alpha = 28°$; $U_j/U_\infty = 1.73$

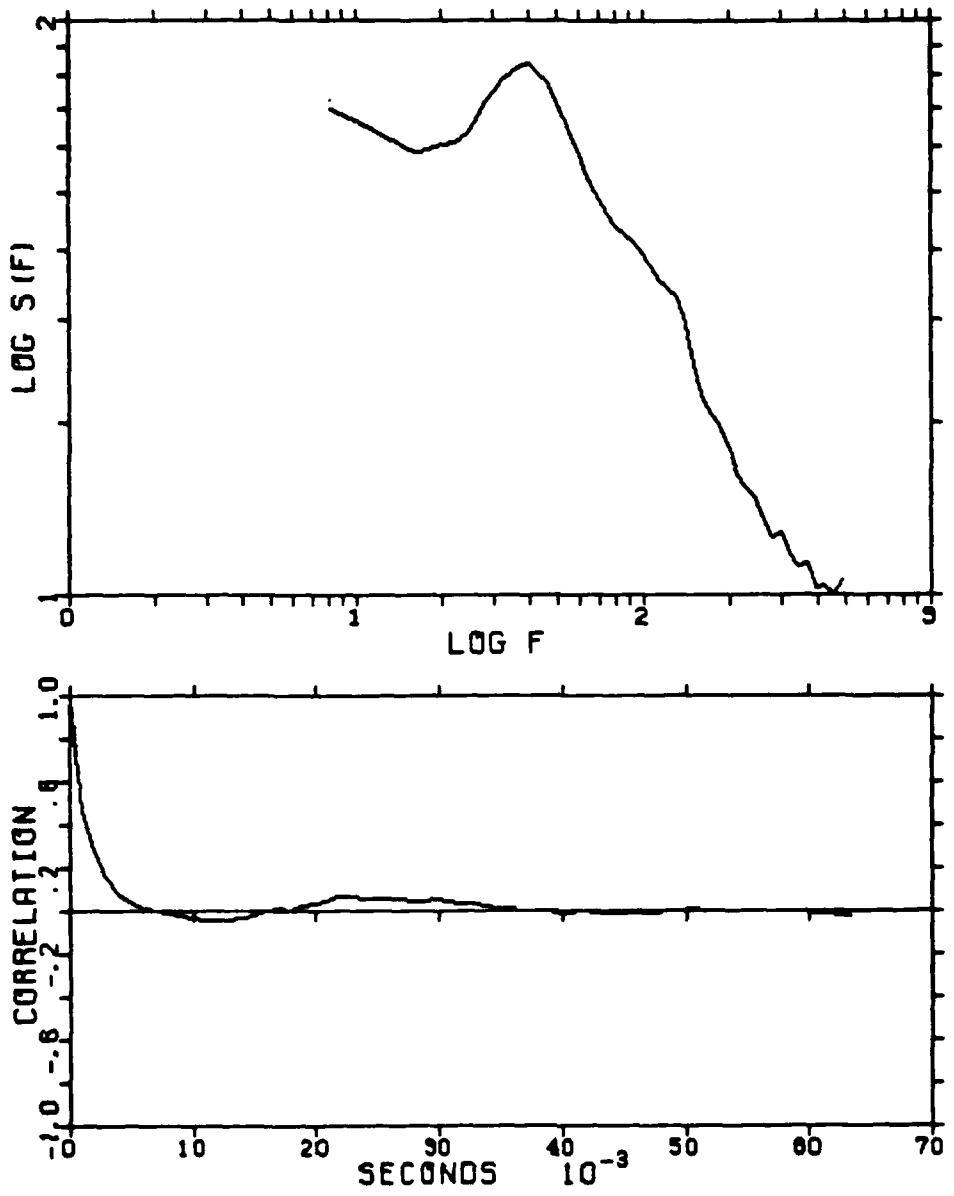

b. z/c = 0.344

Figure 30. (Continued)

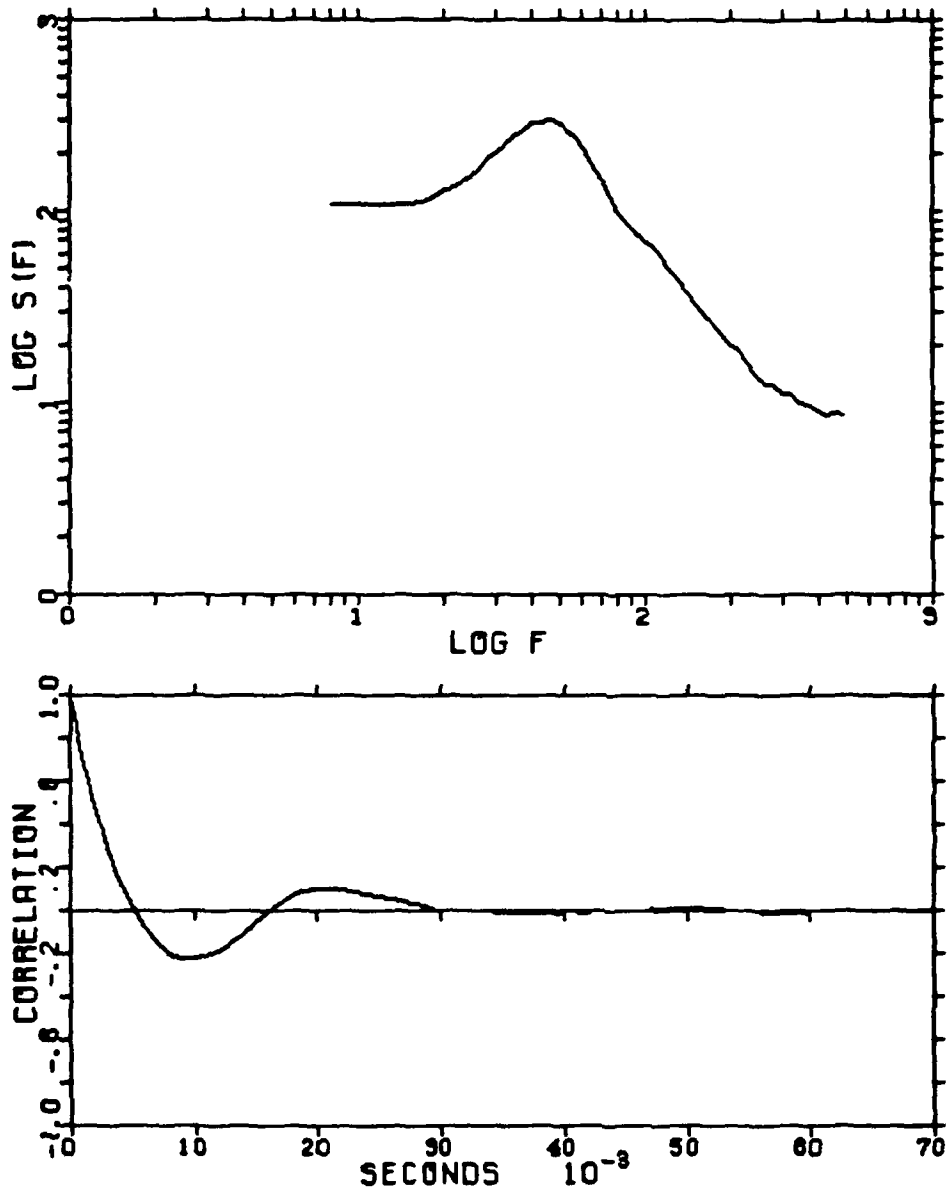

c. z/c = 0.334

Figure 30. (Continued)

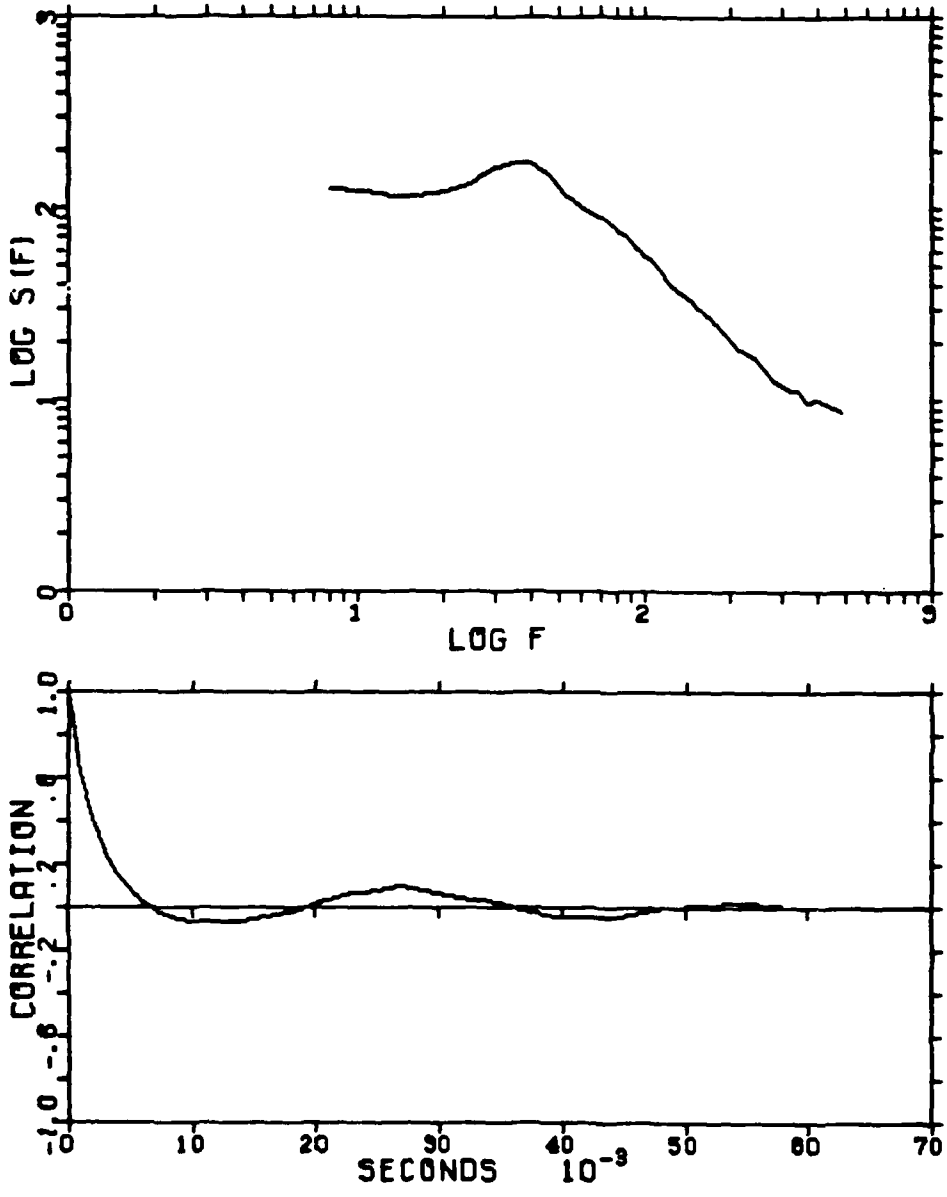

d. z/c = 0.22

Figure 30. (Continued)

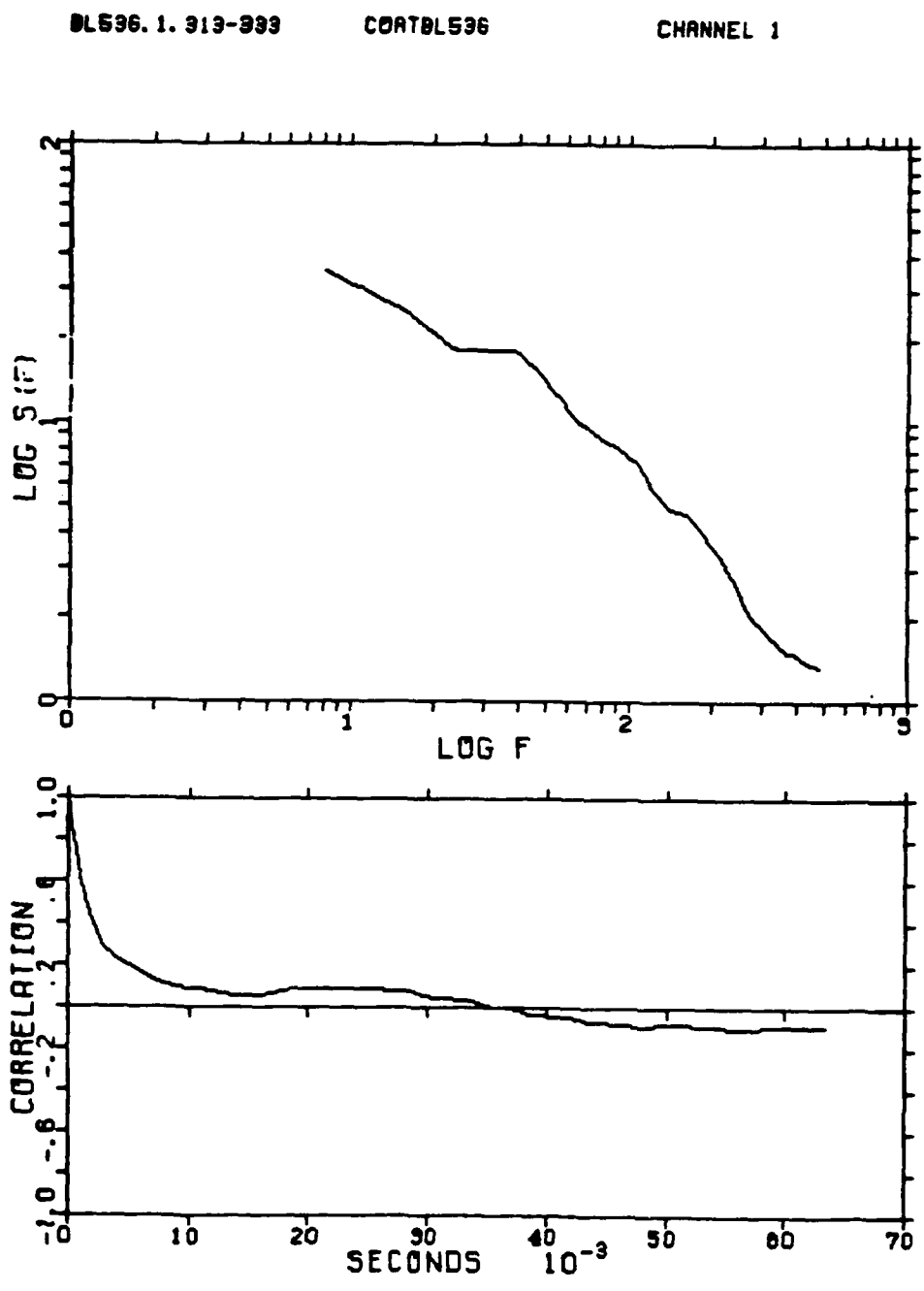

a. z/c = 0.334

Figure 31. Spanwise Variations of Spectrum and Autocorrelation. x/c = 0.6; y/c/ = 0.08; $R_c = 1.3 \times 10^5$; $\alpha = 28°$; $U_j/U_\infty = 1.73$

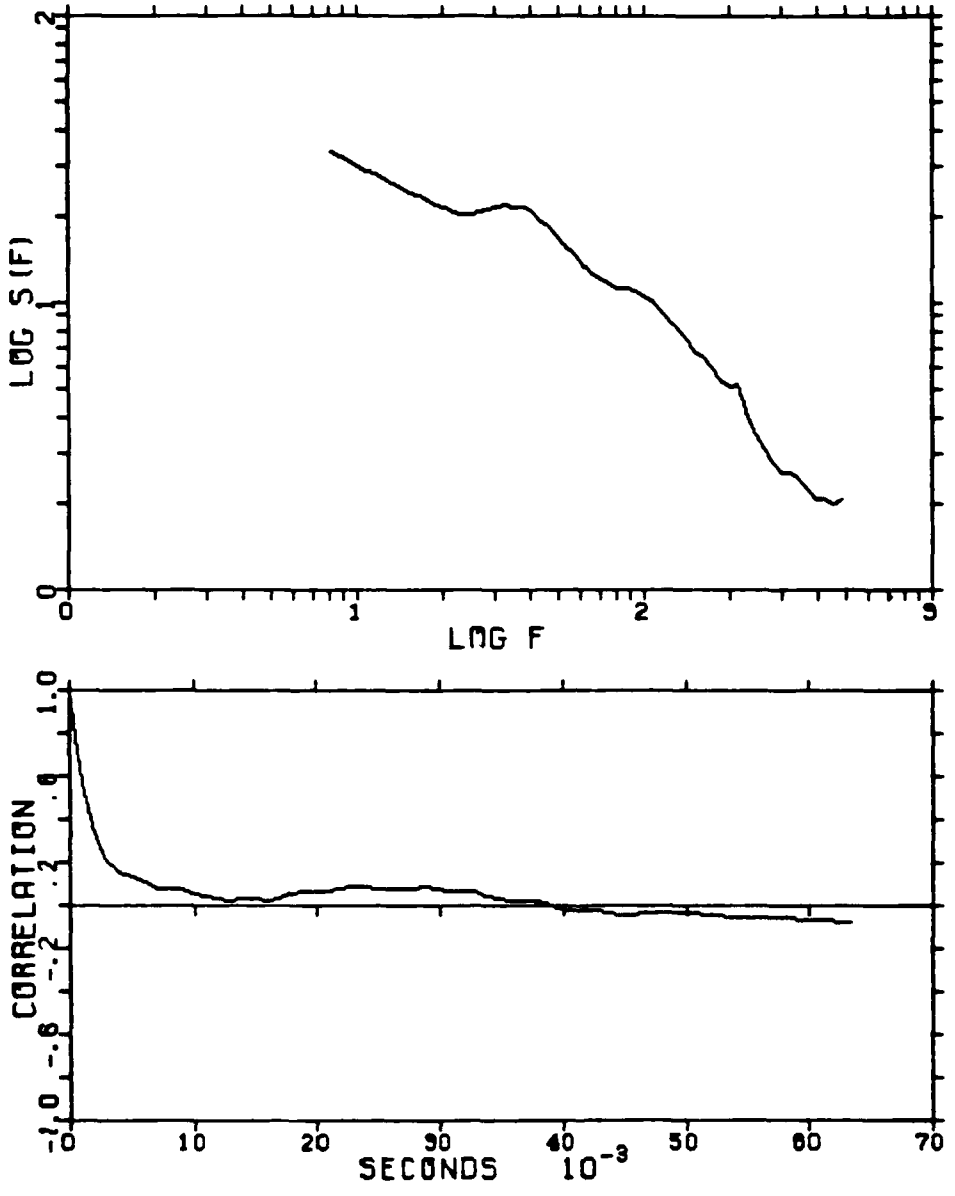

b. z/c = 0.331

Figure 31. (Continued)

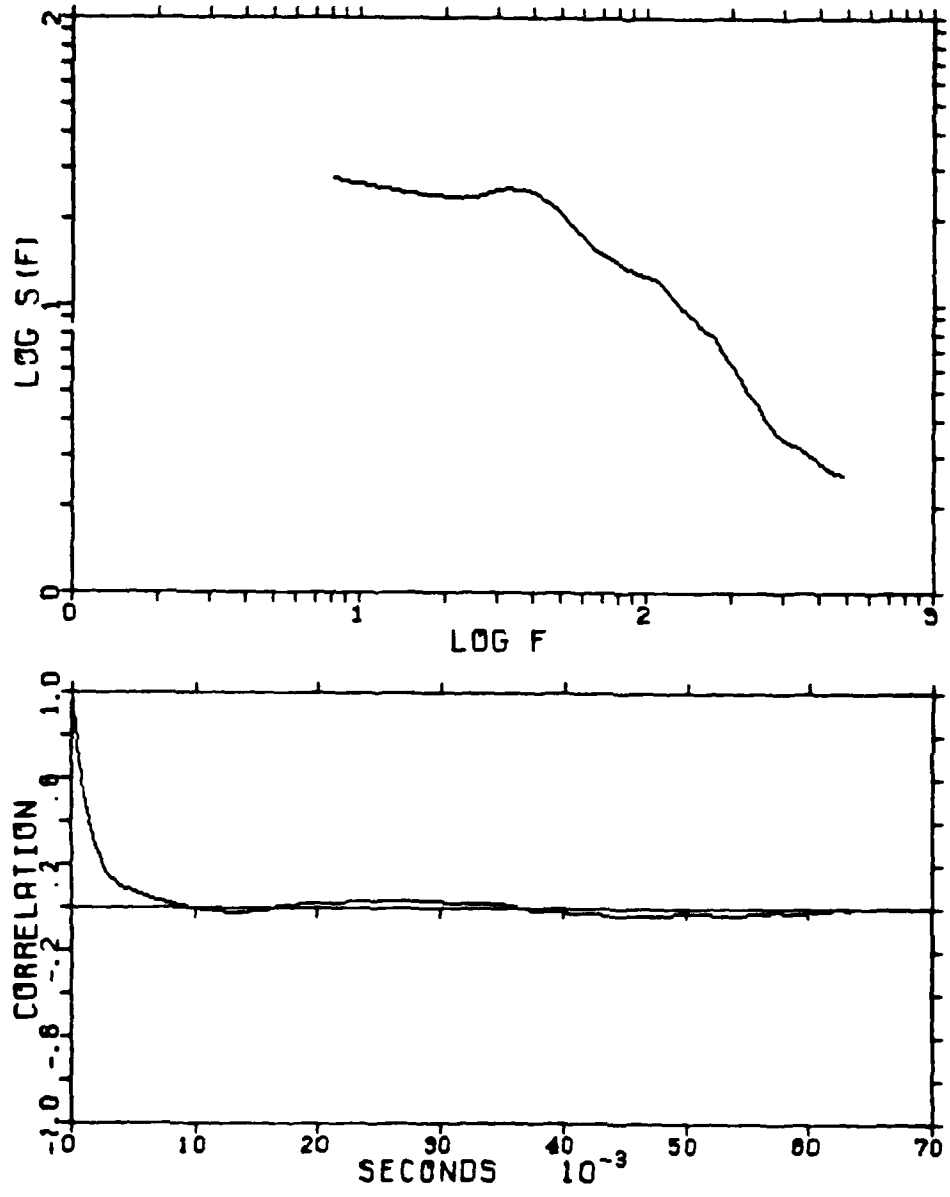

c. z/c = 0.329

Figure 31. (Continued)

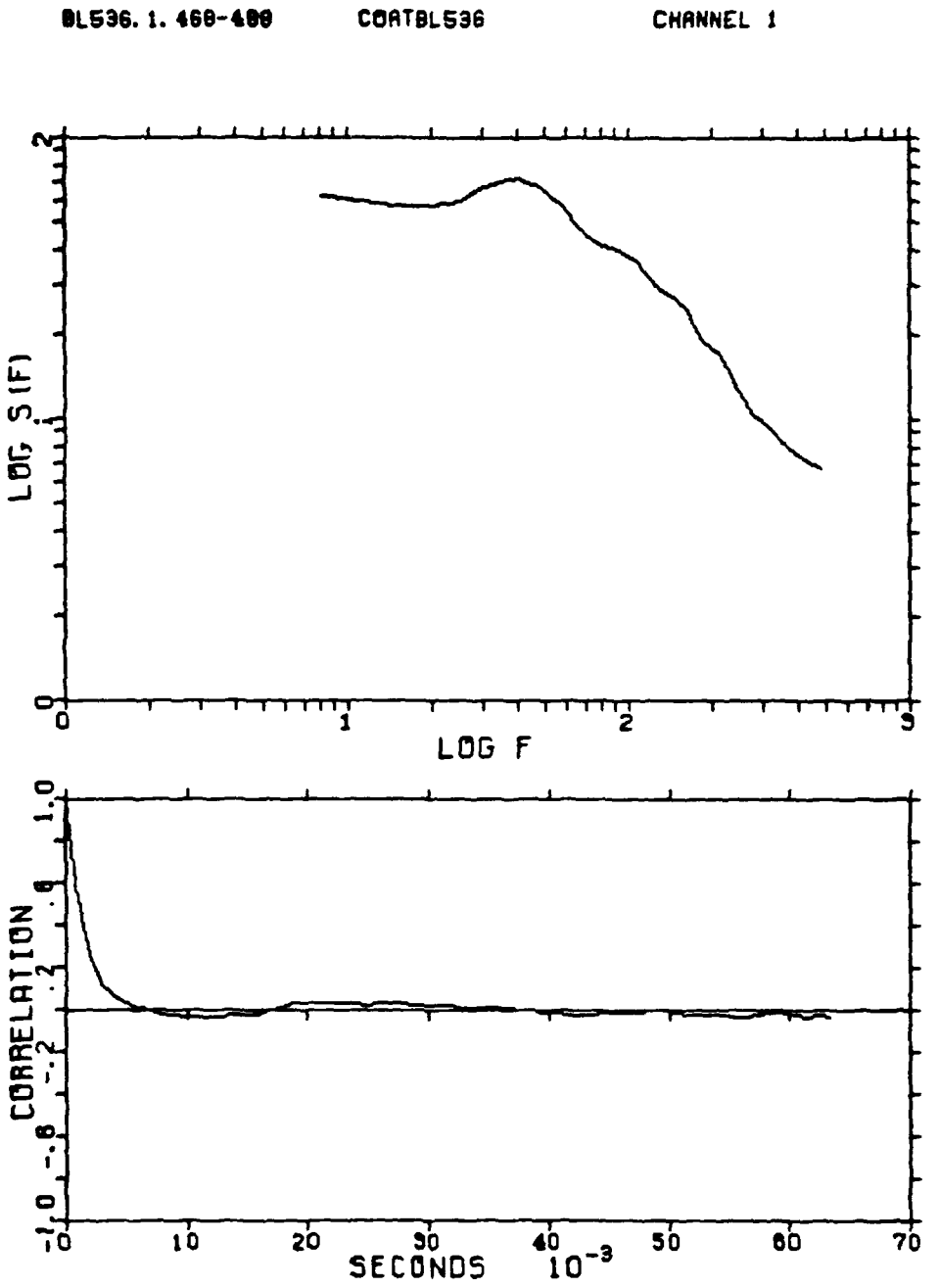

d. z/c = 0.321

Figure 31. (Continued)

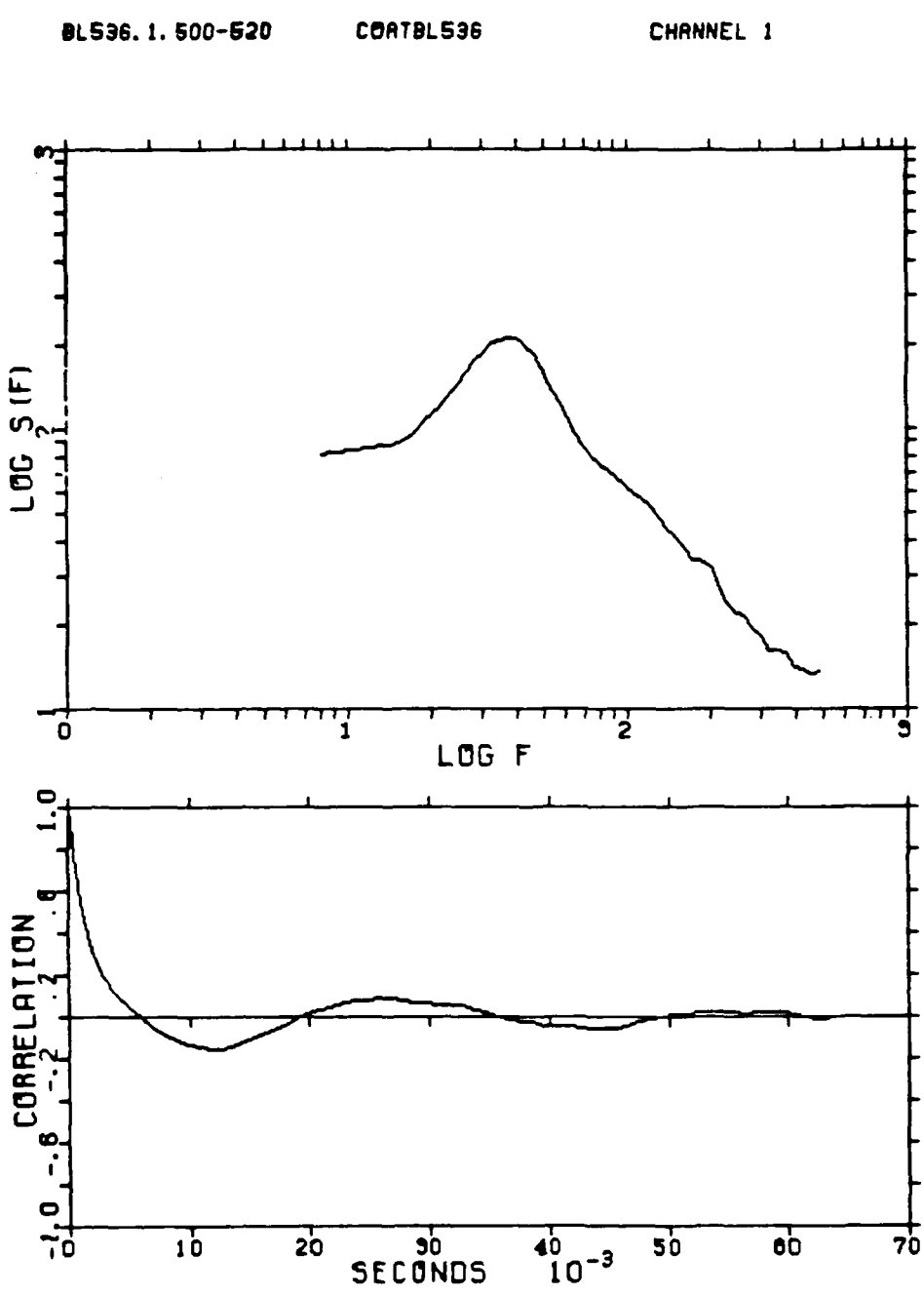

e. z/c = 0.308

Figure 31. (Continued)

8. FORCE MEASUREMENTS

The three-component force balance located in the venturi wind tunnel was used to measure lift, drag and pitching moment on the delta wing model. Three force readings appear on a motor driven beam balance having a resolution of 10 gram, and the readings are used in a computer program that takes into account the balance position with no wind in the tunnel and the effects of the model support. The output of the program is the actual lift, drag and pitching moment on the wing. For the basic unperturbed case, lift, drag and moment coefficients were determined for different wind speeds and angles of attack. The results were in reasonable agreement with the available literature, particularly the exhaustive set of measurements conducted by Wentz & Kohlman (1968) for thirteen different delta wings.

The force and moment coefficients were, as expected, independent of Reynolds number. The sharp leading edge on the delta wing fixes the separation point and the vortex lift is mostly an inviscid phenomenon invarient to the Reynolds number. at an attack angle of $\alpha = 10°$, the three coefficients were $C_L = 0.5$, $C_D = 0.1$ and $C_M = -0.1$. At $\alpha = 28°$, the lift, drag and moment coefficients were $C_L = 1.15$, $C_D = 0.6$ and $C_M = -0.1$.

When the wing was perturbed at the leading edge using subharmonic suction or injection, no measurable change of the forces was observed. This result constituted a setback to the present project and warranted further consideration. The nominal resolution of the force balance used in the present experiment was 10 gram force. However, due to the continuous motion of the balance caused by insufficient damping in the feedback circuit, the needle moved continuously over a range that is about an order of magnitude higher than the nominal resolution. Attempts were made to read a mean position within this range of movement. Changes in the force that are smaller than the needle movement are obviously going to be hard to resolve. At a tunnel speed of $U_\infty = 500$cm/sec and an attack angle of $\alpha = 10°$ the lift force was approximately 70 gram. If the leading edge perturbation device that is being developed in the present project is to change the lift coefficient by 10%,* the change in the balance reading would be only 7 gram; obviously too small to resolve with the present force measuring device. Even at the higher

---

*This is probably a significant change for an actual fighter aircraft.

speed of U_∞ = 1000 cm/sec and the higher angle of attack of $\alpha = 28°$, the resulting lift force is slightly higher than 600 gram. A 10% change translates to about 60 gram change in the reading of the balance. While this is higher than the nominal resolution (10 gram), this reading is within the needle fluctuations due to the insufficient damping in the feedback circuit as noted above.

The short period available for the present project (6 months) did not allow enough time for considering an alternative force balance, particularly building a new one. However, during the second phase of this research a new force balance with sufficient resolution will be designed and built.

9. SUMMARY

Based on our recent finding that a leading edge vortex on a delta wing in steady flight consists of a series of discrete smaller vortices, a device was proposed to modulate these discrete vortices to favorably affect the flow around the wing. The purpose of the present phase of the research reported herein is to establish the proof of concept and to understand the complex flow field under consideration. To this end, the perturbed and unperturbed flow fields around a delta wing at constant angle of attack were studied experimentally in a water towing tank and a high speed wind tunnel. Flow visualization, fast-response velocity probe surveys, as well as force measurements were conducted to study the shear layer formed on the suction side of the wing, and to determine the effects of periodic suction or injection from a leading edge slot on the shedding and pairing of the discrete vortices.

The flow visualization experiments utilized food color and fluorescent dyes illuminated with flood lights or sheets of laser projected in the desired plane. Periodic injection from a leading edge slot significantly changed the shear layer on the suction side of the wing. Subharmonic perturbation with relatively low amplitude seemed to enhance the pairing process and result in a more organized large vortex.

Miniature hot-wire and hot-film probes were used to survey the instantaneous longituding velocity at different positions within the leading edge vortices. Different statistical quantities were computed including the mean, root-mean-square, probability density function, autocorrelation and spectrum. The instantaneous signals clearly showed positive and negative velocity spikes consistent with the passing of the shed vortices by the fixed probe. Leading edge perturbations dramatically affected the intense shear layer as evidenced by the marked changes in the different statistical quantities.

The expected changes in the aerodynamic forces were not observed in this preliminary phase of the research. Careful analysis of the force balance used in the present experiments indicated that these changes are most probably within the accuracy of the balance system.

The results of Phase I research indicate that the discrete vortices could be strongly modulated with periodic suction or injection from a leading edge slot. In the next phase, a force balance with adequate resolution will be designed and built, and the perturbation device will be optimized for field applications.

REFERENCES

Brown, G. L., and Roshko, A. (1974) "On Density Effects and Large Structure in Turbulent Mixing Layers," J. Fluid Mech. 64, p. 775.

Elle, B. J. (1958) "An Investigation at Low Speed of the Flow Near the Apex of Thin Delta Wings with Sharp Leading Edges," ARC Tech. Rep. R&M No. 3176.

Faery, H. F., Jr., Strozier, J. K., and Ham, J. A. (1981) "Experimental and Theoretical Study of Three Interacting, Closely-Spaced, Sharp-Edged 60° Delta Wings at Low Speeds," NASA CR-3460.

Gad-el-Hak, M. (1986a) "The Use of the Dye-Layer Technique for Unsteady Flow Visualization," J. Fluid Engineering 108, No. 1.

Gad-el-Hak, M., and Blackwelder, R. F. (1985b) "On the Discrete Vortices from a Delta Wing," AIAA Journal 23, p. 961.

Gad-el-Hak, M., Blackwelder, R. F., and Ho, C.-M. (1983a) "Coherent Structures in Steady and Unsteady Motions of a Delta Wing," Bul. Am. Phys. Soc. 28, p. 1397.

Gad-el-Hak, M., Blackwelder, R. F., and Riley, J. J. (1981) "On the Growth of Turbulent Regions in Laminar Boundary Layers," J. Fluid Mech. 110, p. 73.

Gad-el-Hak, M., and Ho, C.-M. (1985c) "Three-Dimensional Effects on a Pitching Lifting Surface," AIAA Paper No. 85-0041.

Gad-el-Hak, M., and Ho, C.-M. (1985d) "The Pitching Delta Wing," AIAA J. 23, p. 1660.

Gad-el-Hak, M., and Ho. C.-M. (1986b) "Unsteady Vortical Flow Around Three-Dimensional Lifting Surfaces," AIAA J. 24, No. 5.

Gad-el-Hak, M., and Ho, C.-M. (1986c) "Unsteady Flow Around an Ogive-Cylinder," submitted to J. Aircraft.

Gad-el-Hak, M., Ho, C.-M., and Blackwelder, R. F. (1983b) "A Visual Study of a Delta Wing in Steady and Unsteady Motion," in Unsteady Separated Flows, eds. M. S. Francis & M. W. Luttges, Univ. Colorado, p. 45.

Herbst, W. B. (1983) "Dynamics of Air Combat," J. Aircraft 20, p. 594.

Herbst, W. B. (1981) "Supermaneuverability," presented at the Joint Automatic Control Conference, University of Virginia, Charlottesville, VA.

Hinze, J. O. (1975) Turbulence, second edition, McGraw-Hill.

Ho, C.-M., and Huerre (1984) "Perturbed Free Shear Layers," Ann. Review Fluid Mech. 16, p. 365.

Hoerner, S. F., and Borst, H. V. (1975) Fluid Dynamic Lift, L. A. Hoerner publisher, Brick Town, NJ.

Konstadinopoulos, P., Mook, D. T., and Nayfeh, A. H. (1983) "Numerical Simulation of the Subsonic Wing-Rock Phenomenon," AIAA Paper No. 83-2115.

Lumley, J. L. (1970) Stochastic Tools in Turbulence, Academic Press.

Roshko, A. (1976) "Structure of Turbulent Shear Flows: A New Look," AIAA. 14, p. 1349.

Tennekes, H., and Lumley, J. L. (1972) A First Course in Turbulence, MIT Press.

Wentz, W. H., Jr., and Kohlman, D. L. (1968) "Wind Tunnel Investigations of Vortex Breakdown on Slender Sharp-Edged Wings," NASA CR-98737.

Werlé, H. (1973) "Hydrodynamic Flow Visualization," Ann. Review Fluid Mech. 5, p. 361.

Winant, C. D., and Browand, F. K. (1974) "Vortex Pairing: the Mechanism of Turbulent Mixing-Layer Growth at Moderate Reynolds Number," J. Fluid Mech. 63, p. 237.

4181R

END

2-87

DTIC